Effect of Anode Purge on Polymer Electrolyte Membrane Fuel Cell Performance

by

Rebecca Christine Sauder

A thesis
presented to the University of Waterloo
in fulfillment of the
thesis requirement for the degree of
Master of Applied Science
in
Chemical Engineering

Waterloo, Ontario, Canada, 2009

AUTHOR'S DECLARATION

I hereby declare that I am the sole author of this thesis. This is a true copy of the thesis, including any required final revisions, as accepted by my examiners. I understand that my thesis may be made electronically available to the public.

Abstract

Polymer Electrolyte Membrane Fuel Cells (PEMFC) are promising power generating devices that use an electrochemical reaction to convert the energy from hydrogen fuel into usable electricity. One cell produces a small voltage so many cells are combined in series in order to produce a useful voltage, this configuration is referred to as a stack. Hydrogen is supplied to the anode of the stack in amounts greater than the electrochemical reaction requires to guarantee that enough hydrogen is available for every cell in the stack and to provide enough pressure throughout the cell flow channels for good mass transfer. For reasonable fuel efficiency, the anode outlet gas containing unconverted hydrogen is recycled (or recirculated) back to the anode inlet. PEMFC performance is highest when pure hydrogen fuel is supplied, however, nitrogen at the cathode will permeate through the membrane and accumulate in the anode gas with recirculation. Nitrogen buildup dilutes the hydrogen gas which adversely affects fuel cell performance at the anode. Also, in practical applications hydrogen-rich gas produced from reformed methane, called reformate, is used as the fuel. Reformate contains impurities such as, nitrogen, carbon dioxide, carbon monoxide, and sulfur compounds. This thesis will focus on trace levels of carbon monoxide entering in the hydrogen fuel stream, and the impact of contaminant build-up due to anode recirculation. Carbon monoxide adsorbs readily onto the platinum catalyst sites, called poisoning, thus decreasing PEMFC performance. In efforts to minimize the buildup of impurities and crossed over nitrogen, a portion of the anode outlet gas is periodically and continuously purged to the exhaust. How often the outlet gas is purged depends on a variable called the purge fraction. The purpose of this research is to study the effect of purge fraction on PEMFC performance, measured by the average cell voltage, for a Hydrogenics 10 cell stack. The operating parameters used for testing and the experimental apparatus were designed to mimic a Hydrogenics 8kW Hydrogen Fuel Cell Power Module. A pump connected between the anode outlet and anode inlet form the anode recirculation loop. In Phase 1 of the test program the effect of purge in the absence of carbon monoxide was studied to see if hydrogen dilution from nitrogen crossover and accumulation would cause significant cell voltage

degradation. In Phase 2 the effect down to 0.2 ppm carbon monoxide was evaluated. The results showed that nitrogen buildup, in the absence of carbon monoxide, did not significantly penalize the cell performance in the range of purge fractions tested. However, for the same purge fraction but with as little as 0.2 ppm carbon monoxide present, the voltage loss was significant. A discussion of the effect of purge on the impurity concentration and the associated cell voltage degradation is detailed with particular emphasis on carbon monoxide poisoning.

Acknowledgements

I owe my deepest gratitude to my supervisor, Dr. Michael Fowler, whose encouragement and guidance from the start to the end enabled me to develop an understanding of the subject.

It is an honor for me to thank my industrial supervisor, Dr. Rami Abouatallah; without his guidance and persistent help this project would not have been possible. As well, I am grateful for having the opportunity to collaborate with Hydrogenics Corporation and especially Natasha Beydokhti, David Rebello, and Kwok Chan for their technical help and their enthusiasm in regard to teaching.

Lastly, I would like to thank my mom for her unlimited support and encouragement in reaching my goals.

Table of Contents

List of Figures

List of Tables

Nomenclature

a_i	-	Activity of component i	-	-
E	-	Thermodynamic equilibrium potential	-	V
E°	-	Standard potential at 25°C and 1 atm	-	V
F	-	Faraday's constant	-	$C\cdot(mol\ e^-)^{-1}$
FC	-	Fuel Cell	-	-
i	-	Current density	-	$A\cdot m^{-2}$
I	-	Total current running through the stack	-	A
l	-	Separation distance between each anode and cathode	-	m
n_{cell}	-	Total number of cells in the stack	-	-
n_e	-	Number of electrons transferred	-	-
OCV	-	Open Circuit Voltage	-	V
$P_{average}$	-	Average cell power	-	W
P_{stack}	-	Stack power	-	W
PEM	-	Polymer Electrolyte Membrane or Proton Exchange Membrane	-	-
Q	-	Volumetric flow rate of the gas consumed by the stack	-	$L\cdot min^{-1}$
R	-	Ideal gas constant	-	$L\cdot atm\cdot mol^{-1}\cdot K^{-1}$
λ	-	Stoichiometric ratio/coefficient	-	-
T	-	Absolute Temperature	-	K
$V_{average}$	-	Average cell potential	-	V
V_{cell}	-	Voltage produced by the cell	-	V
V_{stack}	-	Stack voltage	-	V
V_{STP}	-	Volume occupied by an ideal gas at standard temperature and pressure (0°C, 1 atm)	-	$L.mol^{-1}$

Chapter 1 - Introduction

1.1 Objectives

For fuel cells to flourish commercially they must provide a clean, energy-efficient technology that performs comparably, if not better than, the current technologies and at a comparable cost. However, the technical issues that constrain fuel cells from prevailing must first be overcome. Through investigations such as this study, it is the intension of researchers in industry, government and academia to advance the development of polymer electrolyte membrane fuel cells (PEMFC). This work will address the critical issue of anode stream purge rates, and the impact of purge rates on degradation of PEMFC performance.

1.2 Rationale for the Transition to Fuel Cells

Today's principal methods for producing energy still rely on burning fossil fuels and as a result society is facing serious global issues: the adverse effects that pollutants have on human health and the environment, climate change from the accumulation of carbon dioxide in the atmosphere, the earth's finite stores of fossil fuels are dwindling, and the lack of security of countries without oil resources as a result of energy import dependence [1].

These issues are the major driving force for scientists and engineers investigating energy generation methods that use hydrogen rather than fossil fuels. Hydrogen serves as an energy carrier that can be used to power factories, heat homes, and run cars, just as gasoline does now [2]. No pollutants are emitted in converting hydrogen to power, making it a "green energy" source. Hydrogen can be produced by various methods and from various sources (e.g. electrolysis of water) which alleviates energy dependence as countries become more self-reliant.

The promise of the hydrogen economy lies with the production of hydrogen from clean sources of electricity and then using the hydrogen,

- to power vehicles and industrial equipment (i.e. lift trucks),
- as distributed energy generation, and
- for electricity generation as a supply and load management tool.

Especially important is the role that hydrogen can play to enable additional penetration of intermittent power generation sources such as wind and solar. Also, hydrogen vehicles can significantly improve urban air quality [3].

Hydrogen can be produced by the electrolysis of water from electricity. Hydrogen, when made from renewable sources and nuclear energy, is a zero-emission fuel, and is viewed as a way society can reduce green house gas (GHG) emissions in the transportation sector to 80% below 1990 levels [4]. The transportation sector is a significant contributor to GHG emissions. Hydrogen use also reduces dependence on non-renewable resources by establishing a wide local energy base from which hydrogen can be obtained. Figure 1 outlines the comparison of various technology options for transportation.

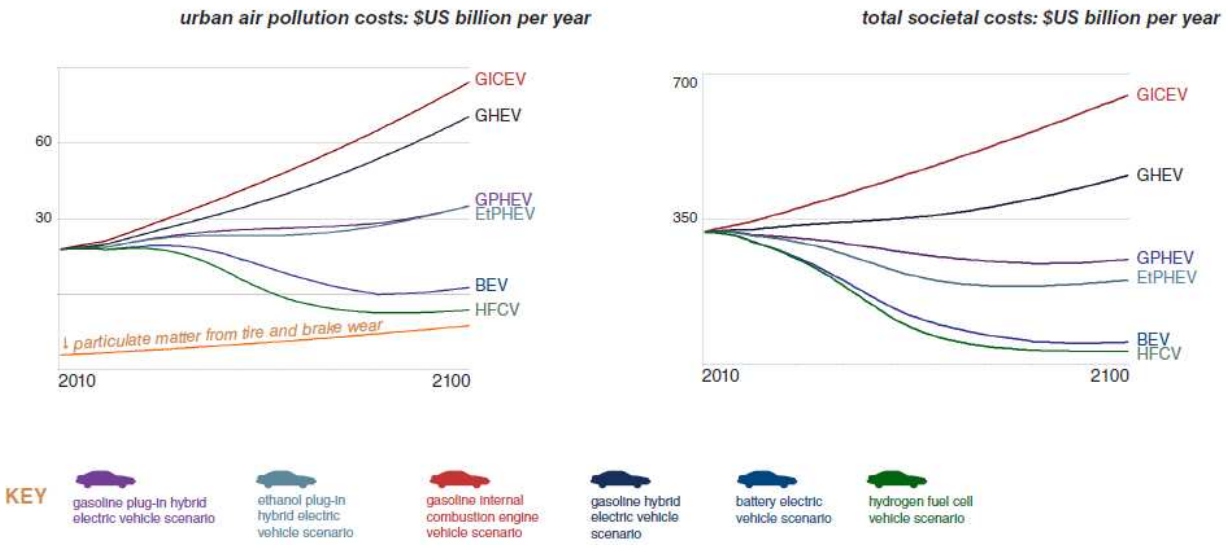

Figure 1: Comparison of Various Propulsion Technology Options for Air Pollution Costs [5]

Fuel cells are an attractive technology for energy production from hydrogen primarily because the method of energy conversion provides many advantages over combusting fossil fuels. First, pure water is the only emission produced during the conversion. Second, fuel cells convert the chemical energy of the fuel directly into electrical energy, thus fuel cells are theoretically more efficient than internal combustion engines which are limited by the Carnot cycle. Finally, the technology can be easily scaled as a power source for something as large as a power plant to something as small as a cellular phone.

Some viable classes of fuel cells are under consideration for the hydrogen economy, including alkaline fuel cells, polymer electrolyte membrane fuel cells (PEMFC), and solid oxide fuel cells [6]. The different fuel cell types are distinguished by their type of electrolyte. This thesis will focus on PEMFC which employ a solid polymer electrolyte and hydrogen and oxygen reactants.

1.3 Introduction to PEM Fuel Cells

From a historical perspective, fuel cell technology was invented by Sir William Grove, a Welsh judge and scientist in 1839. It wasn't until the Gemini and Apollo space programs that fuel cells saw their first practical application in generating electric power (and drinking water). Since then, fuel cells have been used in transportation and stationary power generation applications but for the majority they have been used in laboratory settings.

The theory behind the fuel cell is relatively simple. A fuel cell is a device that uses an electrochemical reaction to directly convert the chemical energy of a fuel into useable electricity. Similar to batteries, fuel cells are made of two electrodes with an electrolyte sandwiched in between. Unlike batteries, fuel cells operate for as long as fuel and oxidant are supplied, much like a combustion engine does. Yet, combustion engines are less efficient than fuel cells because fuel is combusted in order to produce heat that is then used to produce useful work by moving a piston, and thus such engines are limited by the Carnot cycle. The theoretical thermodynamic derivation of the Carnot Cycle shows that even under ideal conditions, a heat engine cannot convert all the heat energy supplied to it into mechanical energy; and some of the heat energy must be rejected. In an internal combustion engine, the engine accepts heat from a high temperature source (T_H), converts part of the energy into mechanical work and rejects the remainder to a heat sink at a low temperature (T_L). The greater the temperature difference between source and sink, the greater the efficiency. The maximum efficiency of a heat engine = $(T_H-T_L)/T_H$.

PEMFCs offer many benefits. They are highly efficient, as they convert chemical energy directly to electrical energy; therefore there is no requirement for a conversion of heat to mechanical energy. Depending on the type and design, fuel cells have an actual electric energy efficiency range from 40 to 60 percent. Practically internal combustion engines in a typical car will only get an efficiency of 10-20%. A PEMFC stack operates with a relatively flat efficiency

profile based on the load. Emissions from this type of a system are much lower than emissions from the cleanest fuel combustion process as the operating temperature is not high enough to create NO_x emissions. There are no moving parts in the energy converter, which means that high reliability is possible. Modular installations are used to match loads and improve reliability while providing size flexibility. Fuel cells can be quickly recharged or refueled (unlike a traditional battery), and this can be repeated through a large number of cycles, thus PEMFC have refueling advantages over battery systems. High-quality and low-quality heat is available for co-generation, heating, and cooling in residential, commercial, and industrial applications.

There are still some barriers to overall market acceptance of PEMFC technology:

- PEMFC material and manufacturing cost are high, and cost reduction targets associated with mass production have not been fully demonstrated at this time;
- there has yet to be a fully developed supply chain of balance of plant components, so component options such as anode recirculation pumps are not optimized for the specific application;
- endurance and reliability has not been adequately demonstrated;
- hydrogen distribution and refueling infrastructure is not in place; and
- purity of the hydrogen fuel remains an issue.

Aside from manufacturing and material cost issues, the two main issues constraining commercialization of fuel cells are optimization of the reaction rate at lower catalyst loading and optimization of operating conditions [7].

1.3.1 Principal of Operation

Fuel cells are electrochemical devices that convert the energy of a reaction into usable electricity. This thesis will focus on the PEMFC which utilizes hydrogen and oxygen as reactants and a solid

polymer as the electrolyte (Figure 2). The general structure consists of an electrolyte sandwiched between two porous electrodes. Hydrogen fuel is supplied to the anode and oxygen (in air) is supplied to the cathode. The anode and cathode are at a high energy state and combine to reach a lower energy state. Essentially, they are two halves of the electrochemical electrooxidation-reduction reaction

$$H_2 + \tfrac{1}{2}O_2 \Leftrightarrow H_2O \qquad \textbf{(1-1)}$$

Hydrogen is oxidized at the anode, releasing protons and electrons

$$H_2 \rightarrow 2H^+ + 2e^- \qquad \textbf{(1-2)}$$

The solid polymer electrolyte permits proton, but not electron or reactant gas, migration to the cathode. Without the polymer electrolyte, electrons would travel directly to the cathode and all the energy created by the reaction would manifest itself as heat. Instead, the electrodes are connected with a circuit that includes an electrical load, so electrons travel the circuit doing useful work on their way to the cathode. The protons and electrons are necessary to complete the reduction reaction at the cathode

$$\tfrac{1}{2}O_2 + 2H^+ + 2e^- \rightarrow H_2O \qquad \textbf{(1-3)}$$

As the reaction completes, product water is formed at the cathode and subsequently removed for further reaction to occur. A PEMFC must be kept below the boiling point of water in order to ensure that the membrane remain in a hydrated state so that it can conduct protons. At the low operating temperatures of PEMFC (~80^{o}C) the above reactions could not occur without the use of a catalyst. In effect, the gas-porous electrodes are impregnated with platinum metal particles which provide the necessary electrocatalysis.

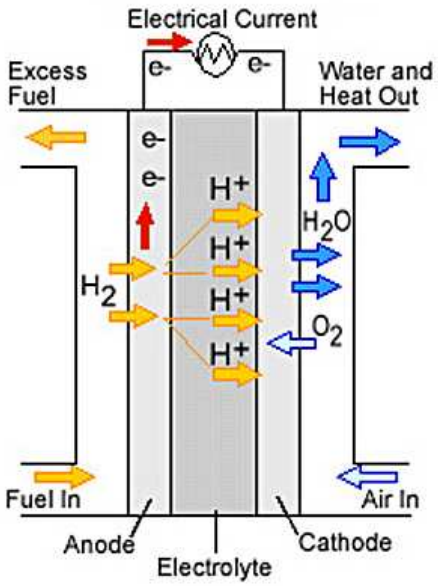

Figure 2: Electrochemical reaction within a PEM Fuel Cell [8]

1.4 Components and Construction of a PEMFC

1.4.1 Fuel Cell Stack

One cell produces a small voltage, usually 0.7 volts, when providing useful current [9]. To produce a useful voltage many cells are connected in series to form a fuel cell stack (Figure 3), generating a voltage of 0.7 multiplied by the number of cells in the stack. Connecting cells in series to produce a stack is accomplished by connecting the anode of one cell to the cathode of its neighboring cell via a bipolar or flow field plate. A PEMFC is composed of many components with each serving an important role. Below is a description of these components.

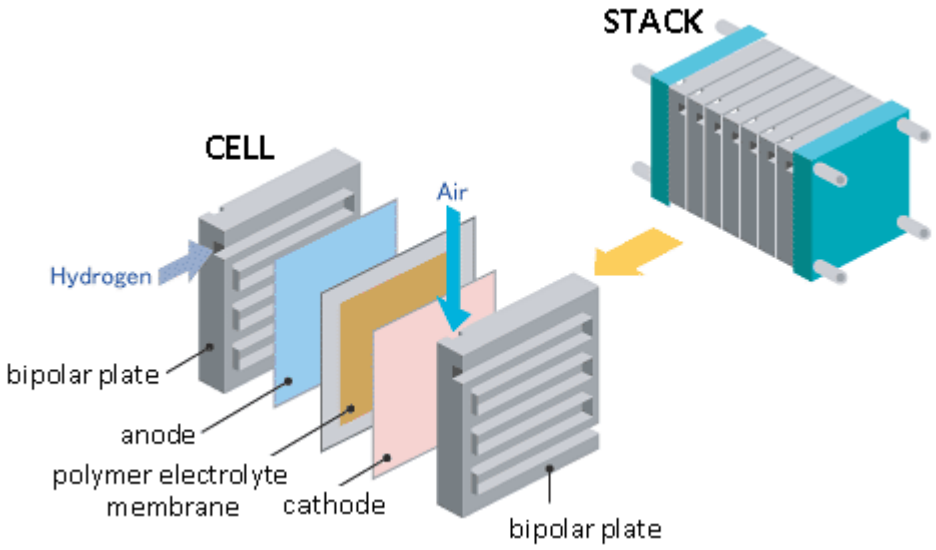

Figure 3: Demonstration of the components of a PEM fuel and a stack [10]

Endplates

The endplates provide structural stability to the entire fuel cell stack and also provide a surface with which the stack can be compressed using bolts. They require sufficient mechanical strength to withstand the tightening pressure, must be light weight not to impact overall system or device weight, and have stable chemical and electrochemical properties. Historically, the most common materials used for endplates were metals such as aluminum, titanium or stainless steel alloys. Plastics, partial non metals and composites are now being considered due to the corrosion susceptibility of metal plates.

Bipolar Plates

Bipolar plates connect individual cells in series. Plates contain internal flow fields which distribute gases to the electrodes and carry off excess gas and water. In addition to providing electrical conduction pathways, they keep oxidant and fuel gases separate from one another. The plate material conducts electrons from the surface of the electrode to current collectors, while providing mechanical structure. They have high electronic conductivity, excellent gas

impermeability, and chemical stability under both oxidizing and reducing conditions. Fuel cells often use lightweight metals, graphite and carbon/thermo-set composites as bipolar plate material.

Gas diffusion layer

On either side of the membrane is a thin gas diffusion layer (GDL) which serves three main functions. It distributes reactant gases over the catalyst layer, conducts electrons to the bipolar plate and facilitates water transport away from the electrodes [11]. It is made of a highly porous carbon paper treated with hydrophobic polymer like polytetrafluoroethylene (PTFE) and has a large impact on cell performance. These materials provide the effective diffusivity and permeability that allows mass transport and flow of hydrogen, oxygen and water vapour through the cell to the catalyst layers. As such the GDL provide mechanical stability to the membrane, electron conduction, reactant distribution, and product water removal.

Catalyst

Electrocatalysts facilitate the oxidation of hydrogen at the anode and reduction of oxygen at the cathode. The highest performing catalyst for these reactions is platinum. A catalyst layer structure is formed with the Pt catalyst on carbon support bonded to the electrolyte membrane in a porous structure, forming the membrane electrode assemblies (MEA). The MEA is responsible for the reaction catalysis, reactant transport (i.e. hydrogen and oxygen) to the reaction site, electron and proton transport, and transport of product water away from the reaction site. [12].

Electrolyte

The electrolyte in a fuel cell has three main requirements; it must (i) conduct specific ions from the anode side to the cathode side; (ii) serve as a barrier between the anode and cathode reactant gases; and (iii) serve as an electronic insulator [13]. The electrolyte used in PEMFC are sulfonated polymers such as Nafion® made by DuPont. These solid electrolyte systems prevent the need to contain corrosive liquids and are thus preferred. They comprise of perfluorinated

back-bones, which provide chemical stability, and of sulfonated side-groups which allow for the high mobility of protons through the membrane and the immobility of other ions, as well as aggregate and facilitate hydration.

1.4.2 Fuel Cell Performance

In this thesis, performance means the voltage of a fuel cell or the average cell voltage of a fuel cell stack and does not take efficiency into account. The words performance and voltage are used interchangeably.

The purpose of this section is to discuss the performance of a fuel cell and describe the various operating parameters which impact its performance. First, the ideal performance will be defined using thermodynamic and electrochemical principals. Then, the polarization curve which characterizes a fuel cell's actual performance will be introduced and used to illustrate the effect of operating parameters on fuel cell performance.

Gibbs Free Energy and Nernst Potential

The amount of energy released during the fuel cell reaction is called the enthalpy of reaction (ΔH). For a PEM fuel cell which operates at standard temperature and pressure and produces liquid product water, the enthalpy of reaction is:

$$\Delta H = -285 J \cdot mole^{-1}_{H_2O(l)}$$

The negative sign represents energy being released during the reaction. All of the enthalpy of reaction is not available to do useful work; some is lost as entropy ($T\Delta S$) and the remainder is known as Gibbs free energy (ΔG). For a cell operating reversibly, $T\Delta S$ is the amount of heat produced and ΔG is the maximum amount of electrical energy available (free) to do useful work. At standard operating conditions

$$\Delta G = -237 J \cdot mole^{-1}_{H_2O(l)}$$

so the maximum operating thermodynamic efficiency of a PEMFC 83% (at standard operating conditions).

The voltage difference across the electrodes (ΔE), or reversible cell potential is related to ΔG by

$$\Delta E = -\frac{\Delta G}{2F} \qquad \textbf{(1-4)}$$

where 2 is the number of electrons involved in the reaction and F is Faraday's constant (96,486 coulombs/mole-electron).

For a fuel cell reaction operating at different temperature and pressure, the change in Gibbs free energy can be expressed by the equation

$$\Delta G = \Delta G^o + RT \ln\left(\frac{P_{H_2O}}{P_{H_2} P_{O_2}^{1/2}}\right) \qquad \textbf{(1-5)}$$

where the standard Gibbs energy (ΔG^o) at the reference state is a function of temperature only, R is the ideal gas constant, T is the temperature in Kelvin, and P_{H_20} , P_{O_2} , and P_{H_2} are the partial pressures of water, oxygen and hydrogen, respectively. By substituting Equation (1-4) into Equation (1-5), the reversible voltage of a cell is determined by the Nernst equation

$$\Delta E = \Delta E^o - \frac{RT}{2F} \ln\left(\frac{P_{H_2O}}{P_{H_2} P_{O_2}^{1/2}}\right) \qquad \textbf{(1-6)}$$

Ideal (Reversible) Performance

The ideal performance for a fuel cell is the maximum cell potential for a reversible reaction. The maximum potential always exists when there is no load (open circuit) and the reactants are at their highest energy state. For a reversible fuel cell reaction at 25^{o}C and 1 atm Equation (1-4) is used to calculate an ideal performance of 1.23 V. For different operating conditions, the ideal

performance can be calculated using Equation (1-6). A cell typically operates using gas mixtures at higher temperatures and pressures so the theoretical voltage reduces to 1.16 V [1]. In a working fuel cell the open circuit voltage (OCV) is below this value mostly due to crossover of the reactants.

The efficiency of a fuel cell is often characterized by the efficiency of the electrochemical reaction. It is therefore defined as the ratio of the actual voltage produced with respect to the ideal voltage

$$\eta = \frac{V_{actual}}{\Delta E} = \frac{V_{actual}}{1.2} \qquad \textbf{(1-7)}$$

In reality, actual operation voltages are roughly 0.7 V which results in electrochemical efficiencies of approximately 58%.

Actual Performance

Fuel cell performance is most commonly characterized by a polarization curve (Figure 4). Theoretically, a fuel cell performs at 1.2 V at all operating currents; practically this is not the case. Voltage decreases as more current is drawn from the cell and this voltage loss is referred to as polarization. Voltage versus current is plotted and a point on the curve represents the actual steady-state voltage delivered for a given size of electrical load placed across the cell. The electric power is the product of voltage and current for a point on the curve. Also, the polarization curve shows the electrochemical efficiency at any operating current since the efficiency is the proportion of actual voltage with respect to the ideal voltage.

Polarization is the result of chemical and physical factors that adversely affect the electrochemical reaction. The shape of the curve can be divided into three sections; activation polarization, ohmic polarization, and concentration polarization. The maximum voltage which exists at open circuit (when there is no load) doesn't reach the ideal voltage because of hydrogen

crossing over to the cathode resulting in a mixed potential. At low current, activation polarization is caused by slow reaction rates due to the energy barrier that reactants must overcome. This effect is greatest at the cathode.

As current increases the curve exhibits linear behavior that is governed by ohmic polarization which is the combination of, (1) resistance to ion flow through the electrolyte, (2) resistance to ion and electron flow within the electrodes, and (3) resistance to electron flow within the electrical terminals.

Concentration polarization or mass transfer polarization dominates at large current densities because reactants are consumed faster than they are supplied and products are produced faster than they are removed.

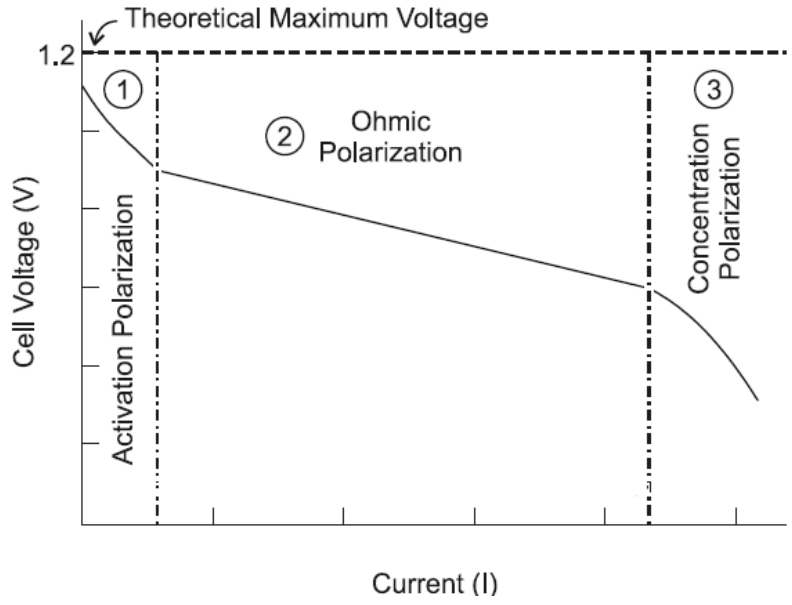

Figure 4: Typical polarization curve for a fuel cell.

1.4.3 Effect of Fuel Cell Operating Parameters

This section will discuss the impact of operating conditions on fuel cell performance. An understanding of how parameters such as pressure, temperature, and humidity affect PEMFC performance is essential to the design and optimization of fuel cells.

Temperature

In general, higher operating temperatures result in better performance. PEM fuel cell performance correlates with temperature in terms of faster reaction kinetics, increased diffusion mass transport and increased ionic conductivity of Nafion® membranes at higher temperatures. However, the electrolyte relies on liquid water to facilitate proton conduction, so this limits the temperature below the water boiling point. Furthermore, at high enough temperatures whereby water evaporation rate is faster, the membrane can dehydrate resulting in lower proton conductivity and thus lower fuel cell performance.

Pressure

Fuel cell performance typically increases with increasing gases inlet pressure. The Nernst equation clearly demonstrates that an increase in the partial pressure of hydrogen and oxygen will increase the cell potential. Increasing pressure also increases the partial pressures of hydrogen and oxygen gas thus allowing them to reach the reaction site more readily. However, due to pressure drop limitations of the flow field plates and that additional air compression requires more gross power, PEM fuel cells are usually operated at no more than a few atmospheres. The differential pressure between the oxidant and fuel is kept to a minimum because large pressures gradients across the membrane will cause the reactant at a higher pressure to permeate through the membrane to the opposite electrode where they will chemically combust without the production of useful energy and even cause membrane failure.

Water Balance

Sufficient hydration of the membrane is an essential determinant of PEMFC performance because without it the membrane can dry out thus increasing ohmic polarization or even membrane failure. To achieve optimal performance it is very important to have a sufficient water balance not to only ensure that the membrane is properly hydrated for sufficient proton conductivity, but to avoid flooding in the cathode channels and dehydration at the anode. The degree of hydration in the membrane is determined by reactant stream hydration and water production and transport phenomena through the membrane. Water management will be described in greater detail later.

Reactant Stoichiometry

The reactant stoichiometric ratio is a measure of the excess in which reactant is fed to the cell. It is defined as the ratio of the amount of reactant input to the electrode (F_{in}) to the amount of reactant that is consumed in the electrochemical reaction (Q) to produce a certain current density. The volumetric flow rate of the former is determined by Faraday's Law

$$Q = \frac{I \cdot nV_{STP}}{Fn_e} n_c \qquad \textbf{(1-8)}$$

where Q is the volumetric flow rate through the stack, I is the total current flowing through the stack, n_e is the moles of electrons transferred based on the electrode reaction, n is the moles of reactant consumed, n_c is the number of cells in the stack, and V_{STP} is the volume an ideal gas occupies at STP. Using this flow rate and knowledge of F_{in}, the stoichiometric ratio can be calculated:

$$\lambda = \frac{F_{in}}{Q} \qquad \textbf{(1-9)}$$

If λ =1, the exact amount needed for the electrochemical reaction, at a given current, is fed to the cell. If λ >1, excess reactant is provided, and if λ <1, the reaction is limited by insufficient reactant. Increased λ will increase the performance for various reasons [14; 15]: (i) enhancement of mass transfer by a high gas velocity of reactants; (ii) high velocity gas facilitates the removal of water that might otherwise block the flow channels; and (iii) avoidance of operational problems such as stagnant water vapor, catalyst degradation and accumulation of impurities. However, the amount of excess hydrogen must be kept to a minimum because unconsumed hydrogen lowers the overall efficiency of the fuel cell. At higher current densities, fuel cell power systems typically operate at λ = 1.4 for the fuel and λ = 2.0 for the air, but higher λ are employed at lower current densities to avoid flooding at low gas velocities [16].

1.5 Fuel Cell System

Fuel cell stacks alone do not operate as engines. They require various subsystems, each containing different components and functionalities, in order to serve as power supplying devices. The basic features of a fuel cell system are illustrated in Figure 5. As this figure indicates, a fuel cell system is composed of six basic subsystems: the fuel cell stack discussed in the preceding section, the fuel processor, air system, water management, thermal management, and power conditioning subsystems. The design of each subsystem must be integrated with the characteristics of the fuel cell stack to provide an optimal system. It should be noted that not all power systems contain all of these basic subsystems.

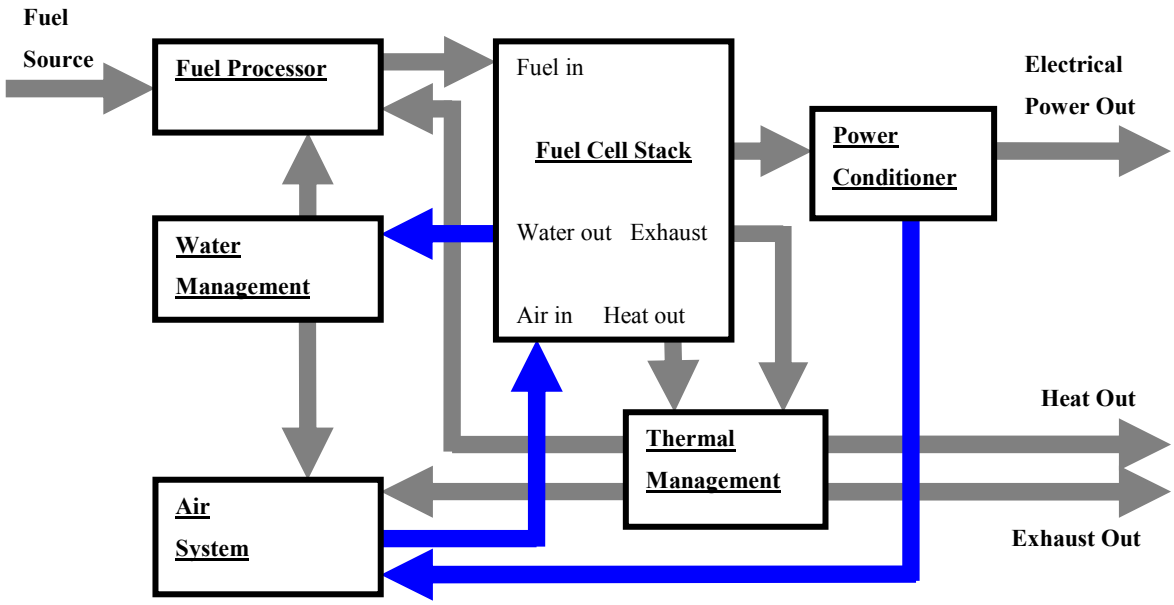

Figure 5: Fuel cell system schematic

1.5.1 Air System

Air is drawn from the outside environment and into the cathode. The incoming air first passes through a particulate and chemical filter before it passes through any other components. The particulate filter traps small particles that can obstruct the air delivery system. The chemical filter provides limited protection against air pollutants (SO_x, NO_x, CO, CO_2) that are formed from vehicles and industrial processes that combust fossil fuels [17]. These chemicals will adversely affect performance, and can cause permanent damage to the MEA. Contaminants such as SO_x, NO_x and CO poison the platinum catalyst, while CO_2 on a platinum catalyst can catalytically convert into CO [18]. An air blower is sufficient for small to medium sized PEMFC applications but air compressors are often used for larger fuel cells requiring higher pressures [7]. Automotive systems generally operate at higher pressures of two to three atmospheres to

increase power density. In some applications, turbochargers that harness energy from exhaust air are used to further increase the air pressure [16]. The air handling system also includes a hydration system to increase the relative humidity of the air stream. Air handling systems often include some type of heat exchanger to improve the efficiency of the hydration system or increase the reactant temperature prior to entering the stack.

1.5.2 Water Management

In a PEMFC system, water is required for the fuel reforming process (if one exists) and to humidify the air (and sometimes the fuel). Polymer electrolyte membranes perform effectively and exhibit high lifetimes only when well hydrated [19]. The humidification system effectively humidifies and raises the temperature of the inlet air stream so that the air can provide water to hydrate the membrane. Water is available from the fuel cell reaction, but it must be removed from the exhaust gas, stored, and pumped to a pressure suitable for the various operations. Due to its importance in this work, water management in the PEMFC stack will be described in greater detail later.

Fuel cells may be humidified by internal and external methods. Internal humidification refers to the addition of water directly into the fuel cell, or a method of keeping the water produced by the fuel within the fuel cell [20]. External humidification involves the use of a humidification unit to provide the fuel cell with humidified gas. External humidification often brings added complexity to the fuel cell system.

A bubbler is a common external humidification system used in stationary systems. In a bubble type humidifier, the reactant stream is passed through a sparger into a heated column of water, in which the air bubbles in contact with water are humidified. Emprise produces the Humidicore Enthalpy Wheel humidifier, which is based around a ceramic honeycomb material named Cordierite. Cordierite absorbs water from the fuel cell exhaust stream, the Cordierite core is

constantly rotating bringing the moist material into contact with the dry inlet reactant stream [21]. Humidification can be achieved in a device consisting of hollow fibre membranes, in a shell and tube type configuration where the tubes are poly-propylene or poly-ethylene [22].

1.5.3 Thermal Management

During fuel cell operation, the electrochemical reaction produces heat at a rate that is roughly equivalent to the electrical power that it produces. A stack cooling system is responsible for maintaining a certain optimum reaction temperature in the stack. This temperature is maintained by coolant flowing through channels in the flow plate and either radiating or absorbing heat. The system consists of a deionized (DI) water polisher, particulate filter, heat exchanger, pump and flowmeter. The thermal energy produced can also be used for a variety of purposes within the fuel cell system, transferred externally to meet the thermal needs of a particular application, or rejected to the surroundings.

1.5.4 Power Management

The power management system regulates, conditions and distributes the unregulated direct current (DC) electrical power produced by the stack to a current and voltage that is suitable for a particular application and supplies power to the other auxiliary systems. A switching power converter is used to match the voltage produced by the fuel cell to the needs of the application and to protect the fuel cell from overcurrent or undervoltage conditions. If the application requires alternating current (AC), the electricity is processed through an inverter, which constructs single or three-phase waveforms as required by the application.

1.5.5 Fuel Processor

Since most fuel cells use hydrogen as a fuel and most primary energy sources are hydrocarbons, a fuel processor is required to convert the source fuel to a hydrogen rich fuel stream. The complexity of the fuel processor depends on the type of fuel cell system and the composition of the source fuel. For PEMFC, the fuel processor is relatively complex and usually includes a desulfurizer, a steam reformer or partial oxidation reactor, shift converters, and a gas clean-up system to remove carbon monoxide from the anode gas stream. The development of a compact economical reformer to supply hydrogen rich fuel for low temperature fuel cells in building and automotive applications is a tough challenge. As such most PEMFC applications will use pure hydrogen and the fuel will be produced in centralized stationary location (so onboard fuel processors are rare). At this time most hydrogen is produced in steam methane reformers (SMR) and purified using pressure swing absorption. This pure hydrogen is then liquefied and disturbed in to distribution centers were the consumer generally gets a high pressure gas cylinder, or hydrogen is loaded onboard to a hydrogen gas cylinder.

1.5.6 Anode Recirculation and Purge System

One reason the chemical to electrical energy conversion is less efficient for fuel cells (in flow-through operation) than for batteries is because batteries are closed systems. In batteries, the chemical reaction only proceeds when an external load is connected and there is no loss of chemical energy from unconsumed fuel exiting the battery. Flow-through fuel cells are open systems in which the reactants are fed continuously, and in excess, and unconsumed reactants exit the cell. Exhausting unreacted hydrogen consequently lowers the fuel efficiency.

To achieve reasonable fuel efficiency, fuel cells can operate in dead end anode operation or anode recirculation operation. Dead end anode operation is a method proposed to improve fuel

efficiency since no unconsumed hydrogen exits the cell. It involves the closure of the anode outlet while a constant pressure is maintained at the anode so hydrogen is only supplied at the rate it is consumed (λ =1). Dead end operation is not suitable for practical applications because such an arrangement leads to the accumulation of impurities, such as nitrogen that has crossed over from the cathode and impurities in hydrogen fuel. Dead end operation also makes water management difficult.

In most practical applications, fuel cell power systems operate with the anode outlet gas recycled, or recirculated, back to the anode inlet where it mixes with the fresh hydrogen fuel stream before entering the anode. Such an arrangement permits 'dry' fuel supply since water that evaporates from the membrane and into the anode gas is recycled thus humidifying the inlet gas [23]. Dry hydrogen operation for PEM fuel cells can have considerable benefits because it means that the humidification system on the anode can be eliminated, saving both space and cost in the design of the balance of plant of a fuel cell system.

Recirculation does have its consequences; it enriches any impurities in the anode gas. The buildup of impurities is controlled by continuously purging a portion of the anode outlet gas to the exhaust. Purging must be kept to a minimum because any unconsumed hydrogen will be lost irrecoverably thus lowing the overall fuel efficiency.

1.6 Water Management in PEMFCs

It is imperative that water be provided to the fuel cell in due proportion in order to eliminate power losses [24]. There are many methods by which the water may be provided to the fuel cell, but normally reactants are kept at a high relative humidity. Of specific interest to this work is that the anode stream is kept humidified with the use of the recycle stream, and the recirculation and purge rates will impact the water content of this stream.

As stated above, PEMFCs use sulphonated fluoropolymer (PFSA) as the electrolyte. It is produced by first perfluorinating a polyethylene chain; in this process hydrogen atoms on the polyethylene chain are substituted with fluorine atoms. This produces polytetrafluoroethylene (PTFE) better known as Teflon. In the next step fluorinated monomers ending in sulphonic acid (HSO_3) groups are added to the PTFE chain [25]. This sulphonation step creates a perfluorosulphonic acid PTFE copolymer, an example of this structure can be seen in Figure 6.

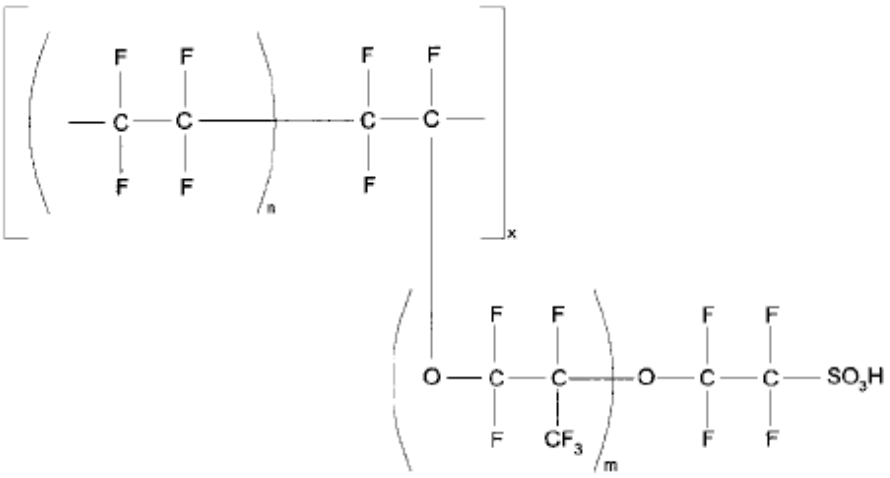

Figure 6: Example of the structure of perfluorosulphonic acid PTFE copolymer (i.e. Nafion^{TM} in this case).

There are two important parts of this polymer that can be seen in Figure 6, (i) the perfluoronated backbone and (ii) the ionically bonded sulphonic acid functional group. The perfluoronated backbone is by nature highly hydrophobic, while the sulphonic acid group is highly hydrophilic. In the presence of water this leads to hydrophilic/hydrophobic nano-separation in the membrane polymer matrix. The sulphonic acid groups form clusters supported by the hydrophobic domain [25]. This can be seen in Figure 7.

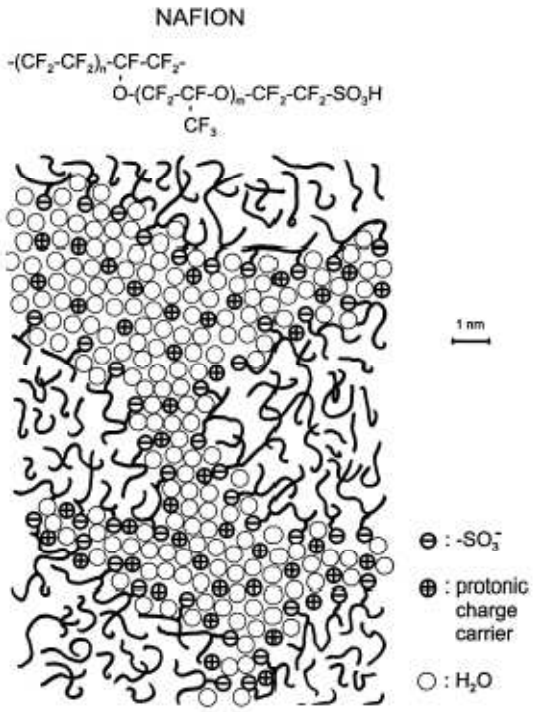

Figure 7: Microstructure of PFSA in the presence of water [26]

The environment created by clustering of the hydrophilic sulphonic groups creates an amorphous acidic environment in which protons will travel from the anode to the cathode during fuel cell operation in the form of hydronium ions (H_3O^+) [20]. The presence of water is important for the proper functioning of PFSA, and on a larger scale the fuel cell system, since protons are carried through the membrane attached to water [26]. An increase in ionic conductivity will lower the Ohmic resistance, which will lead to an increase in the fuel cell voltage at a given current, and thus an increase in overall fuel cell power output. Continuous drying and wetting of the PFSA membrane leads to mechanical stresses in the membrane which may lead to failure.

Water content in the Nafion membrane is essentially affected by four phenomenon; electro-osmotic drag, water production, back diffusion, and reactant stream humidification.

Electro-osmotic drag refers to the water molecules that are brought from the anode to the cathode by the motion of protons in the electrolyte due to the potential gradient [21]. An electro-osmotic drag coefficient is defined which describes the number of water molecules that are transported to the cathode per proton. For Nafion 117 membrane in contact with water vapour this value has been shown to be between 1 and 1.4 which corresponds to a H_2O/SO_3^- ratio of 11 [20]. For membranes saturated in liquid water this value has been reported as approximately 2.5 corresponding to a H_2O/SO_3^- ratio of 22 [27]. Water production occurs via Reaction (1-3) and the water production rate is according to the equation below [7]

$$N_{W,prod} = \frac{I}{2F} \qquad \textbf{(1-10)}$$

Due to the excess water that is collected at the cathode because of electro-osmotic drag and water production, a chemical potential or concentration gradient is created from cathode to anode. This leads to back diffusion of water through the membrane to the anode, following Fick's Law [28]. Still it is essential that the reactant gases are humidified in order to prevent the rapid drying of the membrane, which would lead to fuel cell performance degradation. The vapour pressure (P_w) in the stream is related to the relative humidity by the following equation:

$$RH = \frac{P_w}{P_{sat}} \qquad \textbf{(1-11)}$$

The partial pressure of air (P_a) is unknown, but the overall pressure (atmospheric) and the vapour pressure (P_w) are known. So,

$$P_a = P - P_w \qquad \textbf{(1-12)}$$

and,

$$\omega = \frac{m_w}{m_a} = \frac{P_w \cdot MW_w}{P_a \cdot MW_a} = \frac{P_w}{P - P_w} \cdot \frac{MW_w}{MW_a} \qquad \textbf{(1-13)}$$

This equation defines the amount of water that must be added to a given stream at a given vapour pressure, P_w. If the fuel cell temperature is greater than the temperature of the reactant stream then the relative humidity of the stream will decrease as it enters the fuel cell and the reactant stream is heated. This will cause evaporation of water from the fuel cell, proportionally to the relative humidity. Once the stream is fully saturated at the fuel cell temperature, no further evaporation will occur.

The required oxygen molar flow (N_{O2}) for the fuel cell reaction can be determined from the desired amperage to be drawn from the fuel cell:

$$N_{O2} = \frac{In}{4F} \qquad \textbf{(1-14)}$$

Where n is the number of cells in the stack. From this equation a value for molar flow of air (N_{Air}) to the fuel cell can be determined.

$$N_{Air} = \lambda \frac{N_{O2}}{0.21} \qquad \textbf{(1-15)}$$

In which λ is the desired stoichometric coefficient, which is the desired excess flow of reactant to provide to the fuel cell. Since the flow of air to the fuel cell is known from the above equation and the ratio of water to air is known from Equation (1-13), the required amount of water to be added to the reactant streams can easily be calculated.

From the above equations and knowledge of the process conditions for the fuel cell, the molar flows of water to and from the anode and cathode of the fuel can be calculated. When all the flows are added together an overall molar water balance on the fuel cell can be determined.

The kinetics of the fuel cell reaction are greatly influenced by the partial pressure of the reactant gases and the temperature of the fuel cell (i.e. higher temperatures accelerate the reaction). So, to maximize efficiency, the fuel cell should be operated at elevated temperatures and at gas flow rates greater than a stoichiometric ratio of 1. The accelerated flow of gases through the fuel cell at elevated temperatures will lead to the evaporation of any excess water collected in the membrane or that produced by the fuel cell reaction. As water is removed from the fuel cell, the membrane begins to dry out. This leads to the dissociation of the SO_3^- - H_2O clusters described previously. This in turn limits the rate at which protons can be transported through the electrolyte, which leads to increased ionic or electrolyte resistance. Increased resistance causes more rapid voltage drop with increased current, which may lead to fuel cell failure or decreased performance [29; 30]. The solution is to humidify the fuel cell reactant gases, so that excessive evaporation of water will not occur. Figure 8 shows the effect of humidifying the reactant gases on the cell voltage.

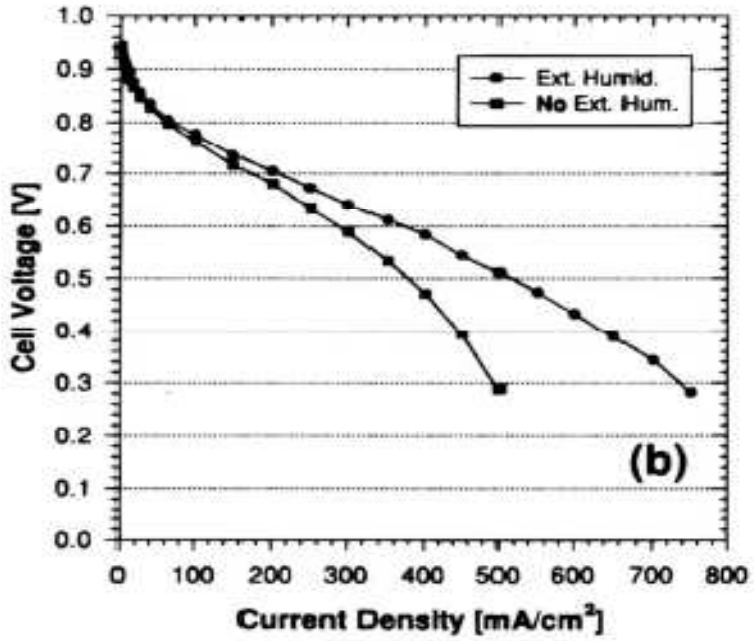

Figure 8: Fuel cell performance under drying conditions [31]

Localized drying in the membrane can lead to areas of high and low resistance in the membrane and thus current gradients throughout the membrane. Areas of low resistance and high current will see increased transport which will lead to accelerated failure at that location [32]. This will also cause temperature gradients across the plane of the membrane which will compound the problem. Localized drying may also cause mechanical stresses in the electrolyte due to the variations in membrane expansion in the presence of water; this may also lead to premature membrane failure.

Excess water accumulation (either in the anode or cathode) in the fuel cell will lead to an increase in water condensation and flooding in the fuel cell. This becomes a problem as water clogs pores in the GDL, and blocks channels in the flow field plates. This excess water will act as a barrier to oxygen mass transport to the cathode catalyst sites [33]. This leads to a decreased effective catalyst active area, and thus an increase in activation losses. This also increases the mass transport voltage losses indicated in Section 1.3.3, leading to further power loss. Figure 9

shows the effect increasing the humidifier temperature beyond the cell temperature and thus causing the condensation of water.

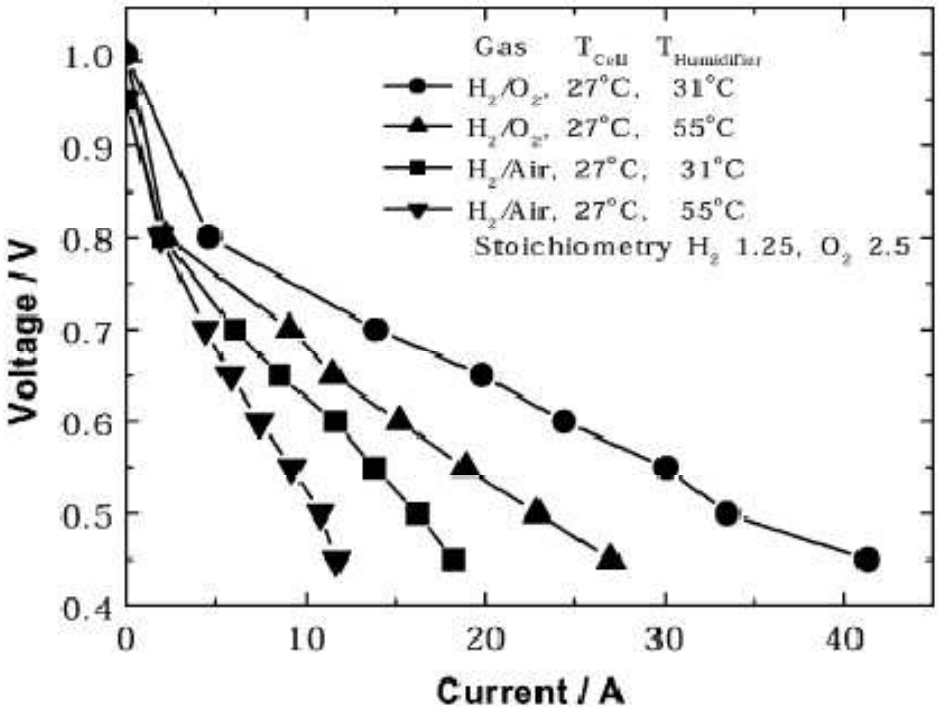

Figure 9: Performance under flooded conditions [34]

1.7 Review of Anode Impurities: Nitrogen and Carbon Monoxide

This section reviews anode impurities, specifically nitrogen and carbon monoxide (CO), and their effect on PEMFC performance. Before the review, the terms used when discussing hydrogen fuel quality are defined, and then the current status of hydrogen fuel quality specifications for PEMFC systems is discussed.

1.7.1 Definitions of Terms [35]

Constituent

A component (or compound) found within a hydrogen fuel mixture.

Impurity

A non-hydrogen constituent in hydrogen fuel.

Contaminant

An impurity that adversely affects the components within the fuel cell system or the hydrogen storage system by reacting with its components. An adverse effect can be reversible or irreversible.

Diluent

An impurity which reduces the concentration of hydrogen, and may be a contaminant or non-reactive in nature.

Non-reactive

Not engaging in chemical reactions such as bonding, deboning, adsorbing and absorbing.

Hydrogen Quality

A description of hydrogen fuel that includes the hydrogen fuel index and the concentration of specific impurities.

Impurity Limit

The concentration threshold level of each specific impurity analyzed in a hydrogen fuel.

Irreversible Effect

The degradation of the fuel cell power system performance that cannot be restored by practical changes of operational conditions and/or fuel composition.

Reliability

The capability of a PEM fuel cell stack to achieve the required performance under a given environment for a period of time. Catastrophic failure and performance losses of the cell can be considered as examples of reliability failure modes.

Durability

The capability of a PEM fuel cell stack to resist permanent change in performance over time. A durability failure may not cause catastrophic failure in the fuel cell. However, this mode of failure will decrease the performance of the fuel cell. It also can involve irreversible failures such as electrochemical surface area reduction, carbon corrosion, etc. and losses mainly related to ageing [18].

Reversible Effect

The degradation of the fuel cell power system performance that can be restored by practical changes of operational conditions and/or fuel composition.

Stability

The capability to recover performance losses during continuous operation. Stability decay is always related to the response of a fuel cell to a given set of operating conditions (such as water management) and reversible material changes [36].

1.7.2 Membrane Contaminants

Membrane contaminants can be undesirable gas-phase, solid-phase or liquid-phase materials that can adversely affect the performance of PEMFC during operation. The presence of these foreign species leads to different modes of fuel cell degradation. Contamination mainly affects the ionomer conductivity of the membrane and the catalytic activity of both anode and cathode electrodes. The effects of contaminants originating from the air stream, fuel stream and fuel cell components on PEM fuel cell performance, life and durability can be significant and have been identified as critical research topics for further study. Common contamination sources and the affected fuel cell properties are listed in

Table 1.

Table 1: MEA contamination sources

Sources	Contaminant	Affected Property
Leaching of bi-polar plate and endplates	Fe^{3+} and Cu^{2+}	membrane conductivity
Fuel	CO, CO_2, NH_3, H_2S	catalyst surface area and proton conductivity
Air mixed with emissions from other automotive exhaust	NO_x, SO_x, CO_x, NH_3, O_3	membrane permeability and conductivity, catalyst-membrane interface and flow fields
Compressors	oils	porosity of the GDL, PEM and catalyst layer
Sealing gasket	Si	catalyst and membrane contamination
Coolant, DI water	Na^+, Ca^+, Si, Al, S, K, Cu, Cl, V, Cr	membrane proton conductivity, corrosion of components
Reformate hydrogen	CO_x, H_2S, NH_3, CH_4	MEA poisoning principally the catalyst

Contaminants in fuel gas stream

Hydrogen used in the PEM fuel cell can be produced using fossil fuels via steam reforming, partial oxidation of natural gas, coal gasification and water electrolysis. Most of the hydrogen fuel is produced by natural gas reforming, a situation that is likely to remain the dominant mode of production for a number of years [37]. Unfortunately, this process generates contaminants such as NO_x, SO_x, CO_x, H_2S, NH_3 and CH_4 that can damage fuel cell components, particularly the membrane and electro-catalyst, and degrade cell performance [38]. Consequently, the quality of

the hydrogen is very important. Thus, it is important to study the reactions of these contaminants with the MEA and procedures to mitigate their effects [39]. Although many details of the interactions between impurities in the hydrogen feed stream, water and the fuel cell components are not completely understood, the need to control and manage their effects is well recognized and remains as a critical challenge for the success of fuel cell technology.

Contaminants in air stream

In addition to the fuel source, contamination can come from the environment or from other fuel cell components. The major sources of the contaminants in the air stream fed to fuel cells are determined by the general air quality standards. Thus, these feed streams will contain contaminants from vehicle emissions such as NO_x, SO_x, CO_x and specific chemical species. The impact of SO_x is particularly critical since its presence can cause fuel cell death depending on its concentration or dosage [40]. Contamination sources can also be from fuel cell components such as the seals, piping or fittings.

1.7.3 Current Status of Hydrogen Quality Specifications

There is currently no Canadian or international standard that specifies an acceptable grade of hydrogen fuel for PEMFC vehicles [35]. In 2005 SAE, formerly the Society of Automotive Engineers, presented an information report on the development of a hydrogen quality guideline for fuel cell vehicles [35]. The report provided The Hydrogen Fuel Quality Specification Guideline; a hydrogen fuel quality specification for commercial hydrogen refueling stations. Hydrogen fuel quality was defined as being measured at the interface between the refueling station's dispenser nozzle and the vehicle, and all impurities that may affect the fuel cell and fuel storage system were considered. The guideline entailed a list of constituents and their

concentration limits, one of which being 0.2 ppm carbon monoxide. The list was established based on a survey of the industry, the published literature and reflects current analytical methods.

The concentration limit of 0.2 ppm for carbon monoxide came from a study, conducted by Japan Automobile Research Institute (JARI), which addressed the influence of carbon monoxide in hydrogen fuel on performance. For a range of CO concentrations, they measured the voltage drop under constant current density for 10 hours of operation on a single cell operating in flow-through mode. The concentration that caused a voltage drop of 2% or more was said to be unacceptable for fuel cells. The limit of 0.2 ppm, however, does not consider the fact that the concentration of CO in the anode gas will increase above 0.2 ppm if the anode is operating in a recirculating mode. For anode recirculation, JARI recommended that the allowable concentration limit must be multiplied by a factor of 0.002 in order to achieve less than 2% voltage drop and reduce the loss of hydrogen by purge to less than 0.2%. However, at the current time there is no published detection method available to measure below 0.2 ppm CO, so JARI's recommendation is not yet realizable. So, it is of great importance to study the effect of the anode purge on the performance when 0.2 ppm CO is present in the hydrogen fuel. Such studies will facilitate moving towards the development of a fuel quality standard that entails concentration limits for realistic operational conditions, such as a recirculating anode.

1.7.4 Hydrogen Dilution by Nitrogen

One of the main requirements of the polymer electrolyte membrane is to serve as a reactant gas barrier. Reactant gas permeation through the membrane, called crossover, adversely affects the fuel cell's performance for a few reasons. Hydrogen and oxygen that crossover are consumed without generating useful work, leading to fuel inefficiency. Oxygen permeation causes the formation of radicals in the membrane which cause membrane degradation, reducing the life of the fuel cell [41]. In addition, nitrogen, a diluent, from the air stream can crossover to the anode.

In an anode recirculation system nitrogen can accumulate in the anode channel which will dilute the hydrogen gas, or in other words it will reduce the partial pressure of hydrogen. As predicted by Equation (1-6), this will lower the cell voltage. Dilution will also increase concentration polarization at the anode.

The buildup of nitrogen can be managed by purging a portion of the outlet gas. The amount of gas purged should be minimized because any unconverted hydrogen will be lost in the exhaust and the anode will have to be replenished with fresh hydrogen. Ahluwalia et al. modeled and analyzed the nitrogen concentration in the recirculating anode gas and its impact on the performance of an automotive 90 kWe PEMFC stack [42]. The results indicated that nitrogen (from crossover) accumulation was mainly a function of the purge fraction and the cell voltage drop was 11-18 mV when the nitrogen concentration at the anode was 20-60% at a 0.1% purge but could be reduced to <5 mV by increasing the purge to 2% which limited the concentration to 6-27%. In this particular study the purge fraction was defined as the ratio of the amount of gas purged to the amount of gas exiting the anode. The voltage decrease was the result of a decrease in the hydrogen partial pressure which caused; (i) a decrease in the theoretical cell potential of Equation (1-6), (ii) an increase in the overpotential of the gas phase in the gas diffusion layer, and (iii) an increase in the overpotential of the gas phase in the anode catalyst. An optimum purge fraction of 2% was determined in the analysis. A purge fraction greater than the optimum caused a decrease in stack efficiency due to the excessive loss of hydrogen in the purge gas. A purge fraction less than the optimum caused a decrease in stack efficiency due to a voltage drop caused by the buildup of nitrogen.

Another study looked at optimizing an anode recirculation operation with respect to the highest electrical energy efficiency for a phosphoric acid fuel cell [43]. The study concluded that at an optimum purge rate a significant amount of inert gas in the anode stream results in relatively low efficiency losses. Moreover, decreasing the purge rate below the optimum is more detrimental to

the electrical efficiency than increasing the purge above the optimum and suffering from decreased fuel efficiency.

The two studies just discussed and many others [44-47], have concluded that the effect of nitrogen in the anode gas is not detrimental to the fuel cell performance. Springer et al. developed a theoretical anode model considering the effect of hydrogen dilution by nitrogen combined with CO poisoning at Pt catalyst sites [48]. The model showed that hydrogen dilution by nitrogen alone did not penalize the anode performance, but in the presence of CO and under the same conditions the voltage loss was large.

1.7.5 Carbon Monoxide Poisoning

Due to the difficulty in transporting and storing pure hydrogen and the lack of hydrogen infrastructure, on-site generation of hydrogen by reforming hydrocarbons and alcohols is the realistic future. The hydrogen-rich gas produced from reformation, called reformate, contains impurities such as, nitrogen, carbon dioxide, carbon monoxide, and sulfur compounds. It is highly recognized that CO adsorbs onto platinum, blocking active catalyst sites and inhibiting hydrogen adsorption and electrooxidation [47]. Of all the PEMFC impurities investigated, carbon monoxide contamination is the most extensively studied and documented. The effect of CO contamination on performance can be seen in the figure below:

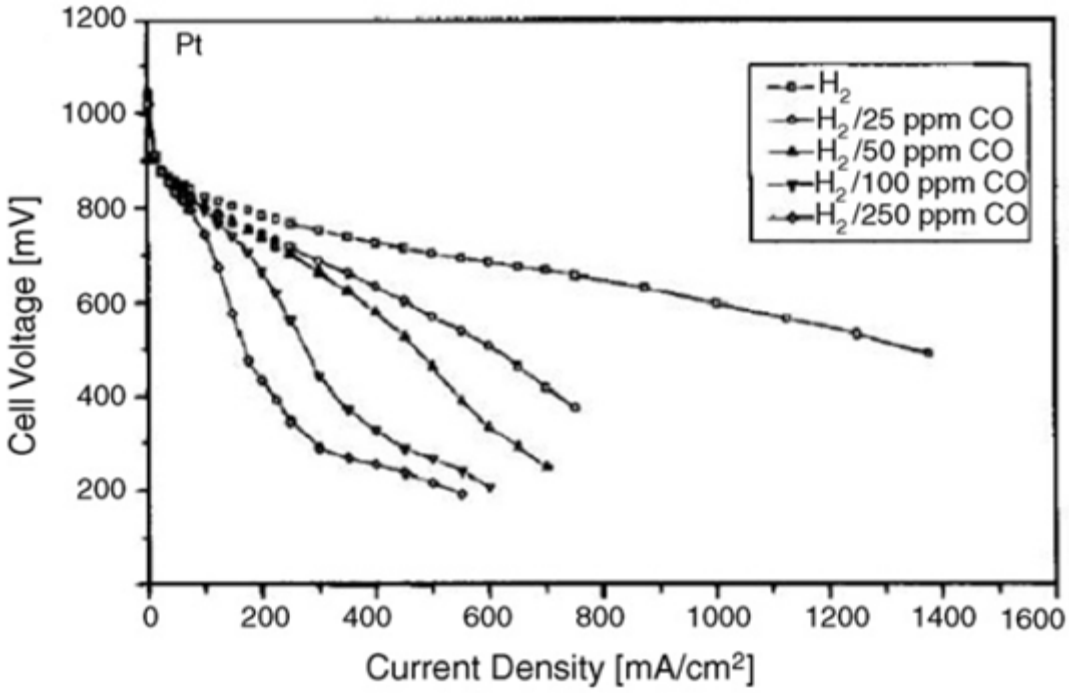

Figure 10: Effect of CO concentration on PEMFC performance for a pure Pt anode catalyst loading.

Currently in the literature, studies on CO concentrations less than 5 ppm are sparse and there is no experimental work that study the effect of CO in hydrogen fuel for an anode operating in a recirculating mode. However, Ahluwalia et al. developed a comprehensive model similar to their nitrogen buildup model described earlier, but which included carbon monoxide in the hydrogen fuel [49]. The model showed that CO can enrich in the recirculating anode gas and that the cell voltage decreased when the purge fraction decreased. One example of their findings was that the hydrogen fuel should contain less than 0.06 ppm CO if less than a 10 mV voltage drop was required at rated power. Also, to achieve the same stack efficiency attained for the case of neat hydrogen fuel, the optimum purge fraction had to be increased by 0.4 % when the fuel contained 1 ppm CO.

Theoretical modeling studies on CO have been imperative to the fundamental understanding of poisoning mechanisms, degradation prediction and advancing mitigation techniques [44; 50; 50-52]. Mitigation techniques for CO poisoning such as air bleeding, increased temperature, and using Pt-alloys have been well documented and will be reviewed, but first the mechanisms involved in CO poisoning will be reviewed.

.

The mechanism for the electrooxidation of hydrogen on Pt is thought to proceed by dissociative chemisorptions (1-16), requiring two adjacent free Pt sites and is therefore rate determining, followed by facile electron transfer
(1-17**)**.

$$H_2 + 2Pt \leftrightarrow 2Pt - H_{ads} \quad \textbf{(1-16)}$$

$$2Pt - H_{ads} \leftrightarrow 2Pt + 2H^+ + 2e^- \quad \textbf{(1-17)}$$

At typical PEM operating temperatures, CO adsorbs strongly on the Pt sites [51], directly blocking the surface active sites which prevents the dissociative electrosorption of H_2. The dissociative chemisorption of CO can occur on bare Pt sites through Reaction* (1-18) *and also at Pt hydride sites via Reaction

(*1-19*).

$$CO + Pt \leftrightarrow Pt - CO_{ads} \quad \textbf{(1-18)}$$

$$2CO + 2Pt - H_{ads} \rightarrow 2Pt - CO_{ads} + H_2 \quad \textbf{(1-19)}$$

The fraction of the catalyst sites that is covered by CO for a PEMFC operating with a recirculating anode and fuel containing 1 ppm can reach 0.80 [49]. At a cell potential of ~ 0.3V,

the elimination of adsorbed CO can occur by the electrooxidation of CO to CO_2 via Reactions (1-20) and (1-21) [53]. Now, some of the former Pt sites are free for hydrogen electrosorption and electrooxidation [54].

$$Pt + H_2O \rightarrow Pt - OH_{ads} + H^+ + e^- \quad \textbf{(1-20)}$$

$$Pt - CO_{ads} + Pt - OH_{ads} \rightarrow 2Pt + CO_2 + H^+ + e^- \quad \textbf{(1-21)}$$

The initiation of CO electrooxidation at 0.3 V is well supported in the literature [55-57]. Water necessary for Reaction (1-20) is provided by the humidified anode gas and/or by the backdiffusion of water from the cathode to the anode. Benesch and Jacksier [58] reported that the time it took for the cell voltage to degrade to a threshold value of 0.3 V was 9 h when the cells were exposed to 10 ppm CO/H_2 for operation in flow through mode.

Reaction (1-20) occurs at an anode potential of 0.5V vs. NHE and Reaction (1-21) occurs at even higher anode potential of approximately 0.6V vs. NHE [18]. At electrode potentials below these Jambunathan et al. obtained the rate constants for hydrogen electrooxidation using scanning electrochemical microscopy on polycrystalline Pt in sulfuric acid solutions. The rate constant was near-zero for the electrode covered with CO while for a CO free electrode the rate constant was greater than 1 cm/s [59]. This demonstrated that Reaction
(1-17**)** can be significantly reduced in the presence of CO, resulting in PEMFC performance degradation.

Qi et al. published their experiments which showed that trace amounts of CO in the fuel can also poison the cathode. They detected CO adsorpion on the cathode catalyst which illustrated that CO had crossed over to the cathode, most likely through pin holes in the membrane. In one study [60], a reference electrode was used to separate the anode and cathode cell performance. The findings revealed that the cathode performance very often decreased with the anode performance when the fuel contained CO. This decrease in cathode potential can be explained

by CO adsorbing onto the cathode Pt catalyst causing a decrease in the available sites for O_2 reduction.

1.7.6 Poisoning Mitigation

Due to the adverse effect that fuel impurities have on PEMFC performance, various contamination mitigation techniques have been developed in efforts to minimize such negative effects. In this section, the literature on the currently most prominent mitigation methods will be briefly reviewed. These methods include, pretreatment of hydrogen-rich reformate, carbon monoxide tolerant electrocatalysts, high temperature operation and oxidant bleeding.

Pre-treatment of Reformate

Since Pt catalysts can be poisoned by even trace amounts of CO, the most obvious poisoning mitigation technique would be to eliminate trace amounts of CO from the reformate gas. Steam reforming of methane is currently the most common method for producing hydrogen [61]. The side products of steam reforming are H_2, CO and CO_2. A water gas shift reactor coverts CO into H_2 and CO_2 and finally a preferential oxidation reactor reduces the CO to less than 10 ppm by further oxidizing CO to CO_2. Other conventional methods include partial oxidation and autothermal reforming. These methods are however not sufficient to bring down CO to tolerable levels without additional purification steps such as Pd membrane technologies.

Carbon Monoxide Tolerant Electrocatalysts

Pure platinum based electrocatalysts are the most common catalyst for hydrogen electrooxidation when pure hydrogen fuel is used. It is well documented that anode electrodes made of platinum alloy catalysts such as Pt-Ru, Pt-Pd, Pt-Mo and Pt-Ru-Mo are much more tolerant to CO

poisoning than pure Pt catalysts [62-64]. Among the alloys mentioned, PtRu has shown to be the most tolerance to CO poisoning [65]. The Ru metal is able to form an oxygenated species (Ru-OH) by Reaction (1-22) at potentials lower than Pt [66]. When adjacent to a Pt-CO site, these Ru-OH species are the oxygen source required for the electrooxidation of CO to CO_2 via Reaction *(1-23)*, thus freeing Pt sites for hydrogen adsorption to take place [67].

$$Ru + H_2O \leftrightarrow Ru - OH + H^+ + e^- \quad \textbf{(1-22)}$$

$$Ru - CO + Ru - OH \leftrightarrow CO_2 + H^+ + e^- + Pt + Ru \quad \textbf{(1-23)}$$

Ralph et al. examined the activity of the electrooxidation of CO to CO_2 on a PtRu half-cell by feeding it pure CO and measuring the outlet gas for CO_2 using mass spectrometry. They found that Reaction *(1-23)* occurred on PtRu at potentials ~0.2V less anodic than required for pure Pt catalysts [53]. Such results reflected the greater capacity of Ru to adsorb water than pure Pt.

High Temperature Operation

It is well documented that high temperature operation reduces carbon monoxide poisoning in PEMFC. In their study, Zamel et al. showed that the carbon monoxide coverage at steady state decreased when the temperature was increased from 50 to 80^{o}C [68], thus freeing catalyst sites for H_2 adsorption. Das et al. showed experimentally that CO coverage on the Pt catalyst sites was higher a lower temperatures [69]. Jiang et al. rational to this phenomenon was that higher temperatures could effectively reduce CO coverage on the catalyst by promoting CO oxidation with an OH adsorbed group [70]. This point was supported by Ehsasi et al. who showed that desorption and adsorption of carbon monoxide increase with an increase in temperature, thus decreasing the overall bond strength of carbon monoxide on the platinum catalyst sites [71]. Results such as these suggest that if PEM fuel cells could operate at higher temperatures then

higher concentrations of CO could be tolerated. In effect, this would permit more of the anode outlet gas to be recirculated (and less purged) which would increase fuel efficiency.

Oxidant Bleeding

Oxidant bleeding is a common technique used for improving PEMFC performance when CO is present in the fuel. Bleeding low levels of air into the anode fuel stream has been shown to reduce CO poisoning in the anode catalyst layer [72]. In one study [72] the author found that the effects of CO poisoning on performance could be eliminated by injecting 4.5% air into a 100 ppm CO in hydrogen fuel. In another study, by injecting 5% air into a fuel stream containing 53 ppm CO in hydrogen, 90% of the CO poisoning was recovered in 60 seconds [73].

The catalytic oxidation of CO occurs by chemisorption of O_2 on a vacant Pt site via Reaction **Error! Reference source not found.**, followed by a surface reaction between Pt-CO and Pt-O to form CO_2 via Reaction **Error! Reference source not found.**

$$O_2 + 2Pt \leftrightarrow O_2 - Pt + Pt \rightarrow 2(O - Pt) \quad \textit{(1-24)}$$

$$CO - Pt + O - Pt \rightarrow CO_2 + 2Pt \quad \textit{(1-25)}$$

However, air bleeding can adversely affect the fuel cell and one issue is that O_2 can recombine with adsorbed H_2 by the following reactions [68] .

$$H_2 + 2Pt \leftrightarrow 2(H - Pt) \quad \textit{(1-26)}$$

$$O_2 + 2Pt \leftrightarrow O_2 - Pt + Pt \rightarrow 2(O - Pt) \quad \textit{(1-27)}$$

$$O - Pt + 2(H - Pt) \rightarrow H_2O + 3Pt \quad \textit{(1-28)}$$

Recombination depletes the hydrogen fuel by only a small extent. The main concern is that this Reaction (1-28) and Reaction **Error! Reference source not found.** are highly exothermic and temperatures above 100^0C have been measured in the MEA of fuel cells operating at 80^0C and an air bleed [53]. The localized increase in temperature can lead to sintering of the catalyst which may lead to pin-holes in the membrane and consequently MEA failure.

Another issue with air bleeding is that chemical degradation of the membrane can occur through the oxygen reduction reaction of hydroxyl ($^{\bullet}$OH) and peroxyl ($^{\bullet}$OOH) radical species [74]. Furthermore, contaminant ions (Fe^{2+} and Cu^{2+}) could induce the radical formation [75]. Studies reveal that the peroxide radical attack on polymer end groups with residual H-containing bonds are chiefly responsible for the severe chemical attack on the membrane at lower humidity, higher temperatures and when using pure hydrogen and oxygen as reactants [76].

Chapter 2 - Experimental

2.1 HyPM® HD8

The overall objective of this work is to determine the effect of anode purge on the performance of a Hydrogenics HyPM HD8 operating with a recirculating anode and being supplied hydrogen fuel contaminated with trace levels of carbon monoxide. HyPM HD8 is the product name for a Hydrogenics 8kW Hydrogen Fuel Cell Power Module (Figure 11). A power module is a portable fuel cell power generating device that uses oxygen in air and hydrogen to produce power based on PEMFC technology. Heat and moisture, the fuel cell by-products, are recovered and recycled to humidify the reactants on both the anode and cathode sides. The HyPM HD8 is used for mobility applications because of its dynamic response from idle to maximum power. In addition to the fuel cell stack, the balance of plant provides reactant and water management, gas conditioning, integrated software controls, and power conditioning. Table 2 displays some of the HyPM HD8 technical specifications and **Error! Reference source not found.** contains a table with the anode and cathode operations conditions for a range of current densities.

Figure 11: Image of a Hydrogenics 8kW Hydrogen Fuel Cell Power Module

Table 2: HyPM HD8 Technical Specifications

Property	*Unit*	*Value*
PHYSICAL		
Overall Dimensions (L x W x H)	mm	853 x 417 x 251
Mass (overall)	kg	60
Volume	L	89
PERFORMANCE		
Net Rated Electrical Power	kW	8
Operating Current Range	A	0 – 170
Operating Voltage Range	V	47– 76
Peak Efficiency	%	52
FUEL SYSTEM REQUIREMENTS		
Gaseous Hydrogen (dry)	%	99.99
CO	ppm	< 0.2
Sulfur (total, ex. H2S, COS)	ppb	< 4
Total Hydrocarbons	ppm	< 2

An actual HyPM HD8 was not used in the experimental work for two reasons. First, manipulation of the purge and measurement of all the desired parameters for analysis would be

quite difficult in the actual power module. Second, given that fuel cells are easily scaled, a smaller stack would show the same effect at a fraction of the capital and operation cost. So instead of the HyPM HD8, an apparatus that mimicked the operation of the HD8 was designed and assembled. The experimental setup (Figure 12) consisted of a fuel cell stack, anode recirculation balance of plant components, and a Hydrogenics Fuel Cell Automated Test Station (FCATS^{TM}).

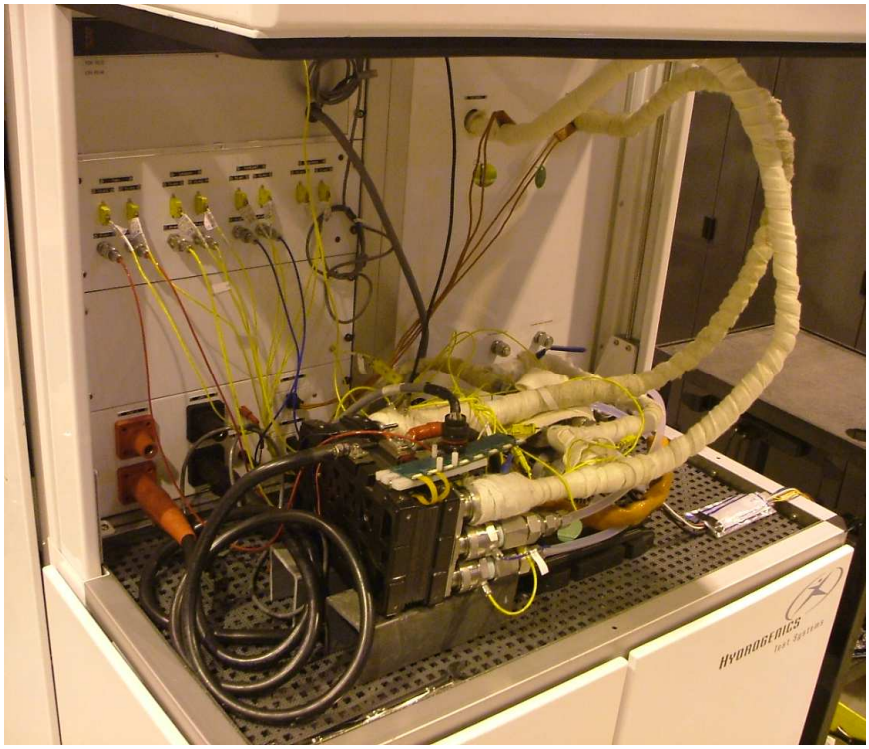

Figure 12: Photo of the experimental setup. The apparatus consists of a fuel cell stack, anode recirculation balance of plant components, and a Hydrogenics Fuel Cell Automated Test Station (FCATS^{TM}).

2.2 Fuel Cell Stack

An HyPM HD8 consists of a fuel cell stack containing 80 cells, each having an active surface area of approximately 196.5 cm^2. Given that that fuel cells can be easily scaled, it was concluded that a Hydrogenics 10 cell stack with a 196.5 cm^2 cell area would suffice for the purpose of the experimental work. The serial number of the stack used was H204-2007-12-002. The flow field plates were graphite plates with a proprietary flow path. The stack was operated in a vertical orientation, with the cathode and anode inlet ports at the top of the stack and the corresponding outlet ports at the bottom. The cells were numbered from 1 to 10, starting at the anode endplate. Each cell had a voltage pin so that the voltage across every cell could be measured. Two load cables were connected to the current collector plates.

The membrane electrode assembly (MEA) is compressed between the anode and cathode gas diffusion layers. The membrane was a reinforced Perfluorinated sulfonic acid (PFSA) membrane made to operate at low (<50%) reactant humidification levels. This is currently the most common type of membrane used in PEM fuel cells. It consists of a Teflon backbone with sulphonic acid groups attached to the ends of branching chains. The membrane is bounded by a layer of platinum catalyst, supported usually by carbon particles. Other membrane specifications are confidential.

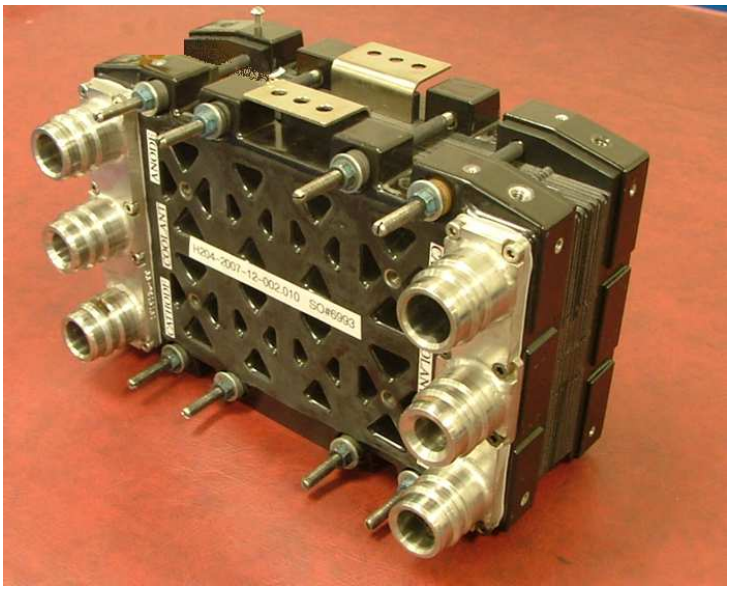

Figure 13: Photo of the 10 cell Hydrogenics stack used in the experimental work. Stack ID number: H204-2007-12-002; active surface area 196.5 cm^2.

2.3 Fuel Cell Automated Test Station

A Hydrogenics Fuel Cell Automated Testing Station (FCATS) has the ability to test, control and monitor the performance and durability of individual cells, stacks, and systems over a range of operating parameters. The latest generation of FCATS, known as G-Series FCATS^{TM}, was used for this work (Figure 14). Features of the G-Series include; online gas flow and mixture composition control, gas humidification and dry gas bypass option, temperature and dew point control accuracy, dead-end gas flow mode, high precision back pressure control, and programmable load control.

Figure 14: Photo of the G-Series FCATS^{TM} fuel cell test station

HyWARE is a software application that runs on the test station computer and forms the main user interface. This software allows accurate monitoring and control of temperatures, pressures, gas flow rates and composition, current, and voltage. Figure 15 shows a screenshot of the HyWARE interface. The area on the left of the HyWARE window is called the side-bar, and is always displayed regardless of what has been selected in the main panel (right). The load, gas flow, pressure, temperature and coolant parameters are controlled and monitored in the side bar. The button bar, located at the top of the window, displays all the buttons needed to access the different functional areas of the software. The main panel displays the page an operator is currently working on. Together, all pages available in the main panel enable an operator to set up and manage the system's parameters, access and control custom features, conduct and monitor tests.

HyAL is the scripting language tool used to program script files that run on the test station computer and make automated operation possible. In this work, scripts were used to condition the stack before a test, to control the test parameters and record the test data, to deal with alarm situations, and to safely shut down the system.

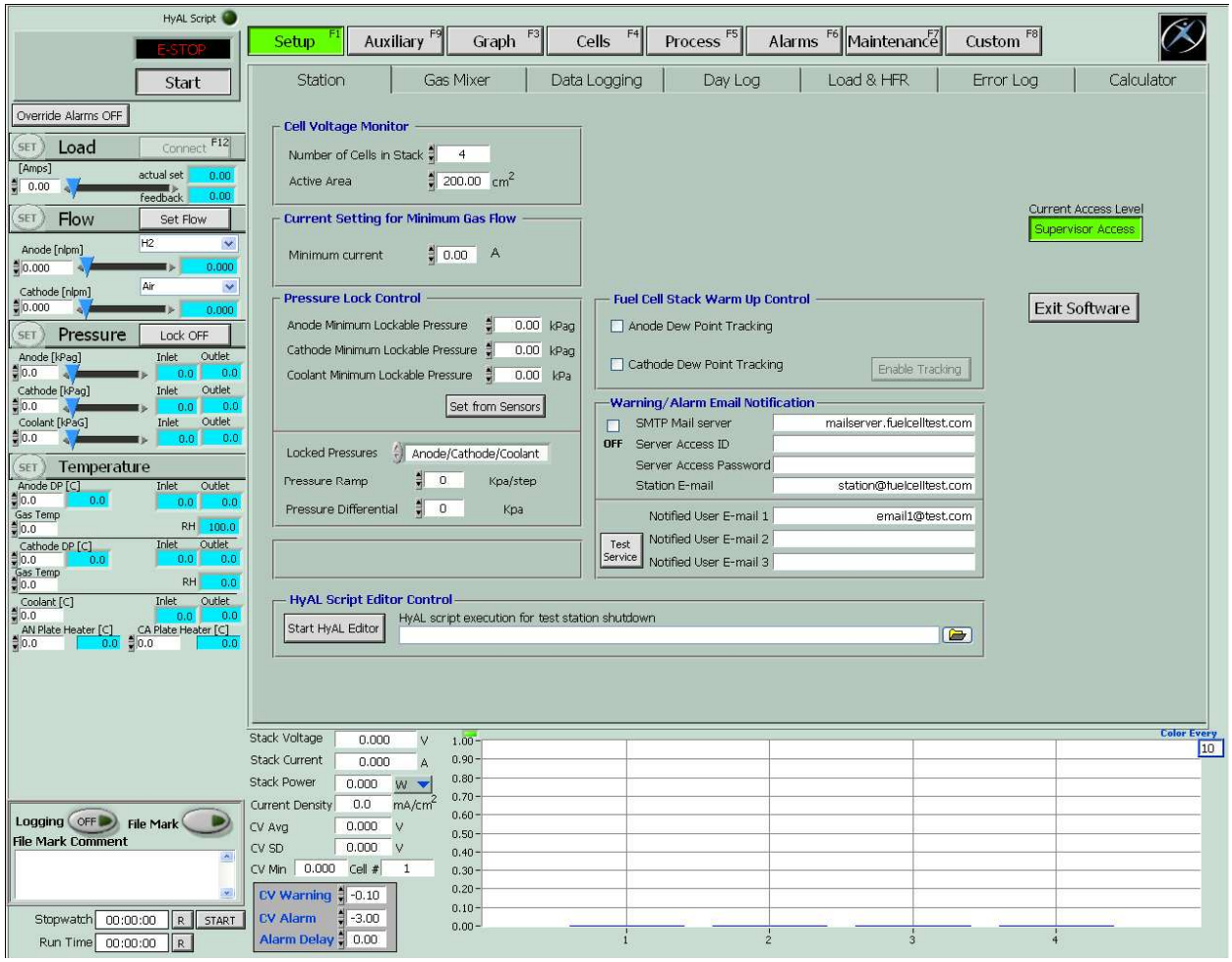

Figure 15: Screenshot of the HyWARE user interface: side panel (left), button bar (top) and main page (center).

2.3.1 Humidification

For humidification, the G-Series FCATS uses a contact humidifier system which bubbles the dry reactant gas through heated water so that the inlet gas stream can absorb moisture and heat. By flowing the gas through a sufficiently long path, the gas dew point approaches the water temperature. This system can quickly heat up the gas stream to the desired temperature when coupled with a PID controller. To prevent condensation of the water vapor after leaving the humidifier, the gas stream travels through heated hosing that maintains the gas stream temperature to at least the same temperature as the saturator. Thus if the cathode is operating at 60°C and a relative humidity of 95% is desired at the cathode, then the cathode air stream is heated to 59°C so that it is fully saturated by water. When this saturated air enters the fuel cell, it will be only 95% humidified relative to the stack temperature. In this experimental work, it is desired to supply the fresh hydrogen stream to the anode completely dry. 'Dry anode' operation is achieved by by-passing the humidification system so that the dry hydrogen is fed directly from utility to the fuel cell stack. Heated hoses are able to heat the dry gas to the desired temperature without any moisture being absorbed by the gas itself.

2.3.2 Stack Temperature

The temperature of the fuel cell stack is maintained at all times by using both active cooling and heating loops to control the flow of de-ionized water through the stack. This gives much faster and more accurate control of stream temperatures. The system continuously polishes the circulated de-ionized water by removing unwanted ions and maintaining the resistivity of the water between one and four mega-ohms.

2.4 Reactant Supply

The reactants are delivered to the stack via the FCATS in the same mode that reactants are delivered to the HyPM HD8. Specifically, air was supplied to the cathode in 'flow-through mode' while hydrogen was supplied in 'dead end mode'. Table 3 gives a summary which compares the different parameters that are characterized by these two reactant delivery modes and Figure 16 shows the basic FCATS flow configuration and components. The following sections will give a complete description of the different flow modes.

Table 3: Comparison of the cathode and anode reactant supply modes

	Cathode	**Anode**
Reactant:	Air	Hydrogen
Gas Supply Mode:	Flow-through	Dead End
Reactant flow rate determined by:	Stoich Set point	Inlet Pressure Set point
Pressure controlled by:	Downstream pressure regulator	Upstream pressure regulator and purge valve
Reactant is supplied:	Humidified	Dry

2.4.1 Air Supply System

Air is supplied to the FCATS from the atmosphere and fed through a carbon filter and into a pressure-swing adsorption system where moisture is removed from the stream. Air is delivered to the cathode in flow-through mode. The name is representative of the air flowing into the inlet and oxygen deficient air flowing out the outlet and to the exhaust. Air passes through a

humidifier and heated hose before entering the cathode. The system controls the overall volumetric flow to the cathode based on the cathode stoichiometric ratio. Once the stoichiometric ratio and current density is set, HyWARE calculates and creates set points for the respective mass flow controllers (Figure 16) and will activate the related isolation solenoid valves automatically.

The pressure at the cathode is controlled by a downstream pressure regulator (Figure 16) which closes to reduce the amount of gas leaving the stack thus increasing the gas pressure at the cathode.

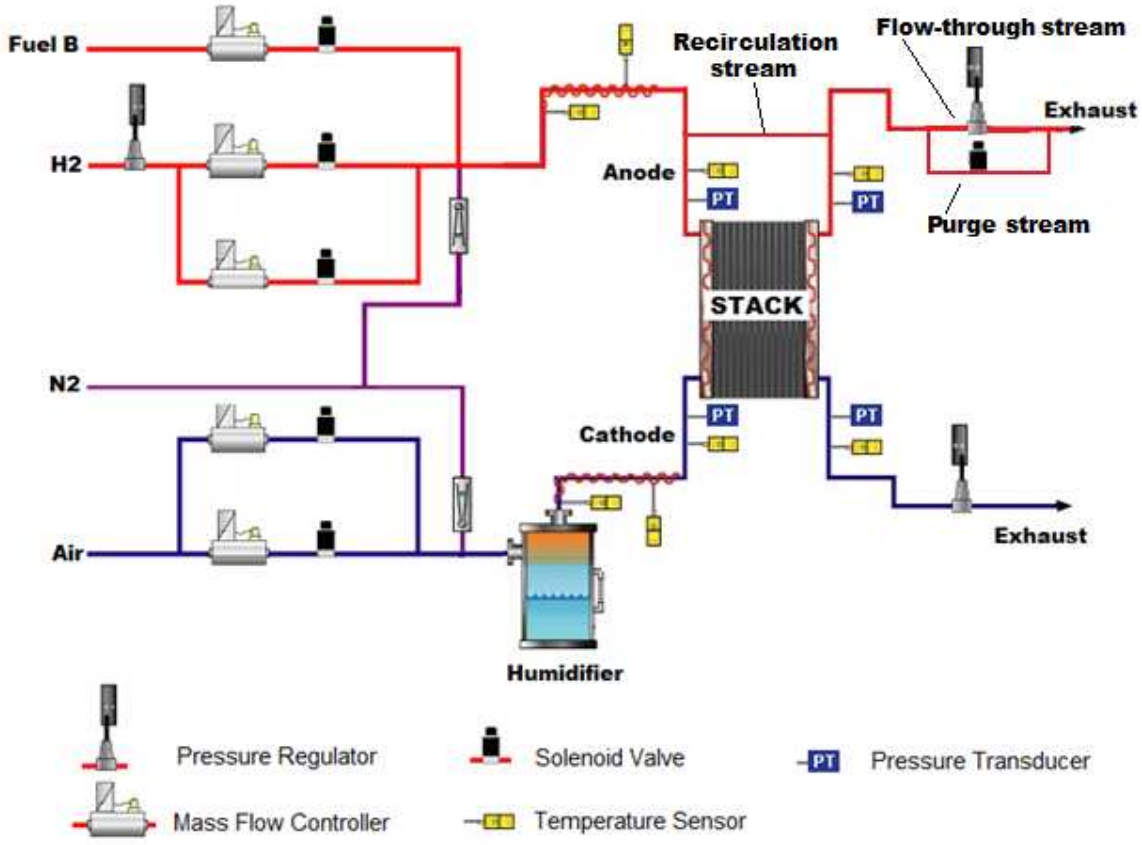

Figure 16: Diagram of basic FCATS flow configuration

2.4.2 Hydrogen Supply

Hydrogen (purity 99.999%) is supplied to the FCATS from a large hydrogen vessel distributed by Air Liquide. This hydrogen comes from an SMR facility in a liquefied hydrogen transport. In the test station hydrogen bypasses the humidification system and is delivered to the anode via 'dead end mode'. The Custom button in HyWARE (Figure 17) contains options that simulate the operation of a fuel cell power system. The *Dead end option* (top) controls the purge valve, the *Humidifier dry gas bypass option* (right) dictates if the reactant is to bypass the humidifier, and the *Dew point meter option* (bottom) displays dew point sensor measurements in the system.

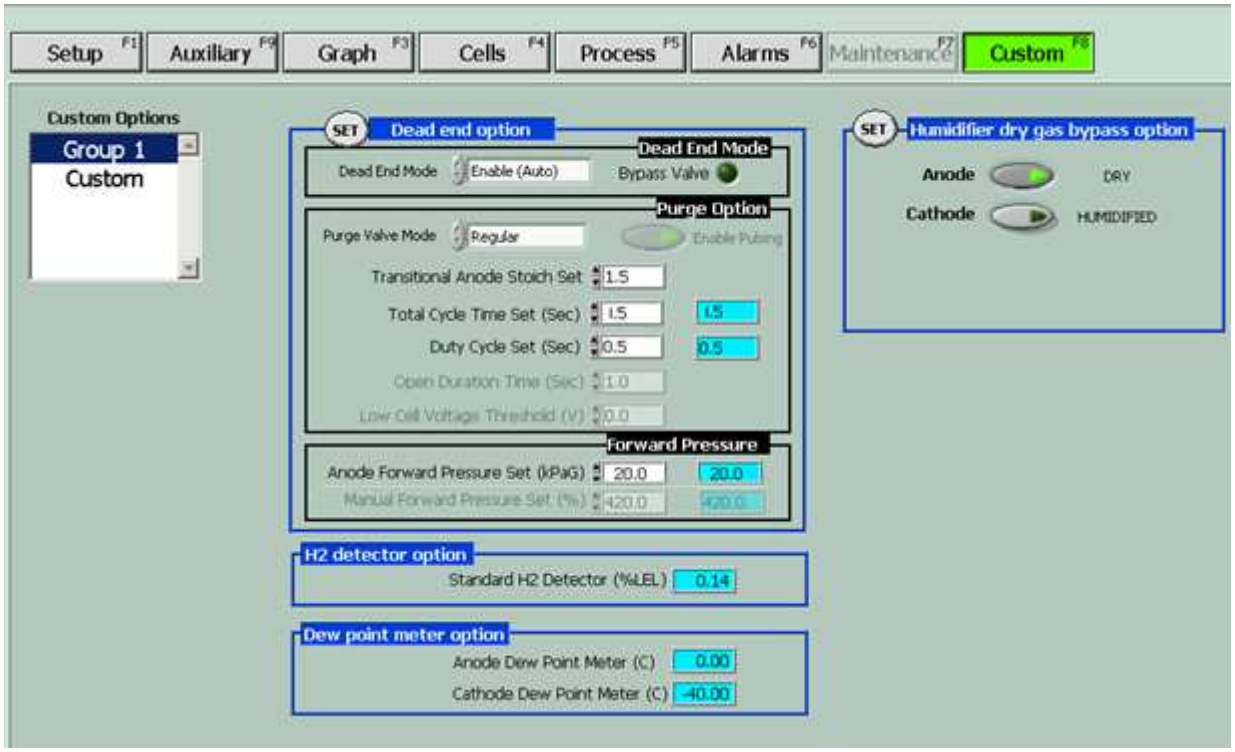

Figure 17: Screenshot of Custom main page including, Dead end option (top) Humidifier dry gas bypass option (right) and Dew point meter option (bottom).

The name dead end is representative of the anode outlet being closed off, or dead-ended. Such a configuration is accomplished by completely closing the downstream pressure regulator that would otherwise function to control the back pressure in flow-through mode. The exiting gas and water are rerouted through a solenoid valve to the exhaust (Figure 16). This solenoid valve functions as the purge valve and will open and close based on a parameter called the purge fraction. The purge fraction is discussed in Section 2.4.3.

The volumetric flow rate of hydrogen delivered to the anode is determined by the anode inlet pressure set point. An adequate amount of hydrogen is supplied to maintain this pressure set point. A pressure drop at the anode results from hydrogen consumption (due to the electrochemical reaction, hydrogen lost due to crossover to the cathode, and due to the combustion of hydrogen with oxygen that has crossed over to the anode) and from gas exiting when the purge valve is open. Therefore, the hydrogen flow rate is dependent not only on the current density (which determines how much is consumed) but also on the recirculation rate and purge fraction. When the actual inlet pressure is less than the set point, the upstream pressure regulator opens to increase the hydrogen flow and thus increasing the pressure. When the purge valve is closed, unconsumed gas remains at the anode consequently increasing the anode pressure. As such, the upstream pressure regulator functions to decrease the hydrogen flow. Figure 18 demonstrates this control strategy.

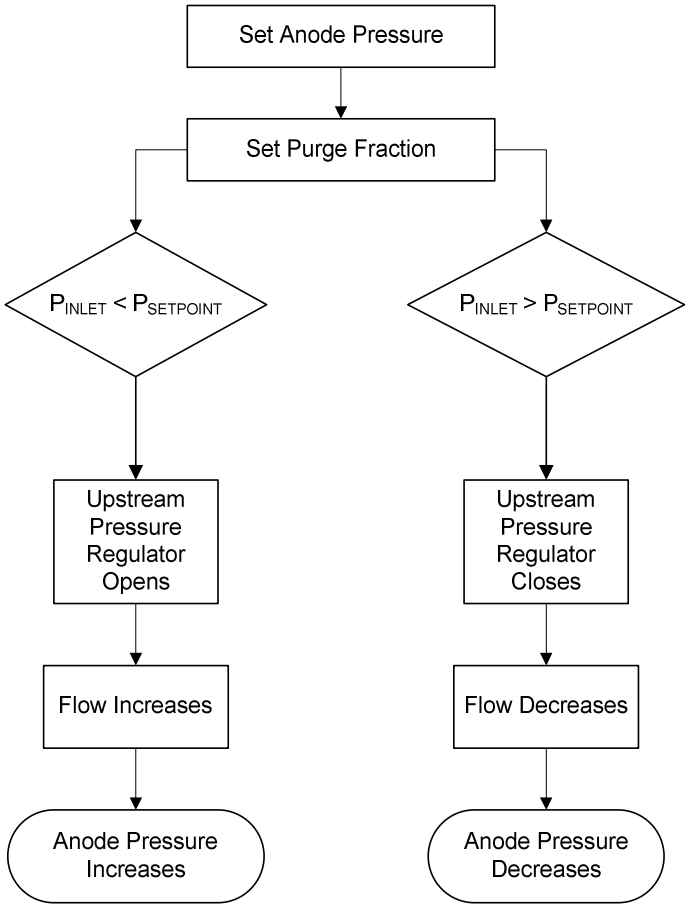

Figure 18: Diagram of dead end mode pressure and flow control

2.4.3 Purge Fraction

The purge fraction (Fp) controls the gas exiting the anode outlet to the exhaust. It is defined as the ratio of the duty cycle time (t_{duty}) to the total cycle time (t_{total}).

$$F_p = \frac{t_{duty}}{t_{total}}, 0 \le F_p \le 1 \qquad \textbf{(2-1)}$$

The set points of t_{duty} and t_{total} are defined in the *Dead end option* in HyWARE (Figure 17). The duty cycle is the time the purge valve is open and the total cycle is the time the purge valve is closed plus the time it is open. In other words, if you subtract t_{duty} from t_{total} the result is the time the purge valve is closed. As an example, if $t_{duty} = t_{total}$ (i.e. the purge valve is always open), Fp = 1.0 but if $t_{duty} = 0$ (i.e. the purge valve is always closed) Fp = 0.0. To mimic the operation of the HyPM HD8, t_{duty} was set constant at 500 ms for all current densities. As such, t_{total} was the only variable changed to adjust Fp.

2.5 Anode Recirculation

In practical applications hydrogen is fed to the anode in excess with the bulk of the spent anode gas being recycled, or recirculated, back to the anode inlet. A positive displacement pump connected between the anode outlet and anode inlet forms the anode recirculation (recirc) loop in the HyPM HD8.

Table 4 shows the anode gas flow rates and stoichiometric ratio for the HyPM HD8 for the three current densities tested in this work. The volumetric flow rate of the recirculation gas (Q_r) is approximately 52 slpm at all current densities. The flow rate of fresh hydrogen to the anode (Q_f) has a stoichiometric ratio of 1. The recirculation gas and the fresh hydrogen combine to give the total flow rate entering the anode and an anode stoichiometric ratio greater than one.

Table 4: HyPM HD8 Anode gas flowrate and stoichiometric ratio for a given current density.

Current Density	Anode Gas Flow Rate			Anode Stoichiometric Ratio
	Recirculation Q_r	Fresh Feed Q_f	To the Inlet (= Q_r + Q_f)	
mA/cm^2	slpm	slpm	slpm	
920	53.53	101	154.53	1.53
570	52.29	63	115.29	1.83
140	51.68	16	67.68	4.23

Since a smaller stack was used for testing, it was necessary to scale down the recirculation flow rate from an 80 cell to a 10 cell stack. Using a ratio of 80 cells to 10 cells, a recirculation flow rate of 6.5 lpm for the 10 cell stack was calculated. With the objective being to mimic the HyPM HD8, it was decided to use the same pump in the experimental setup as is used in the actual power module. However, such a pump is designed for the larger recirculation flow rates of an 80 cell stack. It was decided to adjust the pump power settings in order to decrease the flow rate to 6.5 lpm. In an attempt, the power supply voltage was 'tuned' down but this resulted in a very unsteady flow rate. This occurred because the pump was designed to function in a voltage range suitable for larger flow rates. To resolve this, a bypass line parallel to the pump was incorporated into the recirculation circuit. Figure 19 shows a flow diagram which labels (in red) the different streams of the recirculation circuit and the bypass line. The anode outlet stream entering the recirculation circuit combines with the bypass stream before entering the pump in order to satisfy the pump with a large volumetric flow rate. The gas exiting the pump divides into two streams: one large volume stream which travels the bypass line and 6.5 lpm which combines with the fresh hydrogen stream before entering the anode. Figure 20 shows a photo of the recirculation pipe connected to a Vaisala relative humidity sensor which is connected to the anode outlet manifold. The recirculation pipe exiting the anode outlet manifold was positioned

at an upward angle in an effort to avert liquid from travelling the recirculation circuit. The recirculation pipe and the bypass pipe connect at a T-intersection which connects to the pump. A ball valve was included in the bypass line in order to adjust the pipe diameter. The blue handle of the bypass valve is shown protruding out of the insulation which is wrapped around the piping. A clear plastic tube emerging from the anode outlet forms the purge line. The purge line was positioned on a downward angle in an effort to drive liquid water to the exhaust.

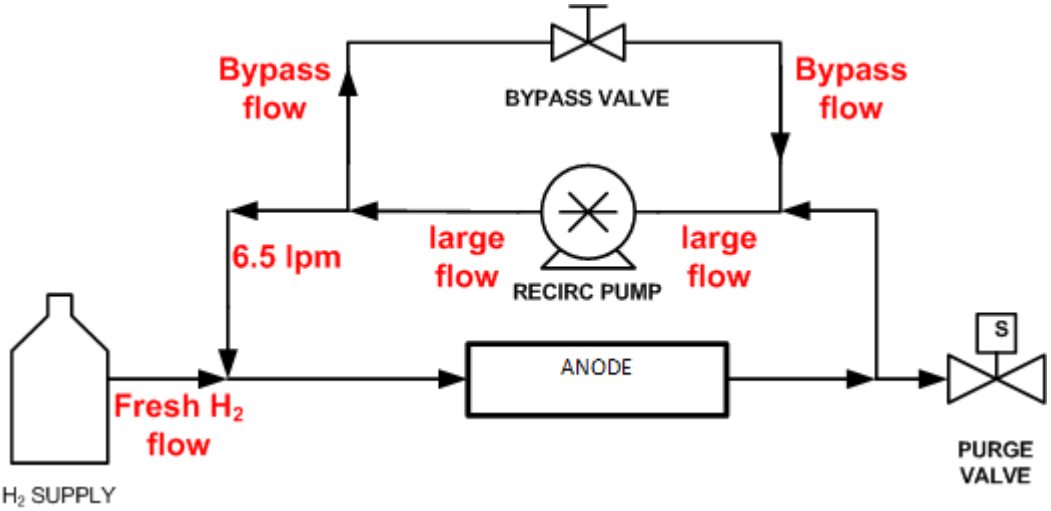

Figure 19: Flow diagram used to describe the purpose of the bypass line in the anode recirculation circuit.

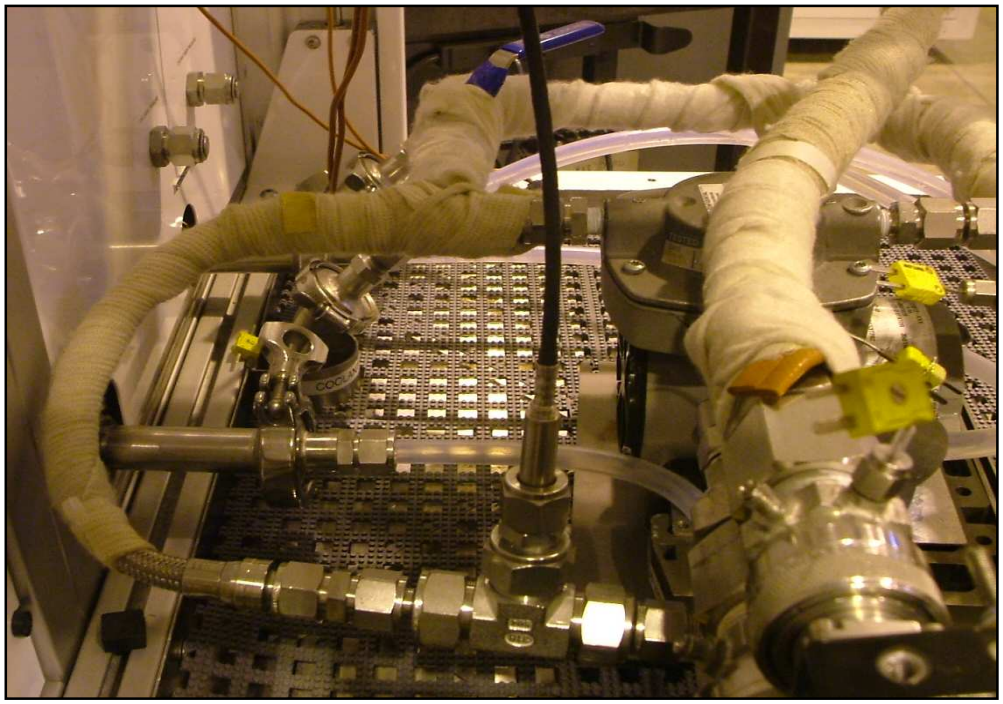

Figure 20: Photo of the anode recirculation circuit including the anode outlet, relative humidity sensor, recirculation pump, bypass line and purge valve.

The setup shown in Figure 21 was used to calibrate the pump power supply voltage to obtain the desired recirculation flow rate through the pump. The recirculation circuit in the calibration setup was the same as in the experimental setup with the exception of a rotameter in the place of the stack. The rotameter was used to measure the volumetric flow rate exiting the recirculation pump. The ball valve was adjusted to fine tune the flow rate through the bypass pipe. The pump voltage was manually changed from a power supply which was connected to a controller and the pump in series. The voltage was adjusted until the rotameter read a flow rate of 6.5 lpm. The pressure fluctuation in the calibration setup (approximately 2 kPag) was nearly the same as the pressure fluctuation in the actual setup with the purge operating. In the final setup the external power supply used for calibration was eliminated and the pump was configured to the FCATS. This arrangement allowed the pump voltage to be controlled from HyWARE or by the HyAL test scripts.

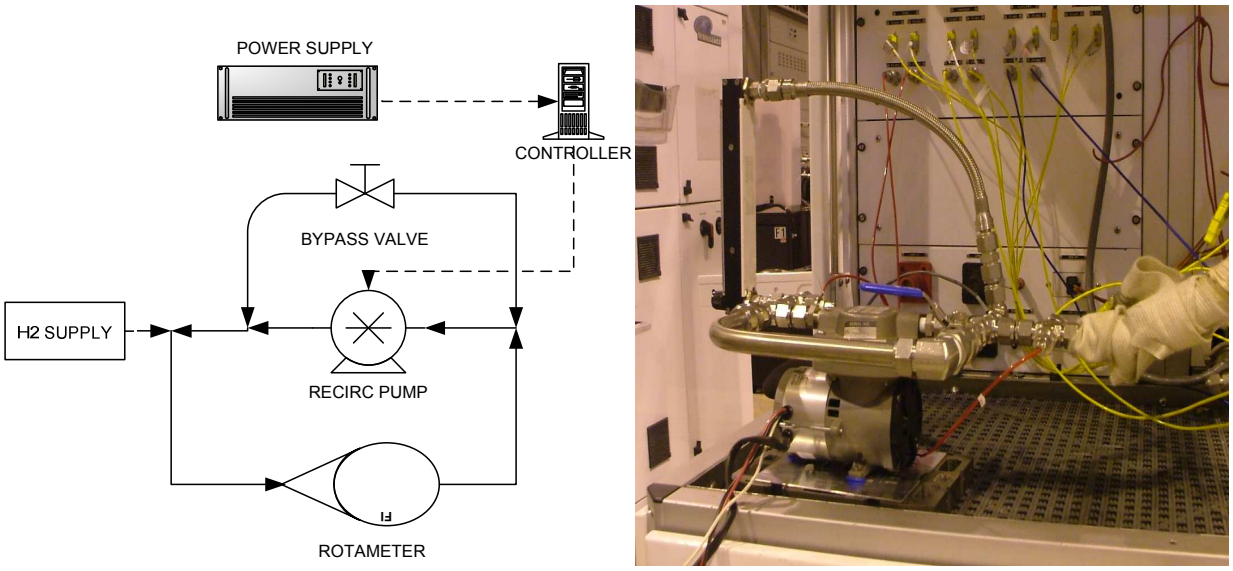

Figure 21: Diagram (left) and photo (right) of the apparatus used for calibrating the recirculation pump to a flow rate of 6.5 lpm.

2.6 Online Parameter Measurements

Measurement of all operating parameters was critical to the overall understanding of the system. Figure 22 shows the location of the online measurement devices used. A mass flow meter indicated the volumetric flow rate of fresh hydrogen entering the anode. Thermocouples and pressure transducers were situated at the anode and cathode inlet and outlet. An additional thermocouple was situated where the recirculation stream meets the fresh hydrogen feed stream and it was assumed that the composition of the gas in the recirculation and bypass circuit was the same as the anode outlet gas. A Vaisala dewpoint temperature sensor was situated at the anode outlet.

The fuel cell voltage monitor measures the voltage across each cell and this information is downloaded and stored on the computer as well as being displayed in real time on the computer screen for the operator to see. Figure 23 shows a screenshot the HyWARE interface used for monitoring the different parameters. The cell voltage monitoring panel located at the bottom of the HyWARE window displays the voltage of each cell by means of a bar graph. The side panel displays the flow rates, pressures and temperatures. The Custom page displays the parameters related to the purge system and the dew point temperature from the Vaisala sensor.

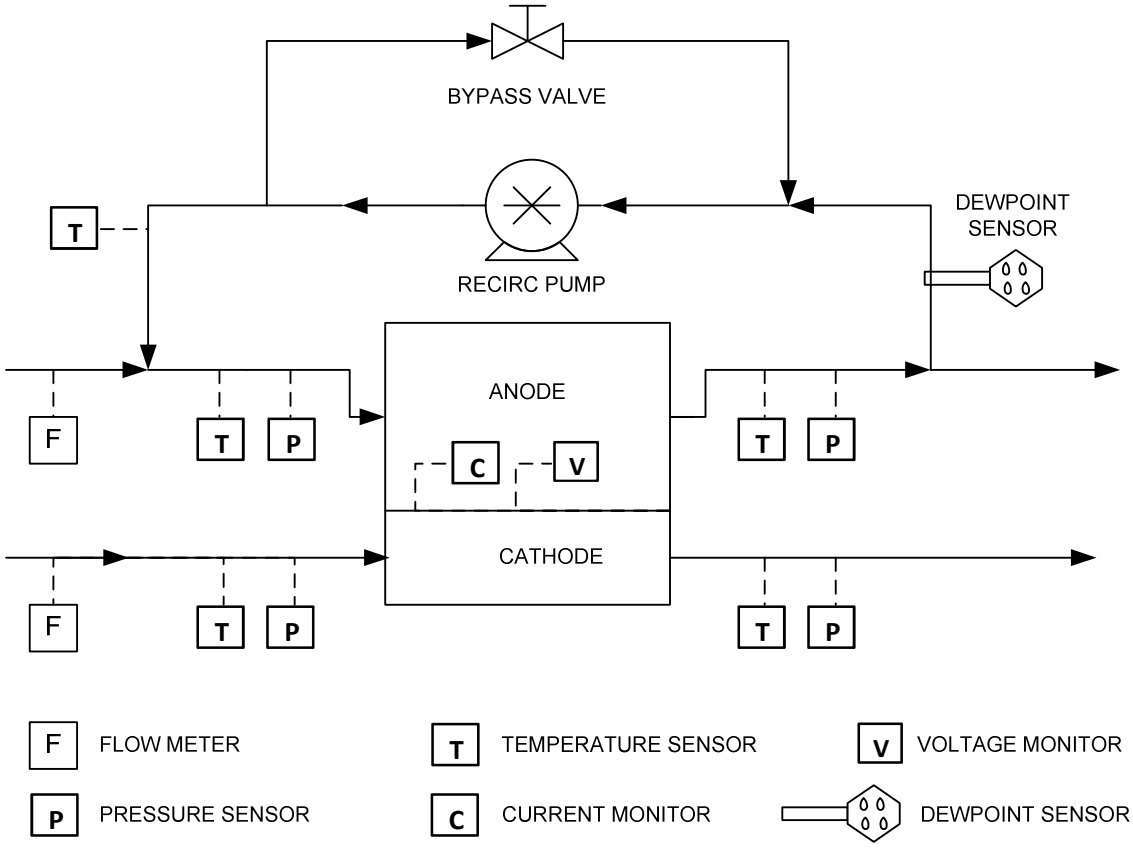

Figure 22: Diagram indicating the location of online sensors for measuring parameters in Phase 1 and Phase 2 testing.

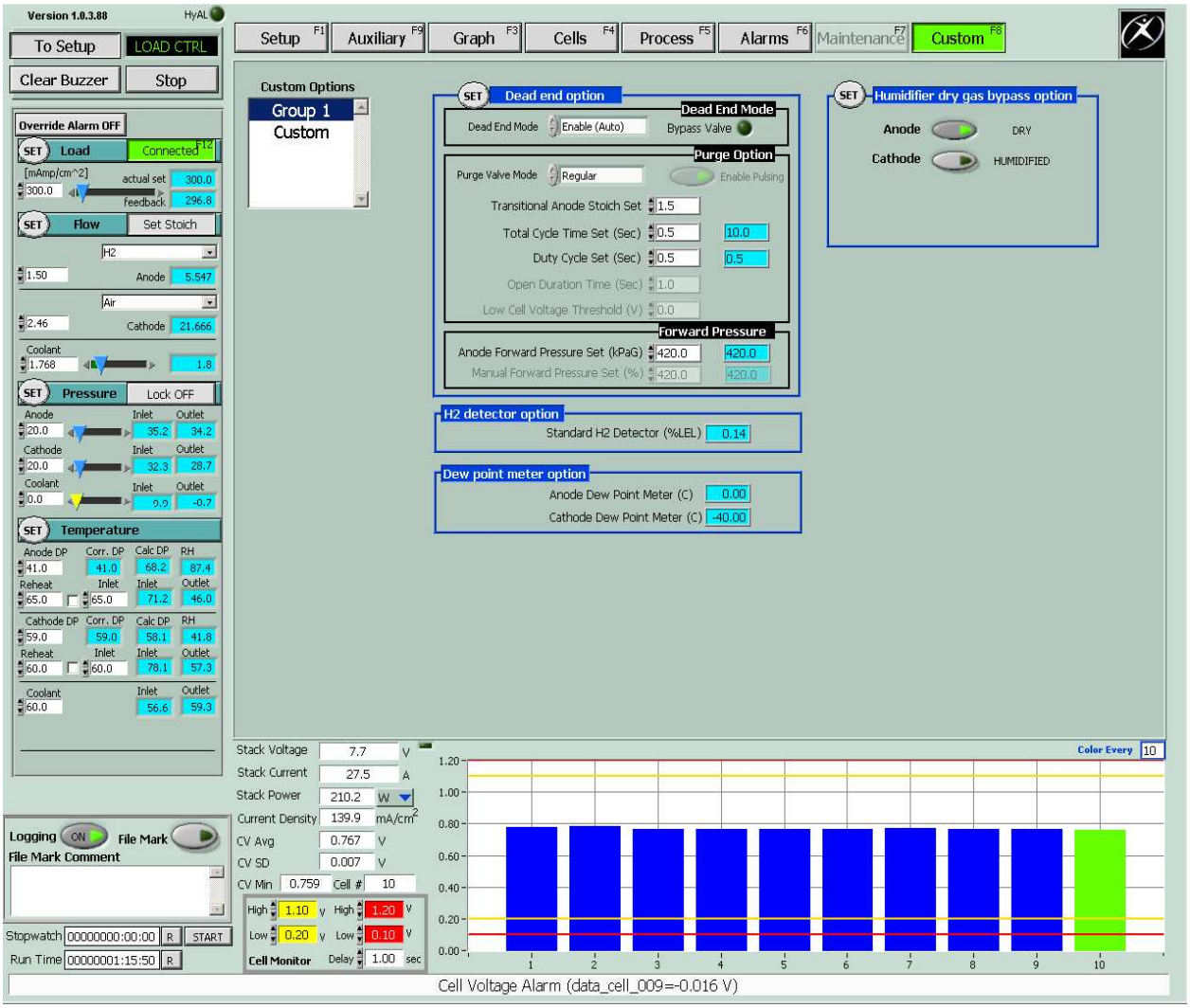

Figure 23: Screenshot of HyWARE window used for controlling and monitoring the various operating parameters.

2.7 Leak Checks

After the initial commissioning period (where extensive leak and crossover checks were performed), leak checks were performed approximately every 60 days. The diagnostic test

determines whether any crossover has occurred between the anode, cathode, and coolant channels. Pure nitrogen was used as the feed gas into the fuel cell stack for each type of crossover check. Anode to cathode crossover was tested at 5 psig, whereas anode/cathode to coolant was at 20 psig. External leaks were investigated at 30 psig. The most important of all is the leak test between the anode and cathode. The detailed procedure for performing the leak checks is outlined in Appendix B.

2.8 Phase 1 Testing

The objective of Phase 1 of the testing was to determine the effect of purge fraction on the average cell voltage when pure hydrogen fuel is fed to the anode. In this case the only impurity in the anode stream is nitrogen that has crossed over from the cathode. Naturally any CO present in the hydrogen itself could also accumulate, but this CO accumulation is thought to be insignificant for Phase 1 as the delivered hydrogen was 99.999% pure. A diagram of the major components in the experimental setup used for Phase 1 is shown in Figure 24 with the measurement devices shown in Figure 22.

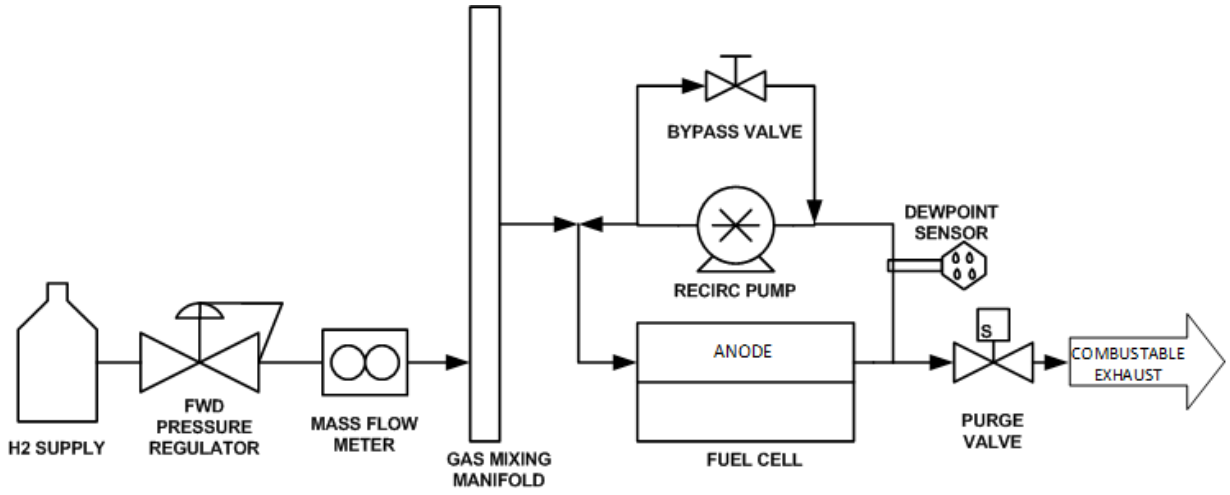

Figure 24: Diagram of major components in the experimental setup used for Phase 1 testing.

2.8.1 Test Protocol

Automation scripts created in HyAL were used to run automated tests on the FCATS. By using test scripts, the same protocol was followed for every test. The flowchart in Figure 25 outlines the basic steps in the protocol: (i) stack conditioning, (ii) test procedure and, (iii) stack shutdown. Automation scripts can be found in 0.

Stack conditioning

Conditioning the stack involves slowly ramping the load to 570 mA/cm^2, and allowing the stack to heat up and equilibrate for 30 minutes. The script maintains the gas at the same temperature as the stack while it is warming up to prevent condensation from forming. The purge valve is set to the always open condition (i.e. = 1.0) during the conditioning period.

Test procedure

Tests were conducted at a constant load condition. This involves leaving the stack running at one current density for the duration of the test. The set points for the operating parameters are also held constant for a given current density. Three current densities representing a low load condition (140 mA/cm^2), medium load condition (570 mA/cm^2), and high load condition (920 mA/cm^2) were tested. A separate test was conducted for a change in Fp. The first test conducted for a given current density was Fp = 1.0. With each following test, Fp was decreased until Fp = 0.0 or the stack can no longer sustain a voltage and consequently shutdown. The minimum purge fraction that could sustain a voltage was defined as Fp_{min1}.

The script first sets the current density and the associated operating parameter set points (Table 5). After five minutes, Fp is set and the test starts. At this point, the data logging is turned on to capture the real-time value of each parameter. Each parameter set point and read back has an associated HyWARE tag name (A list of these can be found in 0). Data points were collected every 30 seconds and stored into an Excel file for the 20 minute test duration.

Table 5: Operating parameter set points for each current density tested in Phase 1.

	Current Density [mA/cm^2]	920	570	140
Cathode	Air flow [nlpm]	567	367	173
	Stoich	2.36	2.46	4.69
	Inlet Pressure [kPa]	9.6	5.4	2.4
	Inlet Temperature [^{o}C]	60	60	60
	Inlet Dewpoint [^{o}C]	59	59	59
Anode	Inlet Pressure [kPa]	16.6	9.7	5.0
	Inlet Temperature [^{o}C]	65	65	67
Coolant	Outlet Temperature [^{o}C]	63	60	60

Shut down

The script will terminate the test and safely ramp down the stack. In the case of a shutdown at Fp_{min1}, the FCATS has an emergency shutdown procedure which returns the load to 0 Amps and sets the parameters back to values that are safe for the stack.

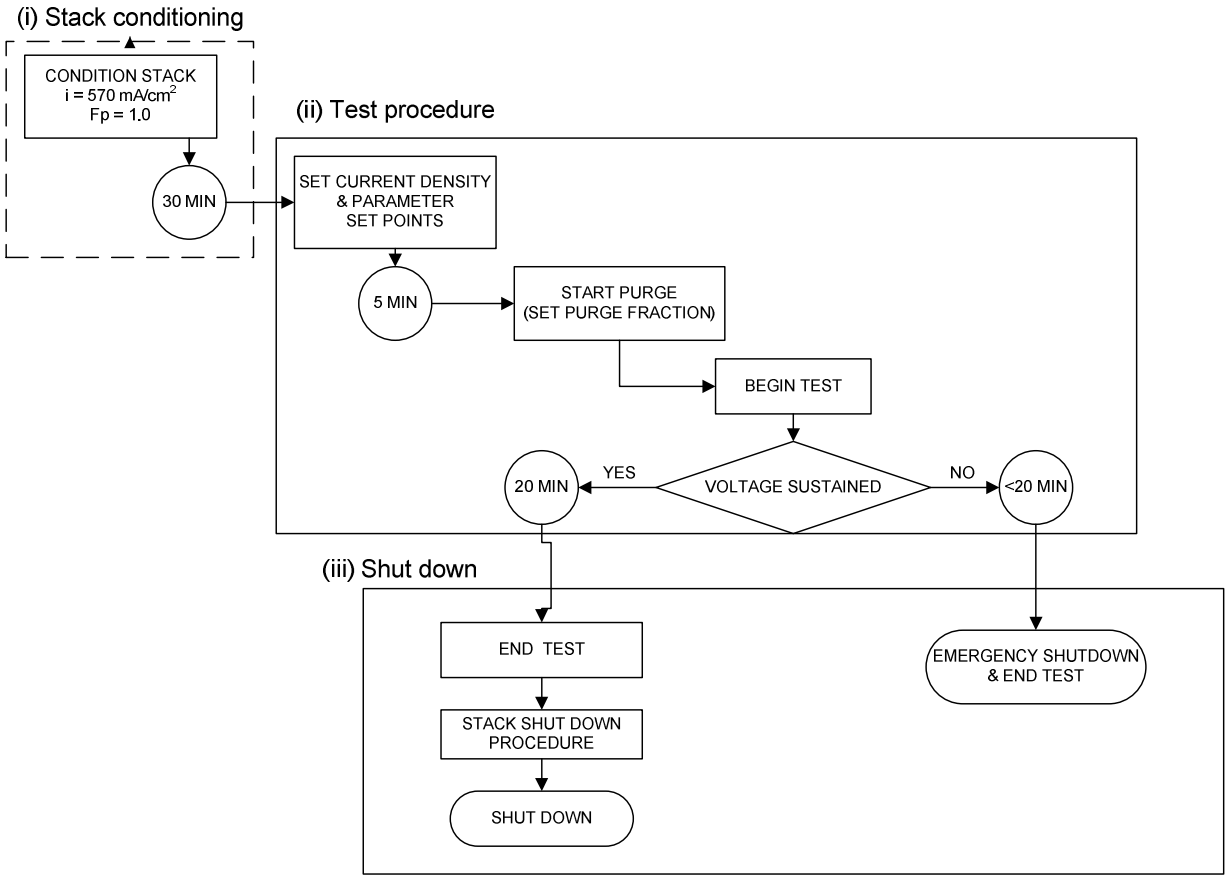

Figure 25: Protocol followed for Phase 1 tests.

2.8.2 Analysis

For each test, the resulting voltage degradation, fresh hydrogen fuel savings, and average anode relative humidity were calculated and plotted against Fp.

Voltage Degradation

Voltage degradation was calculated by taking the average mean cell voltage (MCV) of the last three data points of the test and subtracting it from the average MCV of the first three data points of the test.

Fresh Hydrogen Fuel Savings

This value was calculated for a given Fp and it represents the percentage of fresh hydrogen that can be saved by operating at a purpose fraction less than Fp = 1.0. It is calculated as the reduction in the fresh hydrogen flow rate when operating at Fp < 1.0, divided by the fresh hydrogen flow rate when Fp = 1.0 (Equation (2-2).

$$\frac{Q_{H2}\big|_{Fp=1.0} - Q_{H2}\big|_{Fp=x}}{Q_{H2}\big|_{Fp=1.0}} \times 100\% \qquad \textit{(2-2)}$$

Where, $Q_{H2}\big|_{Fp=1.0}$ represents the volumetric flow rate of fresh hydrogen supplied when Fp = 1.0 and $Q_{H2}\big|_{Fp=x}$ represents the flow rate of fresh hydrogen supplied for a value of Fp less than 1.0.

Relative Humidity

The relative humidity at the anode outlet was calculated as the ratio of the actual vapor pressure to the saturated vapor pressure at the outlet temperature. The actual vapor pressure was calculated from the measured dew point temperature at the anode outlet.

2.9 Phase 2 Testing

The objective of Phase 2 of the test program was to determine the effect of purge fraction on the cell voltage when as low as 0.2 ppm carbon monoxide was present in the fuel supply. A diagram of the major components in the apparatus used for Phase 2 testing is shown in Figure 24. An additional fuel supply stream, 'Fuel B', combines with the fresh hydrogen stream in the gas mixing manifold before entering the anode. Fuel B is a gas mixture containing ppm levels of CO in hydrogen and is supplied from a gas cylinder located beside the FCATS (Figure 27). The flow rate of Fuel B is set by the HyWARE tag *flow_anode_special_gas_mfc_set* which creates a set

point for the respective mass flow controller (MFC). This MFC was calibrated for a range of 0-1000 cm^3/min.

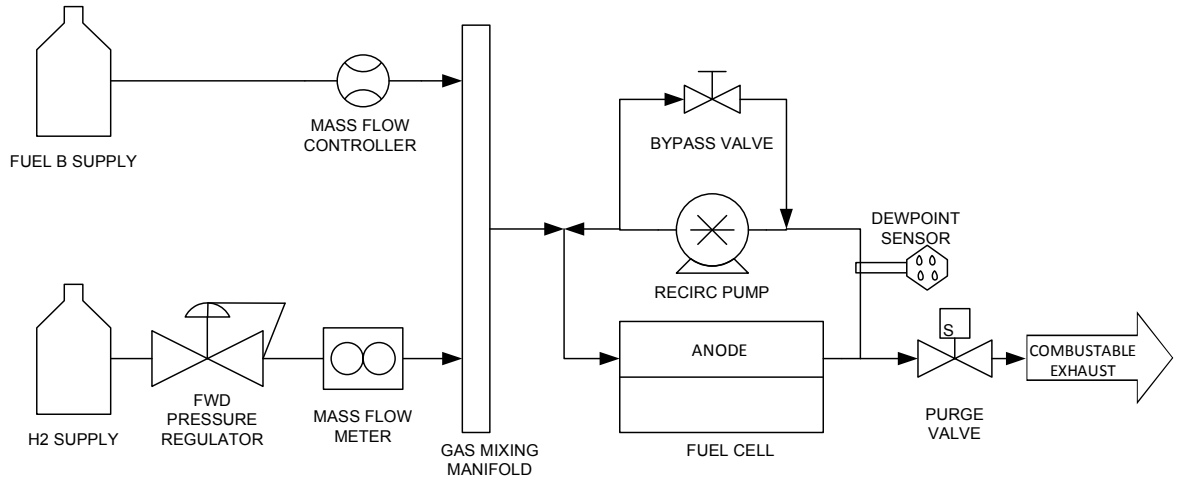

Figure 26: Diagram of major components in the experimental setup used for Phase 2 testing.

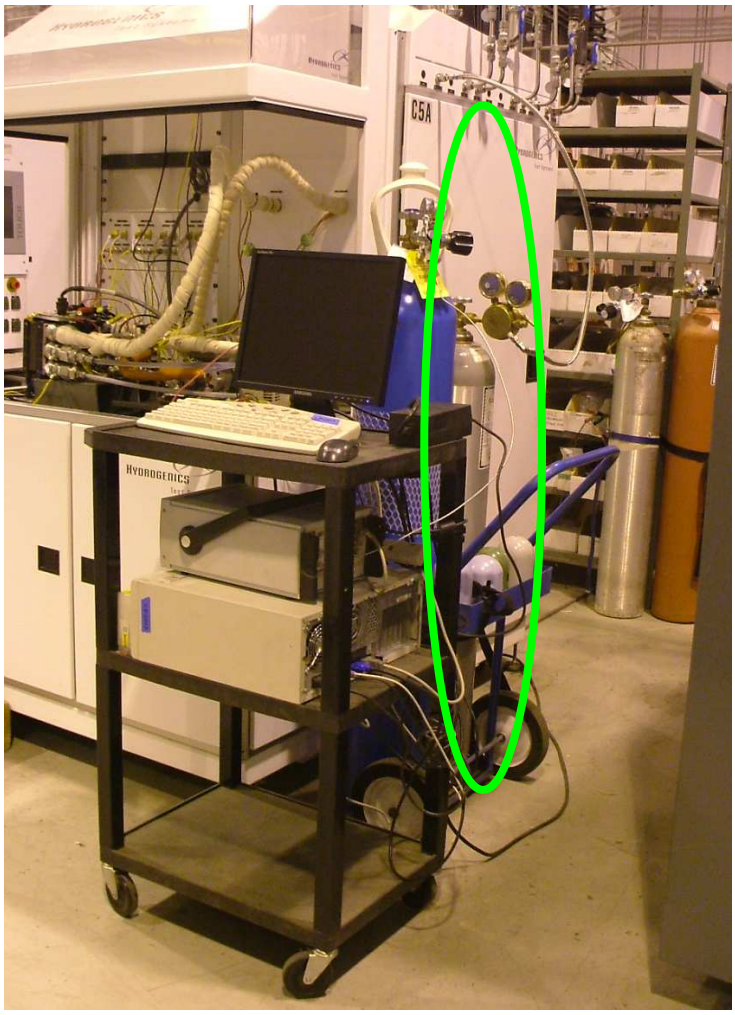

Figure 27: Photo of Fuel B gas cylinder (grey) located beside the test station and connected to the FCATS.

2.9.1 Fuel B Supply

To obtain a desired CO concentration in the fresh fuel supply, the flow rate of Fuel B (Q_{FuelB}) must first be determined. A mole balance was performed on the system shown in Figure 28 to calculate Q_{FuelB}. Neat hydrogen (Q_{H2}) combines with Q_{FuelB} to form the fresh fuel stream that enters the anode (Q_{Anode}). Q_{Anode} is dependent on the anode inlet pressure set point for a given

current density and purge fraction. As an example, by operating the stack at 570 mA/cm^2 and Fp =0.83, Q_{Anode} was determined to be 40 lpm.

The concentration of CO in Fuel B ($y_{COFuelB}$) is known and the concentration of CO in Q_{Anode} ($y_{COAnode}$) is, in the majority of tests, 0.2 ppm. Given that $Q_{FuelB} << Q_{H2}$, it can be assumed that $Q_{Anode} = Q_{H2}$. With this information, Q_{FuelB} can be calculated from the following equation

$$Q_{FuelB} = \frac{y_{COAnode} \times Q_{H2}}{y_{COFuelB}} \qquad \textbf{(2-3)}$$

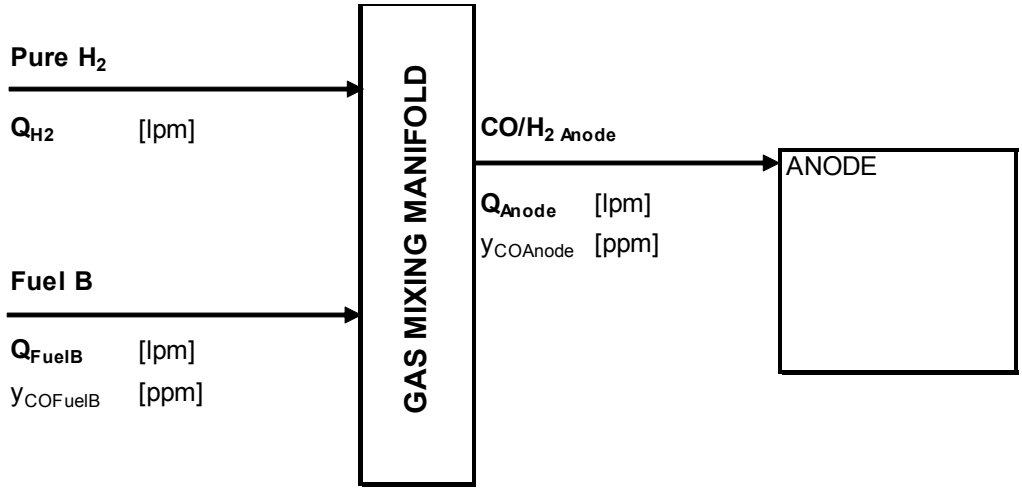

Figure 28: Schematic demonstrating the variables used for calculating the required volumetric flow rate of the Fuel B stream entering the gas mixing manifold.

The next step was to analyze a gas sample from Q_{Anode} to determine the actual concentration of CO delivered to the anode based on the calculated Q_{FuelB} value. This is accomplished by taking a gas sample of Q_{Anode} and using gas chromatography to measure the amount of CO. However,

before such an analysis can be performed the gas chromatography (GC) instrument (Varian) must first be calibrated.

Calibration was performed using a certified standard gas containing 17 ppm CO/H_2. A Tedlar gas sampling bag was filled with the standard gas (Figure 29a) and this bag was connected to the GC inlet (Figure 30b) and injected into the sampling loop. The sample mixes with the carrier gas (nitrogen) and passes through a Molesieve 5Å column The Molsieve 5Å column is designed to separate: hydrogen, carbon monoxide, methane, nitrogen, oxygen, and some noble gases. The column is equipped with a thermal conductivity detector (TCD). This detector responds to the difference in thermal conductivity between the carrier gas (nitrogen) and the sample components. The construction of a TCD is such that the changing signal of the carrier gas stream, due to components present, is compared to the signal of a constant reference gas stream. Digital information of the analysis is exchanged between the GC and a computer. Coefficients for the calibration curve are calculated and saved in a method. The method is then used to perform an analysis of a sample containing unknown amounts of CO.

a) 

b) 

Figure 29: a) Filling a Tedlar gas sampling bag with certified standard gas, and b) connecting the bag to the gas chromatography instrument for calibration.

To measure $y_{COAnode}$, the set up in Figure 30 was used. Different known amounts of Q_{FuelB}, $y_{COFuelB}$ and Q_{H2} were supplied to simulate four concentrations (1, 2, 5, and 10 ppm) of $y_{COAnode}$. Gas concentrations lower than 1 ppm were not detected by the GC. Downstream from the gas mixing manifold a hand valve was used to draw ~1L samples into a Tedlar sampling bag. For each sample, three injections into the GC and therefore three analyses were performed.

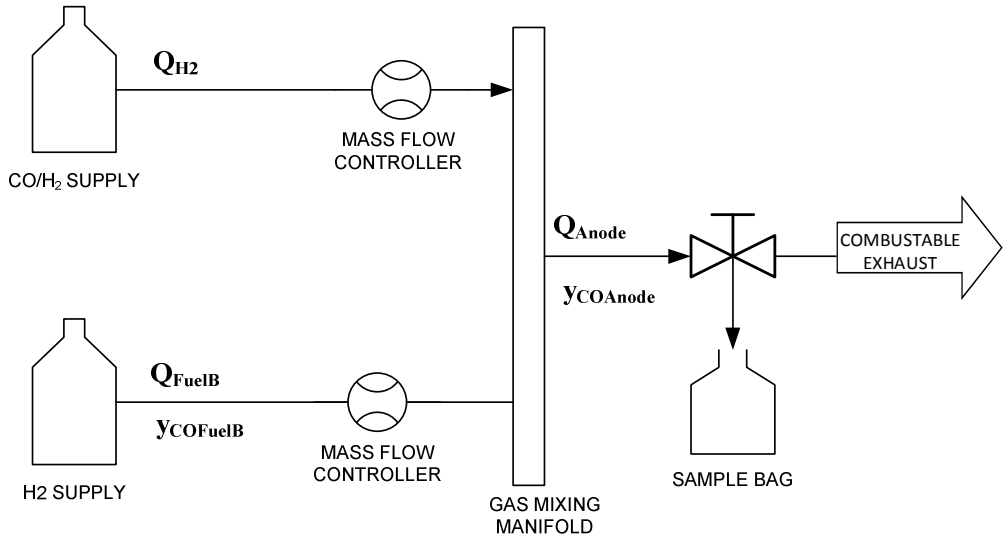

Figure 30: Diagram of the setup used to compare the CO concentration delivered by the FCATS to the CO concentration measured by the GC.

Figure 31 shows the plot used to compare the calculated concentration of CO/H_2 delivered to the anode by the FCATS to the concentration measured by the GC. A linear trend-line forced through the origin shows good linear correlation at higher CO concentrations. Such a result suggests that the FCATS is actually supplying the amount of CO as calculated in Equation (2-2). Conversely, weaker correlation was observed at lower concentrations. As one example for 1 ppm CO, the concentration measured by the GC was closer to 2 ppm. This inaccuracy was thought to be the result of the GC and not the FCATS because measurement uncertainty was likely to occur in this low range of CO concentration given that the reference standard was 17 ppm CO/H_2. In retrospect, a lower concentration reference standard should have been used since

the range of interest was less than 0.2 ppm CO/H_2. Nevertheless, the FCATS was expected to flow the set concentration since Q_{FuelB} was always within the calibrated range of the mass flow controller.

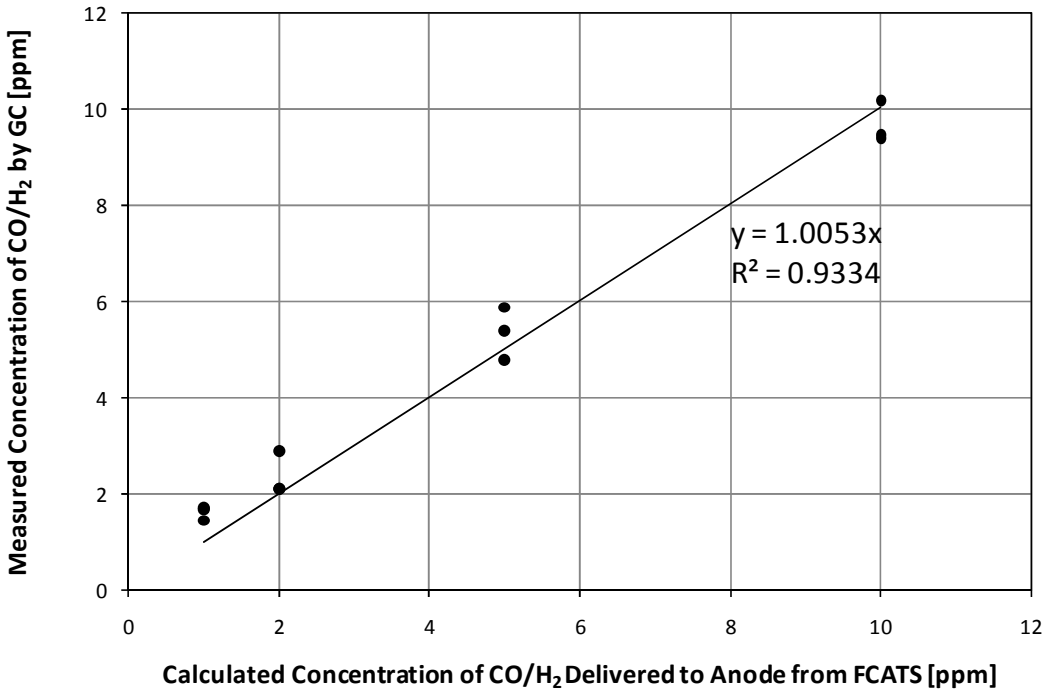

Figure 31: Plot used to compare the Calculated concentration of CO/H_2 delivered to the anode by the FCATS to the concentration measured by the GC

2.9.2 Test Protocol

The protocol followed for Phase 2 tests differed from that of Phase 1 in that a stack recovery procedure was performed before stack conditioning and the test ran for 10 hours rather than 20 minutes. The flowchart in Figure 32 outlines the basic steps in the protocol: (i) Stack recovery, (ii) stack conditioning, (iii) test procedure and, (iv) stack shutdown. Stack recovery is discussed below. Refer to Section 2.8.1 for a description of the other steps. Automation scripts can be found in 0.

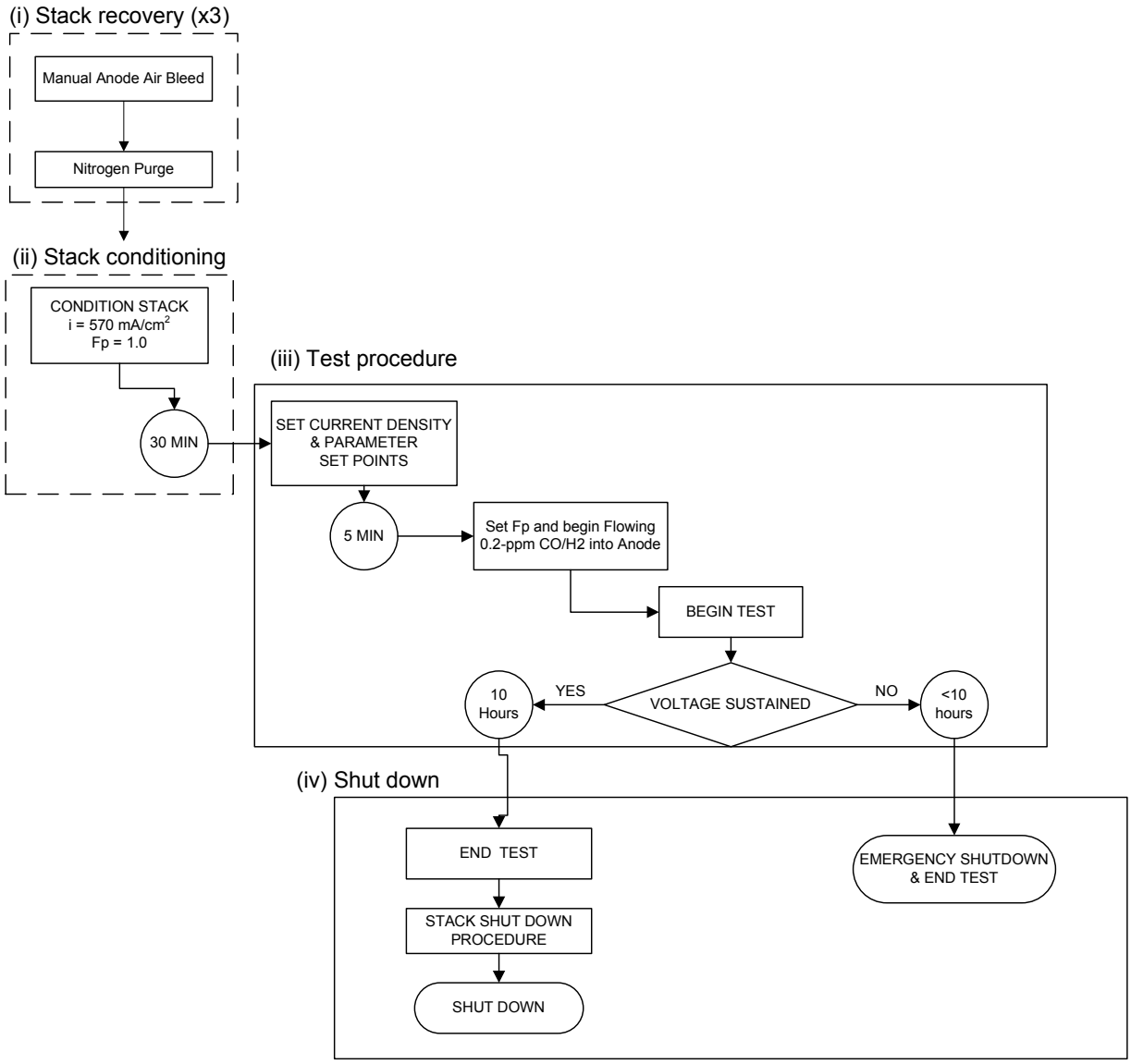

Figure 32: Protocol followed for Phase 2 tests

Stack recovery procedure

Carbon monoxide severely degraded the stack performance during the Phase 2 tests by adsorbing onto the catalyst sites and prohibiting hydrogen adsorption and electrooxidation. It was assumed

that much of the CO that adsorbed onto the catalyst during a test remained there after the test finished. The degree of CO coverage depended on the concentration of CO in the fuel, on the current density and on the purge fraction. In order to start each test from the same operating state, it was crucial to remove the remaining CO that adsorbed on to the catalyst sites from a previous test. CO poisoning is often mitigated while the fuel cell is in operation by bleeding oxygen, or air, into the fuel so that CO can be oxidized to CO_2 by heterogeneous catalysis (Reactions **Error! Reference source not found.** and**Error! Reference source not found.**). The FCATS has an integrated oxidant bleeding option, but this was not utilized because it involved swapping the Fuel B line for the oxidant line. As such, it was decided to introduce air to the anode after a test was completed and the stack was discharged. A method of this kind was not found in the literature so before employing this technique, it must first be determined if Reaction (2-4) proceeds spontaneously at ambient temperature and pressure.

$$\tfrac{1}{2}O_2 + CO \rightarrow CO_2 \qquad (2\text{-}4)$$

To satisfy the second law of thermodynamics the Gibbs free energy (ΔG) of Reaction (2-4) must be negative. Given the free energies of formation for CO, O_2 and CO_2, ΔG was calculated as -123.0 kcal. Therefore at these conditions and in the presence of a platinum catalyst, it was assumed that introducing air to the anode would remove CO from the catalyst when the stack was shutdown. However, it was not known how much of the adsorbed CO would oxidize to CO_2.

The following procedure was followed to perform the air bleed:

(i) The hydrogen inlet fitting was disconnected and a quick connect reduced to a 3/8" tube fitting was connected in its place (Figure 33).

(ii) A 2L tedlar gas sampling bag was connected to the pilot air supply (Figure 34a) and filled with air

(iii) This bag was connected to the anode inlet fitting and its contents were forced into the anode by compressing the bag.

(iv) The air bag was disconnected and a long plastic tube, attached to the anode inlet, was connected to a nitrogen supply on an adjacent FCATS (Figure 34b).

(v) Nitrogen was supplied to the anode at a pressure of 1 psi in order to purge the anode channels of any CO and CO_2.

(vi) This procedure was repeated 2 more times.

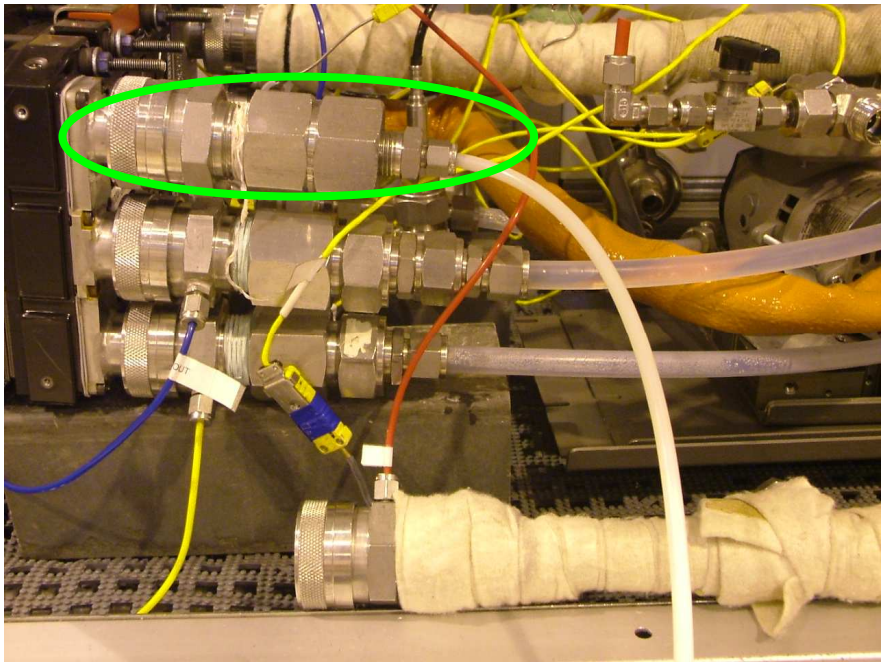

Figure 33: Photo of plastic tubing connected to the anode to supply air and nitrogen to the anode.

a) 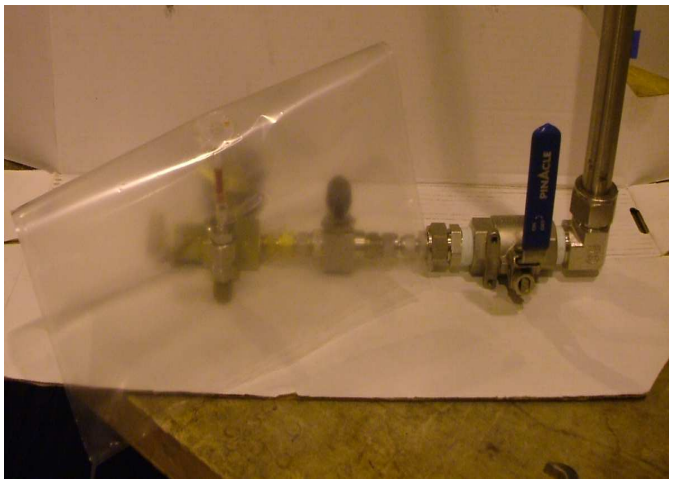 b) 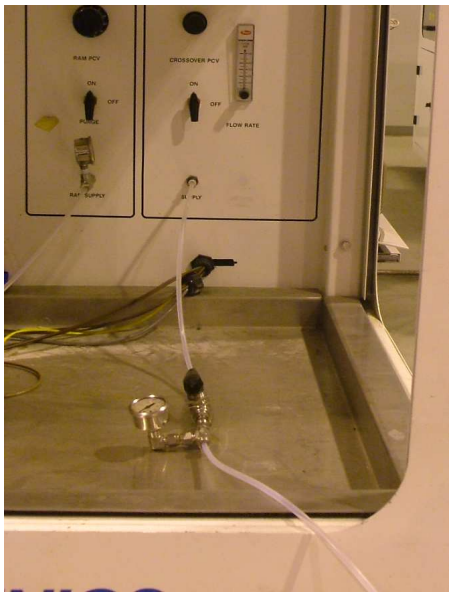

Figure 34: Photo of the equipment used to a) fill the gas bag with air and b) supply nitrogen from an adjacent FCATS to the anode.

Chapter 3 - Effect of Anode Purge on Performance

The overall objective of the experimental work was to quantitatively evaluate the effect of the anode purge fraction on PEMFC stack performance when operating with a recirculation anode stream and trace levels of carbon monoxide present in the hydrogen fuel. First, in Phase 1 the effect of purge in the absence of carbon monoxide was studied to see if hydrogen dilution from nitrogen crossover and accumulation would cause significant cell voltage degradation. In Phase 2 the effect of trace levels of carbon monoxide was evaluated.

3.1 Phase 1 - Effect of Purge in the Absence of Carbon Monoxide

In Phase 1 the objective was to determine the effect of purge on the cell voltage when hydrogen dilution occurred as a result of nitrogen accumulation in the anode gas stream. It should be noted that nitrogen was not present in the hydrogen feed so any nitrogen in the anode channels was the result of nitrogen crossover from the cathode.

Separate experiments were run for 20 minutes at current densities of 140 mA/cm^2, 570 mA/cm^2, and 920 mA/cm^2; the results of which are presented in Figure 35, Figure 36, and Figure 37, respectively. Each plot depicts the cell voltage degradation and the fresh hydrogen savings, as defined in Section 2.8.2, as a function of purge fraction (Fp). Each data point is the average of three different runs at the same conditions. The very left of the horizontal axis (Fp = 1.0) represents when the purge valve was open for the duration and therefore resulted in the smallest amount of impurity accumulation. The very right of the horizontal axis (Fp = 0.0) represents when the purge valve was closed for the duration of the test and therefore resulted in the largest amount of impurity accumulation. Recall that the cell voltage degradation was defined as the lowering of the average cell voltage compared to the average cell voltage when Fp = 1.0 and the fresh hydrogen savings for a given Fp represents the percentage of fresh hydrogen that can be saved by operating at a purge fraction less than Fp = 1.0. When Fp = 1.0, the largest amount of

anode gas is purged and the largest amount of fresh hydrogen is supplied, so performance is greatest. However for reasonable fuel efficiency, the amount of gas to be purged must be kept to a minimum because hydrogen in the purge gas is lost permanently. For each current density, two key purge fractions were of interest:

(i) the minimum purge fraction that could sustain a voltage without the stack shutting down (Fp_{min1}), and

(ii) the minimum purge fraction that would be tested in Phase 2 (Fp_{min2}).

Fp_{min2} was selected based on the voltage degradation and fresh hydrogen savings at that purge. It was rationalized that a purge resulting in a voltage loss too large did not merit testing in Phase 2 as the voltage loss would be far greater. With this criterion and the consideration of fuel efficiency, Fp_{min2} was selected.

Low Load Condition

Figure 35 depicts the effect of purge on the cell voltage for a wide range of Fp ($1.0 \geq Fp \geq 0.001$) at 140 mA/cm^2. Compared to the hypothetical case of Fp = 1.0, the cell voltage decreased by 28 mV when the nitrogen concentration in the anode channels increased as happened when Fp = 0.001. Recall that Fp = 0.001 means that the purge valve remained closed for 500 seconds and open for 0.5 seconds, repeatedly, for 20 minutes. The data point at the lowest purge (Fp_{min1}), represents the minimum purge at which the stack could sustain a voltage; anything lower than Fp_{min1} caused the stack to shutdown. The voltage loss was attributed to an increase in nitrogen concentration in the anode gas from the contribution of recirculated nitrogen build-up. This was expected since at smaller Fp the partial pressure of hydrogen decreases significantly as nitrogen accumulates. The Nernst equation predicts that the equilibrium potential of the cell decreases when the hydrogen partial pressure decreases. The decreasing hydrogen content also leads to reduced mass transfer rates which cause polarization. The voltage degradation was reduced to 5.1 mV by increasing the purge to Fp = 0.05, which reduced the N_2 concentration in the anode channels (Figure 35). At this purge the fresh hydrogen feed requirement was 90% lower than the

case of Fp = 1.0. Although a smaller Fp results in greater fuel savings, the trade off is an increased impurity concentration resulting in greater voltage degradation.

In conclusion, for the case of 140 mA/cm^2 and in the absence of carbon monoxide, reducing the purge to Fp = 0.05 avoids the excessive loss of hydrogen in the purge gas, while also avoiding excessive buildup of nitrogen in the anode channel which results in a higher voltage degradation. With carbon monoxide in the fuel, the voltage degradation is expected to be greater so Phase 2 tests would be conducted using $Fp_{min2} = 0.05$.

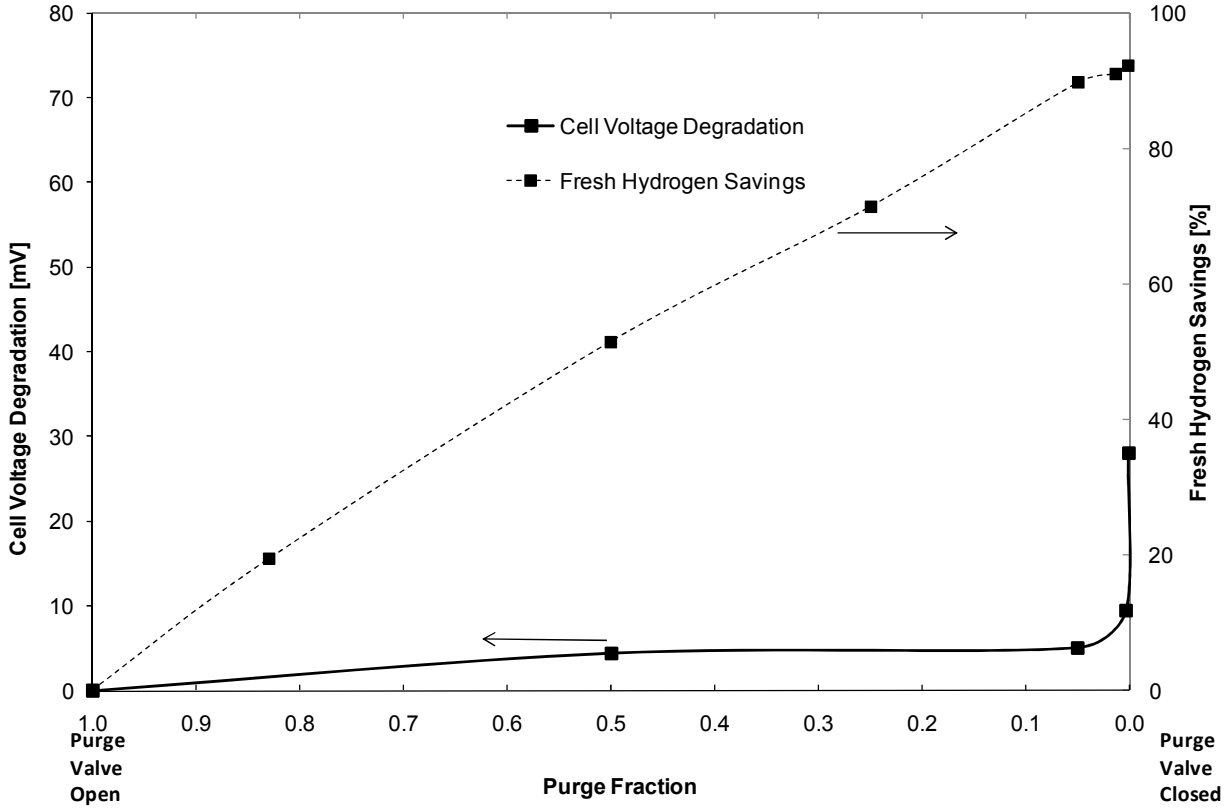

Figure 35: Cell voltage degradation (left) and fresh hydrogen savings (right) as a function of anode purge fraction for a current density of 140 mA/cm^2.

Medium Load Condition

Figure 36 depicts the effect of Fp on the cell voltage and fresh hydrogen savings for a smaller range of purge ($1.0 \geq Fp \geq 0.05$) at 570 mA/cm^2. Compared to 140 mA/cm^2, there was an exponential increase in the voltage degradation as the purge decreased. The cell voltage decreased by 100.5 mV when the nitrogen concentration increased as happened with Fp=0.05. The larger voltage degradation was thought to be due to an increase in concentration polarization as more nitrogen was accumulating and due to liquid water in the anode channels and in the GDL pores. At the lower purge fractions the liquid water was not being purged out. Water clogging the pores in the GDL and blocking the channels in the flow field plates act as a barrier to hydrogen mass transport to the anode catalyst sites. This leads to a decreased effective catalyst active area, and thus an increase in activation losses. This also increases the mass transport voltage losses leading to further voltage loss.

The source of the flooding was assumed to be due to a net flux of water to the anode via back diffusion due to a concentration gradient from the cathode to the anode. This occurs at higher current densities at which more water is produced from Reaction (1-3). Janssen and Overvelde were able to draw some general conclusions about water transport for a low temperature PEMFC (~60^{0}C) operating on dry hydrogen. The net flux of water for such conditions was very high from the cathode to the anode [77]. The occurrence of such phenomenon is supported in Figure 38. Water in the anode outlet gas, as measured by the dew point temperature sensor, must have come from the cathode given that fresh hydrogen is supplied completely dry. Also, Figure 38 shows that relative humidity is higher at higher current density due to more product water being produced at higher currents. The possibility of water vapor super-saturating and condensing in the anode channels was disregarded, and was rationalized as follows. Figure 38 presents the anode outlet relative humidity and calculated inlet relative humidity as a function of Fp at 140 mA/cm^2, 570 mA/cm^2 and 920 mA/cm^2. The outlet relative humidity never exceeded 90%. The calculated inlet relative humidity was on average 50% lower than the outlet because fresh

hydrogen was supplied completely dry. In addition, the actual inlet relative humidity was assumed to be even lower than that calculated because some of the liquid water seen exiting the purge line was probably due to vapor condensation on contact with fittings in the anode outlet. Also, the temperature of the fresh hydrogen stream and the temperature at the recirculation pump outlet confirmed that water vapor exiting the recirculation pump would not condense.

The voltage degradation was reduced to 4.1 mV when the purge was increased to Fp=0.5. At this purge a fresh hydrogen savings of 40%, when compared to the ideal case of Fp = 1.0, was accomplished. Given the results, it was decided to conduct Phase 2 tests at Fp_{min2} =0.5 at 570 mA/cm^2.

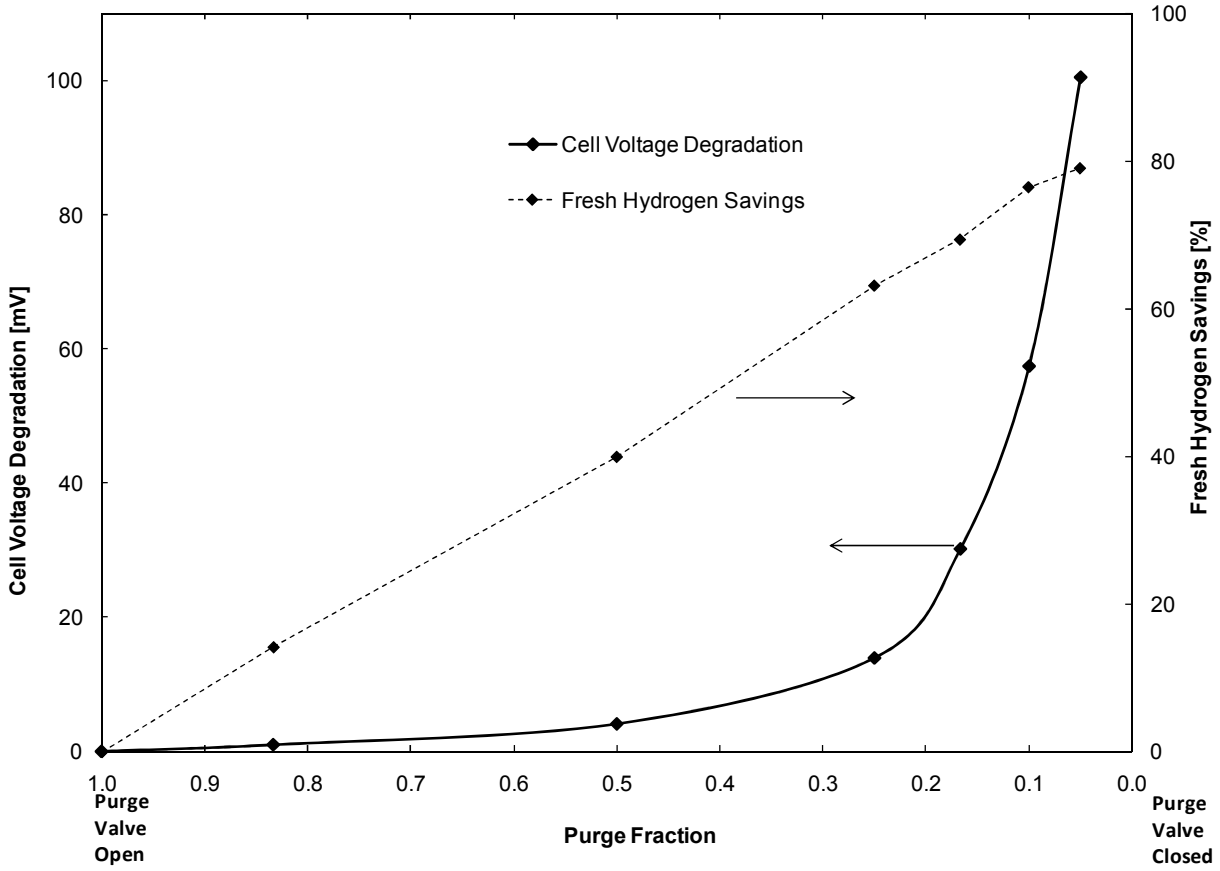

Figure 36: Cell voltage degradation (left) and fresh hydrogen savings (right) as a function of anode purge fraction for a current density of 570 mA/cm^2.

High Load Condition

Figure 37 depicts the effect of Fp on the cell voltage for an even smaller range of purge ($1.0 \geq Fp \geq 0.71$) at 920 mA/cm^2. The purge before which the stack shutdown (Fp_{min1} =0.71) was significantly higher compared to the lower current densities, but the cell voltage at this purge decreased by only 2.1 mV. Given that the nitrogen concentration in the anode channels was probably quite low at this purge and that the anode stoichiometric ratio was 4.6 at Fp = 0.71, the

results would indicate that nitrogen buildup was not causing the stack shutdown at Fp < 0.71. Liquid water in the anode channels and in the GDL pores was assumed to be the sole cause of the voltage loss that resulted in the stack shutdown. Again, the source of the flooding was assumed to be due to backdiffusion of water. However, due to increased water production at a higher current density of 920 mA/cm^2 the flooding occurred at a higher purge fraction than the case of 570 mA/cm^2.

The possibility of water vapor super-saturating and condensing in the anode channels was disregarded for the same reasons explained previously (Figure 38).

Accordingly, because of flooding at Fp< 0.71, Phase 2 testing at 920 mA/cm^2 would be constrained to a small range of Fp ($1.0 \geq Fp > 0.71$).

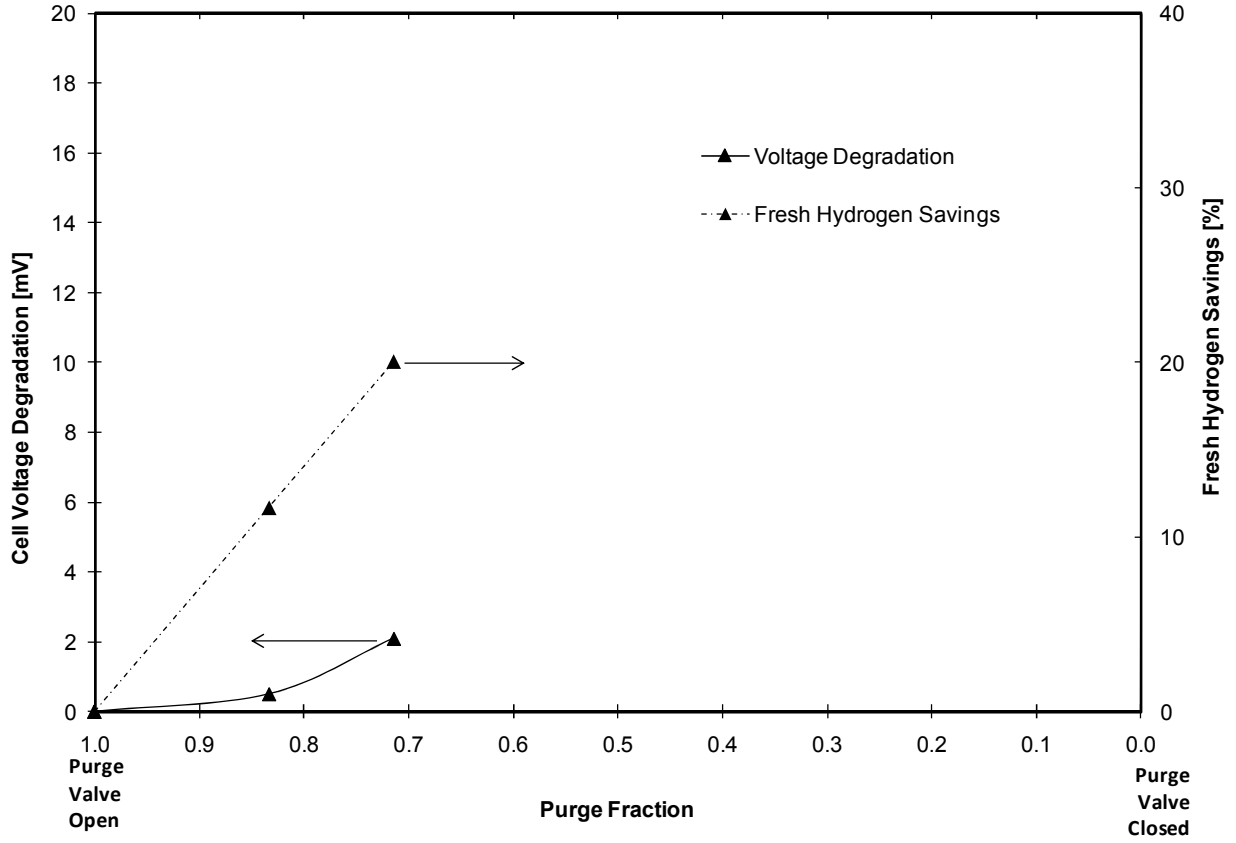

Figure 37: Cell voltage degradation (left) and fresh hydrogen savings (right) as a function of anode purge fraction for a current density of 920 mA/cm^2.

For the experiments conducted in Phase 1 and the upcoming experiments in Phase 2, the gas chromatography instrument used was unable to measure the nitrogen and carbon monoxide in the anode circuit. Gas samples of the anode outlet gas were taken and analyzed for the concentration of N_2 and CO. The concentration of nitrogen in the anode stream was too low for the GC to detect (i.e. there was no peak for nitrogen in the chromatograph). For the lower purge fractions at 570 mA/cm^2 and 920 mA/cm^2 a minute peak for CO was seen in the chromatograph after 10 hours but the peak area and the resulting CO concentration was too low to report with any confidence. Figure 31 shows that the GC could detect the concentration of CO down to approximately 2 ppm with confidence. Therefore it was assumed that the CO concentration in

the recirculation stream was below 2 ppm for the tests studied.

It was however assumed that nitrogen and carbon monoxide contents increased with a decrease in purge. The trend of increasing RH with decreasing purge in Figure 38 helps validate this assumption. In effect, the increasing partial pressure of water was the result of water vapor accumulation due to recirculation.

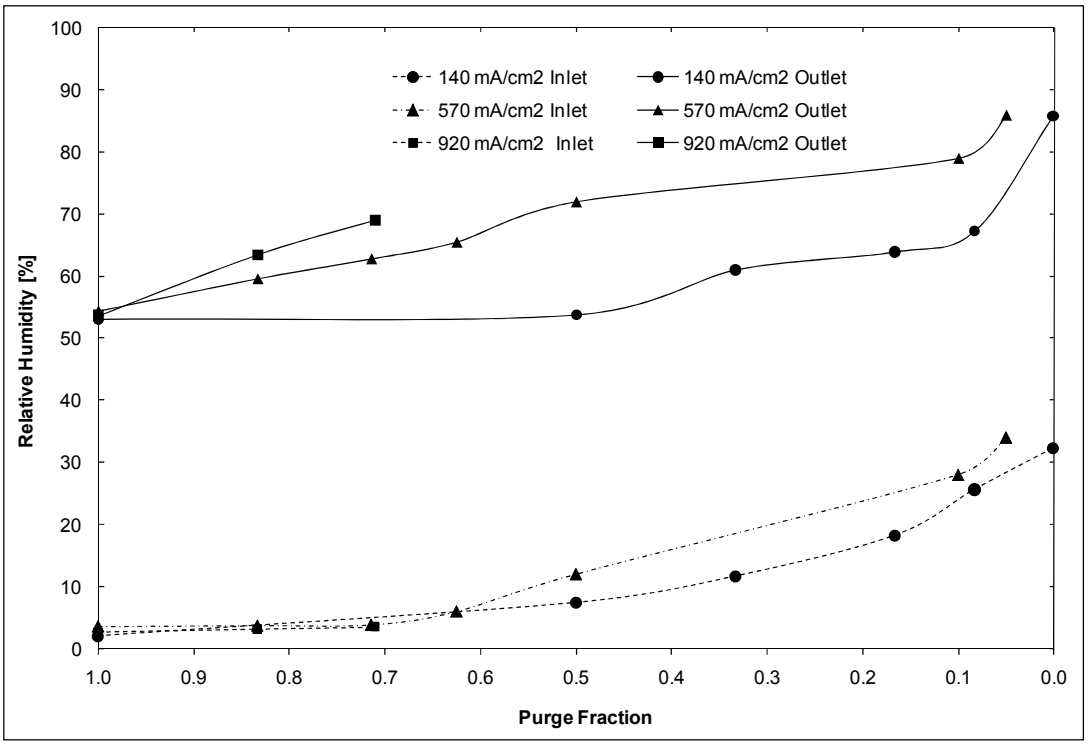

Figure 38: The effect of purge fraction on the relative humidity of the anode outlet (solid) and anode inlet (dotted) gas for current densities 140 mA/cm^2, 570 mA/cm^2, and 920 mA/cm^2.

Table 6 shows a summary of the values of Fp_{min1}, and Fp_{min2} discussed above. For the Fp_{min2} values selected at each current density, the voltage degradation was 5 mV or less and the fresh hydrogen savings was greater than 20%. In the presence of carbon monoxide in the fuel the voltage degradation was expected to be greater so Phase 2 tests would be conducted using $Fp \geq Fp_{min2}$.

Table 6: Summary of the results of Fp_{min1} and Fp_{min2} from Phase 1 tests.

Current Density	Fp_{min1}	Fp_{min2}
140 mA/cm^2	0.001	0.05
570 mA/cm^2	0.05	0.50
920 mA/cm^2	0.71	0.71

3.2 Phase 2 - Effect of Carbon Monoxide in the Anode Fuel

The allowable concentration of 0.2 ppm carbon monoxide in hydrogen fuel for a PEMFC was based on a stack operating in flow through mode [35] so an obvious extension is to evaluate the effect would be for a stack operating with a recirculating anode. As such, the objective of Phase 2 was to determine the effect of purge on the cell voltage when 0.2 ppm carbon monoxide was present in the fuel supply.

3.2.1 Effect of Stack Recovery Procedure

In an effort to start the stack from the same operating state for each test, the stack recovery procedure outlined in Section 2.9.2 was performed before each test. The purpose of the recovery procedure was to remove the remaining CO that was adsorbed on the catalyst from the previous test. The procedure involved forcing air through the anode channels and then purging it with nitrogen. It was performed when the stack was shut down, discharged and at ambient temperature and pressure.

The effectiveness of introducing air to the anode (referred to as "air bleed") was studied by comparing the cell voltage when the stack recovery was performed to the cell voltage when no recovery was performed. For this discussion the former test will be referred to as Test A, and the latter, Test B. Both tests were conducted at identical operating states and were initiated after the stack was running at 920 mA/cm^2, 0.2 ppm CO/H_2, Fp = 0.83 and for 10 hours. Figure 39 shows the effect of the recovery procedure. Over the 1 hour test, the current density was stepped from 140, to 570 and finally to 920 mA/cm^2. Neat hydrogen was supplied at the fuel and the purge valve was open for the duration of the test. In general, the cell voltage for Test A was higher than that for Test B. At 140 mA/cm^2 the cell voltage of Test A was actually 1.4% lower than Test B but close attention to Figure 39 shows that Test A actually initiated at a cell voltage 1.4% lower than Test B. As the current density increased the cell voltage for both tests are near identical until 400 mA/cm^2 where the cell voltage of Test A is noticeably higher. At 570 mA/cm^2 the voltage of Test A was 6.1% higher than Test B and at 920 mA/cm^2 it was 14.7% higher. It was assumed that oxygen from air electro-oxidized CO to CO_2 during the recovery procedure so hydrogen coverage and electrooxidation was greater in Test A than in Test B. The higher performance of Test A demonstrated the effectiveness of the recovery procedure in reversing CO poisoning from a previous test. Due to this recovery technique each test started at the same initial cell voltage.

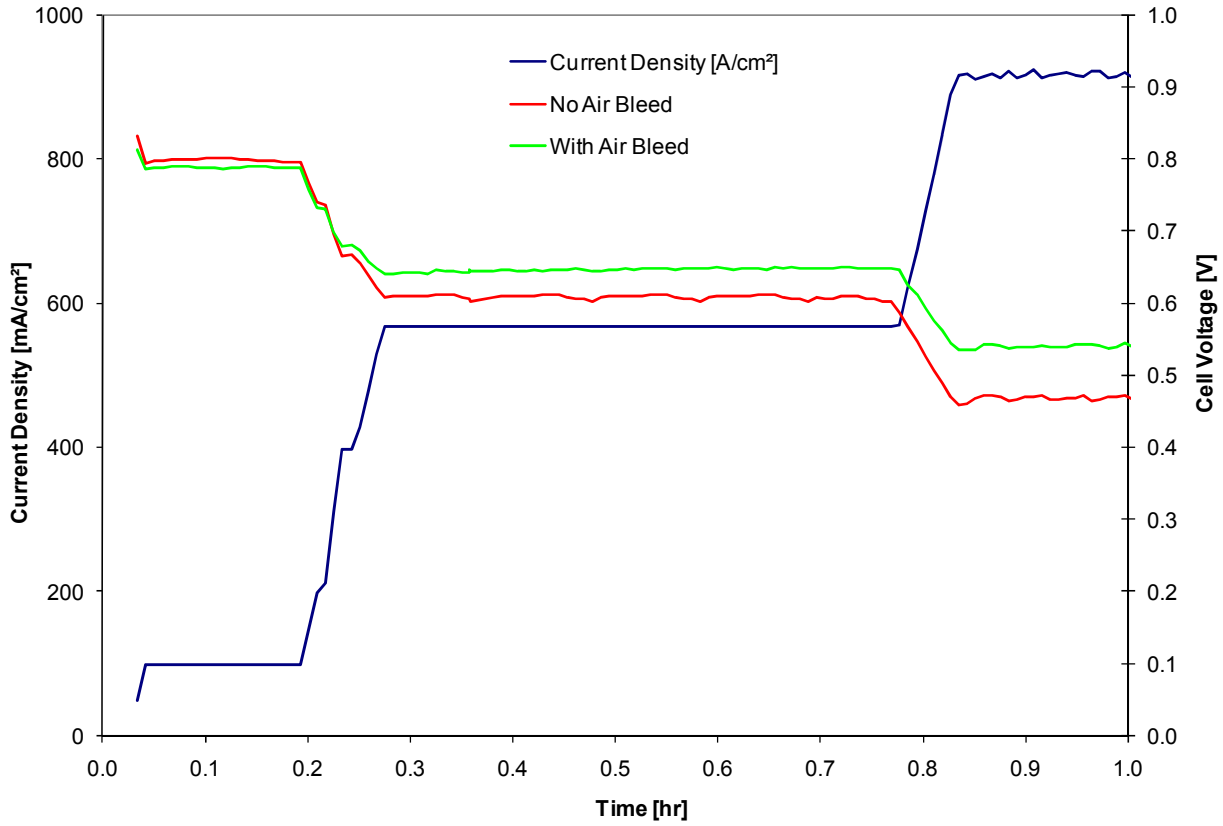

Figure 39: The effect of the stack recovery technique on the cell voltage over the range of current densities tested.

3.2.2 Effect of Carbon Monoxide Concentration

The first set of experiments performed in Phase 2 assessed the impact of the concentration of CO in the hydrogen fuel gas. Figure 40 presents the effect of CO concentration (0.0, 0.2 and 0.5 ppm) in the fresh H_2 fuel on the cell voltage degradation for Fp = 0.08 at 140 mA/cm^2, Fp = 0.63 at 570 mA/cm^2 and Fp = 0.83 at 920 mA/cm^2. Fp_{min2} values from Table 6 caused the stack to shutdown so the higher Fp values just mentioned were used as the minimum purge fraction for testing. The cell voltage degradation was calculated in the same manner as in Phase 1, but over 10 hours rather than 20 minutes. Each data point represents the data from one test only, in other

words they are not the average of repeated tests. The results show less than 5 mV voltage loss for 0.0 ppm CO/H_2 for all current densities. This information is useful in the upcoming analysis when characterizing voltage loss as the result of the combined effects of N_2 concentration and CO poisoning.

At 140 mA/cm^2, Figure 40 shows a voltage degradation of 17 mV for 0.2 ppm CO/H_2 and 18 mV at 0.5 ppm. 570 mA/cm^2 shows a much higher voltage degradation of 162 mV for 0.2 ppm CO/H_2 and 198 mV at 0.5 ppm. Finally, at 920 mA/cm^2 the curve shows a voltage degradation of 171 mV for 0.2 ppm CO/H_2 and 201 mV at 0.5 ppm.

The trend of increasing voltage degradation with increasing CO concentration in the fuel was expected since at higher CO concentrations more CO is available to preferentially adsorb onto the anode catalyst sites leaving fewer sites available for the adsorption and electrooxidation of hydrogen. It is reasonable to assume a constant IR drop and a constant overpotential at the cathode at a given current density so that the change in cell voltage reflects the anode overpotential due to the competing reactions of CO and H_2 adsorption at the catalyst sites.

The trend of increasing voltage degradation with increasing current density occurred because CO adsorbs strongly to platinum at lower potential and therefore higher current density [49]. Also at higher current density there is more CO injected into the anode stream (so more absorbs on the catalyst), and a greater fraction of the catalyst is required to sustain the current, so fewer anode catalyst sites are available for hydrogen electrooxidation.

When comparing the voltage degradation at 570 mA/cm^2 and 920 mA/cm^2 it can be seen that the results are close in value. It was thought that the CO coverage at these two current densities was close in value. This phenomenon was demonstrated by Ahluwalia et al. who showed isotherms for carbon monoxide adsorption on the platinum electrocatalyst when 1 ppm CO was present in the hydrogen fuel. The fractional CO coverage at 500 mA/cm^2 was 0.7 and this increased to

almost 0.8 as the current density approached 1000 mA/cm^2 [49]. Therefore, doubling the current density only resulted in a 10% increase in CO coverage.

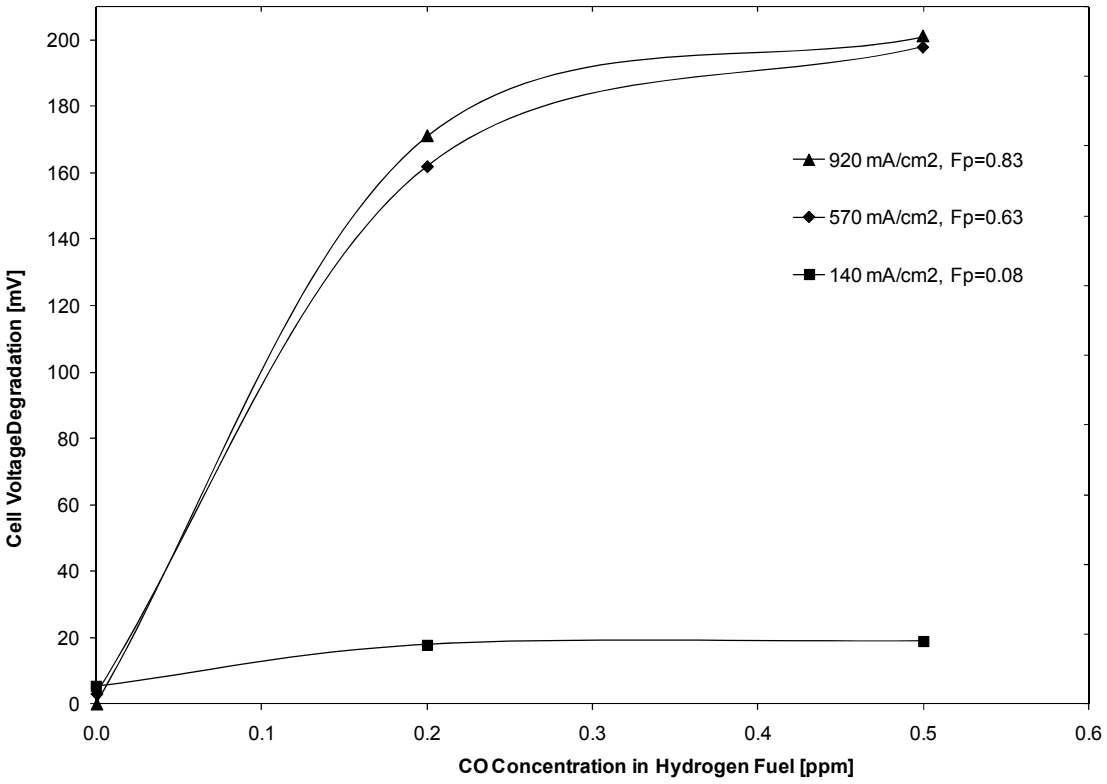

Figure 40: The effect of CO concentration in hydrogen fuel on the cell voltage degradation after 10 hours for a current density of 140 mA/cm^2, 570 mA/cm^2 and 920 mA/cm^2. The Fp for each current density was the lowest purge of the purge fractions tested.

In the context of the individual cell voltages in the stack rather than the average cell voltage, only at 920 mA/cm^2 there was significant non-uniformity in the cell voltages observed. Figure 41 shows the voltage-time curves for Cell 1 to 10 at 920 mA/cm^2, Fp = 1.0 and for neat hydrogen. For the entire 10 hour test, the voltage of Cell 1 was 46.4 mV (or 8.0%) lower than the average

voltage of Cell 2 to 10. This was rationalized as follows. The hot reactant gases enter the stack at the wet-end endplate, which is adjacent to cell 10. Cell 1 is adjacent to the dry-end endplate which acts as a heat sink. Therefore there is a temperature gradient from Cell 10 to Cell 1, with Cell 1 having the lowest operating temperature. The lower voltage of Cell 1 compared to the other Cells is a result of the lower temperature which results in slower reaction kinetics, decreased diffusion mass transport and decreased ionic conductivity of the membrane.

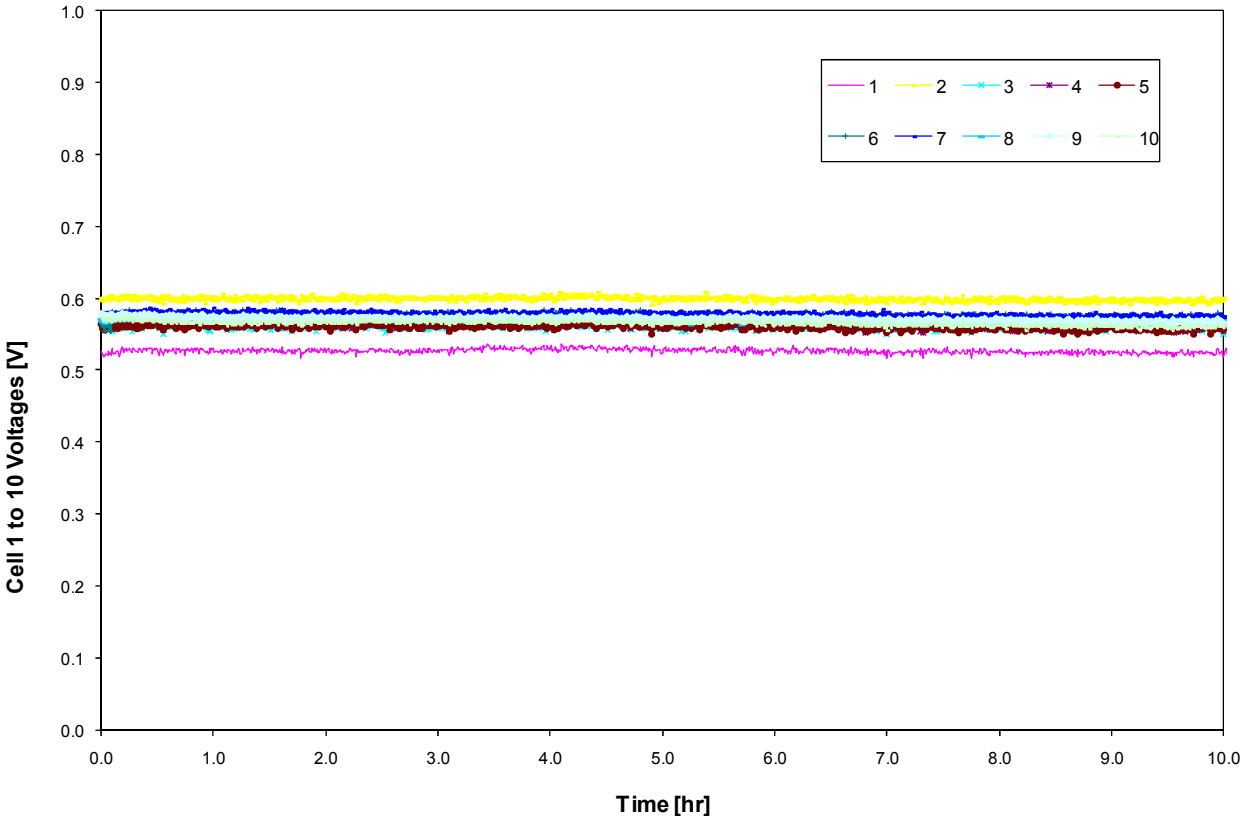

Figure 41: Voltages for Cells 1 to 10 over 10 hours at 920 mA/cm^2, Fp = 1.0 and for neat hydrogen. Cell 1 voltage is on average 46.4 mV (or 8.0%) lower than the average voltage of Cell 2 to 10.

3.2.3 Effect of Purge

In the following analysis, the trend of decreasing cell voltage with decreasing purge will be observed. This correlation was assumed to be the result of increasing CO concentration in the anode gas with decreasing Fp. Figure 40 helped to validate this assumption given that an increase in CO concentration in the fuel definitely caused a decrease in the cell voltage.

Figure 42 presents the effect of Fp on cell voltage over 10 hours at a current density of 570 mA/cm^2 for 0.2 ppm CO/H_2. The temperature was 63^0C, the anode inlet pressure was 9.7 kPag, and as seen at time t=0 the cell voltage for all curves was 0.66 V, since before this time neat hydrogen was being supplied and Fp = 1.0. For neat H_2 at Fp = 0.63, the voltage-time curve was noticeably linear, representing a voltage degradation of only 3 mV over 10 hours. From this result it was concluded that nitrogen buildup did not significantly penalize the cell performance in the range of Fp tested at 570 mA/cm^2. In other words the degradation due to nitrogen is less than 2% of the total degradation observed. As such in the following analysis at 570 mA/cm^2, the voltage loss was attributed to the accumulation of CO in the fuel cell stack. Figure 43 is analogous to Figure 42 but presents a current density of 920 mA/cm^2 at 63^0C, 16.6 kPag and a cell voltage of 0.54 V for all curves at t = 0. For neat H_2 at Fp =0.83, there was no voltage degradation so the effect of hydrogen dilution by nitrogen was neglected for the range of Fp tested.

Whereas dilution did not degrade cell performance in the absence of CO at the range of purge fractions in Phase 2, as can be seen in Figure 42 and Figure 43 the voltage loss under the same conditions is large when CO is present. At t = 0, 0.2 ppm CO/H_2 started being supplied to the anode. As expected, the slope of these curves was negative compared to that measured with neat H_2. The results show that the voltage degradation for all Fp accelerated with time. As one example in Figure 42, at Fp = 0.63 the voltage degradation rate was 3.8 mV/hr over the first 4 hours and 30.8 mV/hr in the last 4 hours. This phenomenon was rationalized as follows. It was

expected that over time CO accumulated in the anode due to recirculation. The extent of this build-up was however not known. In addition to this, in the initial hours of testing CO coverage was primarily distributed over the catalyst sites closest to the gas diffusion layer. The flux of CO in the catalyst layer is at least two orders of magnitude smaller than the flux of H_2 at a current density of 100 mA/cm^2 and greater [78]. With such a configuration, H_2 that diffused through the catalyst layer could adsorb onto, and react with the catalyst sites near the membrane. As time progressed, CO coverage approached sites closer to the membrane. This had an amplifying effect on the voltage loss for a few reasons:

(i) there were fewer sites for hydrogen adsorption and electrooxidation in total;

(ii) the membrane started with excess catalyst, so some of this excess buffered the initial degradation rate until these excess sites were covered;

(iii) even if active sites were available, CO coverage limited hydrogen diffusivity in the anode catalyst layer or hydrogen had to diffuse further to reach these sites; and

(iv) such a distribution had a more severe effect on the anode overpotential than when CO mainly adsorbed onto catalyst sites near the gas diffusion layer because the catalyst sites near the membrane play a more crucial role in determining the electrode performance in that these sites are more active then sites further from the membrane [79].

Furthermore a decrease in the purge was seen to have a negative effect on the cell voltage. At 570 mA/cm^2 (Figure 42) the voltage loss was 162 mV at the lowest purge (Fp = 0.63). By increasing the purge (Fp = 0.83 and 0.71) the voltage loss was reduced to 135 mV and at Fp = 1.0 the voltage loss was further reduced to 96 mV. The similar degradation trends at Fp = 0.83 and 0.71 would indicate that the CO concentration was nearly equal at these two purge fractions. Compared to the hypothetical case of Fp = 1.0, a fuel savings of 12, 15, 21% could be achieved by reducing the purge to Fp = 0.83, 0.71, and 0.63, respectively. At 920 mA/cm^2 (Figure 43) a voltage loss of 178 mV occurred when Fp = 0.83. This voltage loss was reduced to 155 mV

when Fp = 1.0, but at the cost of a 13% increase in fuel requirement. The trend of decreasing voltage at lower purge fractions was due to an increase in CO concentration as less gas is purged.

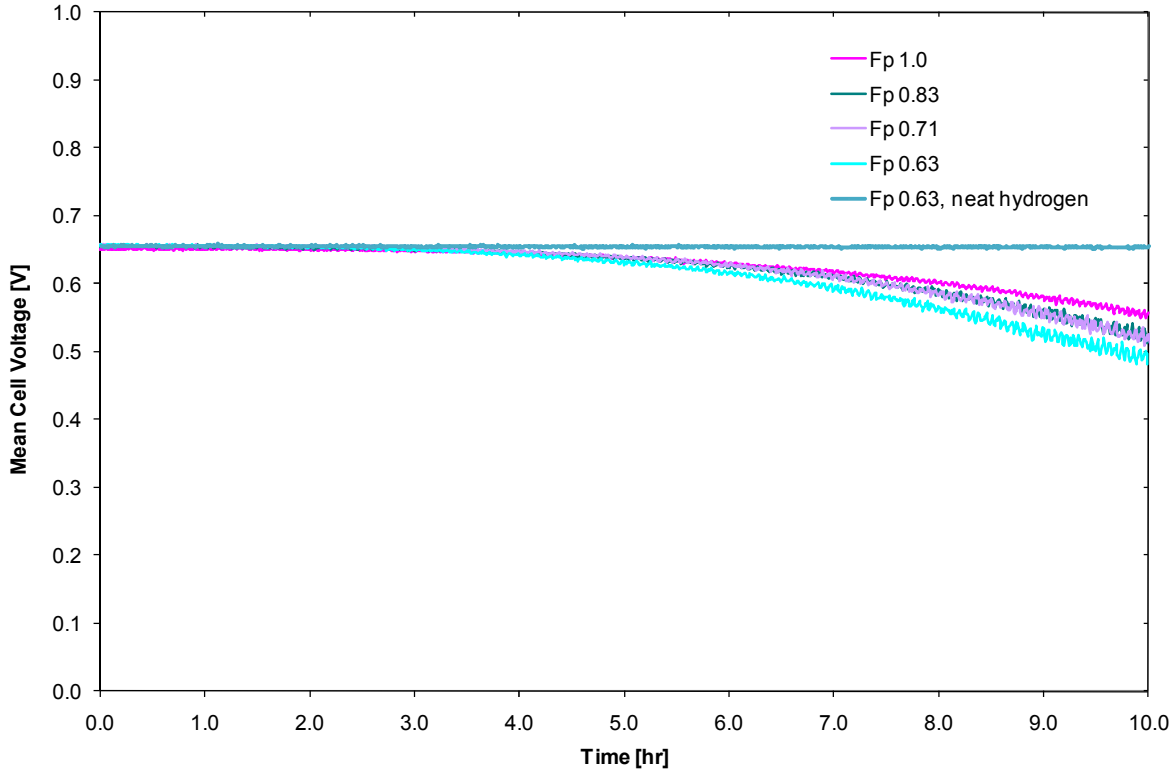

Figure 42: The effect of purge fraction on the stack mean cell voltage for a current density of 570 mA/cm^2 for 0.2 ppm CO/H$_2$. At Fp = 1.0, 0.83, 0.71 and 0.63, a voltage loss of 96, 133, 138, 162 mV was observed, respectively.

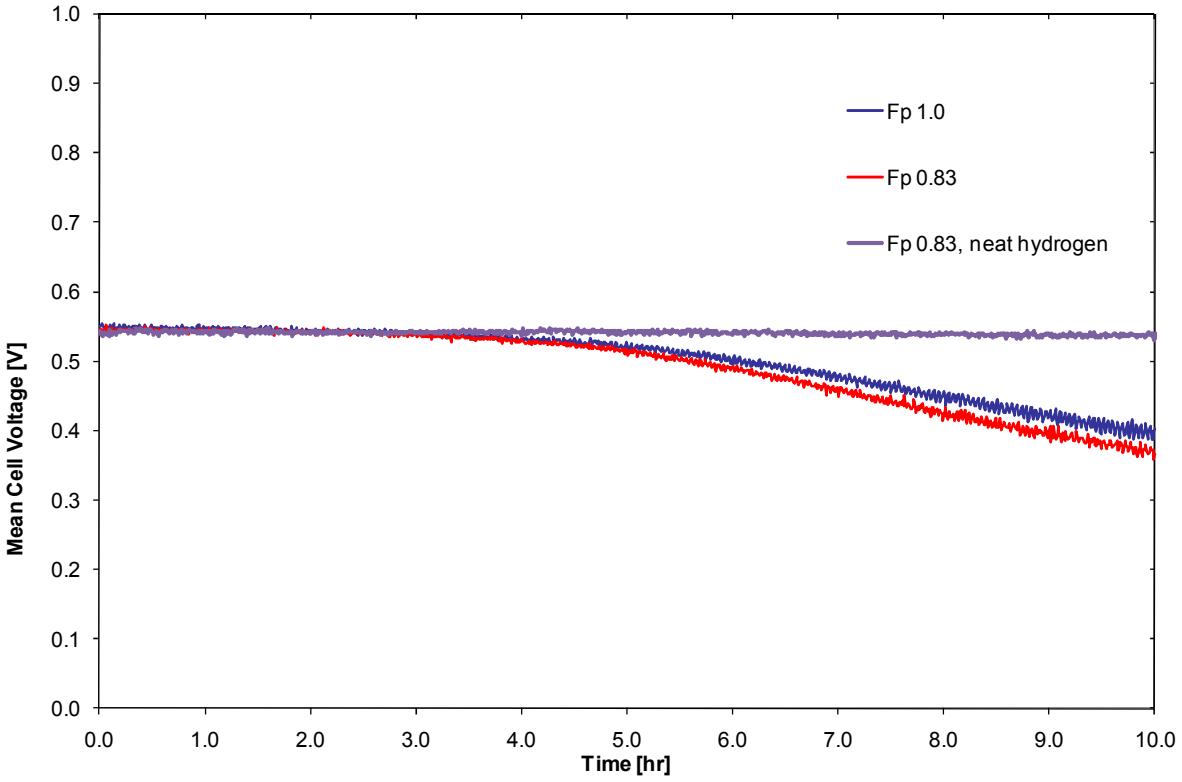

Figure 43: The effect of purge fraction on the stack mean cell voltage for a current density of 920 mA/cm^2 for 0.2 ppm CO/H_2. At Fp=1.0, 0.83, a voltage loss of 155 and 178 mV was observed, respectively.

When comparing the voltage loss of 133 mV at 570 mA/cm^2 and 178 mV at 920 mA/cm^2 for the same purge and CO concentration (Fp = 0.83 and 0.2 ppm CO/H_2), the greater voltage loss at 920 mA/cm^2 was likely the result of two phenomena:

(i) CO adsorbs strongly to platinum at lower potential and therefore higher current density;

(ii) greater mass transfer limitations in that more sites (i.e. deeper into the catalyst layer) are required and involved in the reaction.

Close attention to Figure 43 shows that the cell voltage for the curve of Fp = 0.83 is below 0.4 V near the end of testing. Recall that at a cell potential of ~ 0.3V, the elimination of adsorbed CO

can occur by the electrooxidation of CO to CO_2 via reactions shown earlier. Figure 44 depicts the minimum cell voltage over the last two hours of testing for the same curve just mentioned (i.e. 920 mA/cm^2, 0.2 ppm CO/H_2 and Fp = 0.83). The minimum cell voltage was chosen because it was of interest to see if any of the 10 cells in the stack were in the voltage range where CO can be oxidized. Indeed, the voltage did approach 0.3V in the last two hours of testing.

In the case that CO oxidized to CO_2 at some of the anode electrodes, higher reaction rates for hydrogen adsorption and electrooxidation would result. As such, the increase in hydrogen electrooxidation would effectively lower the anode overpotential to maintain the same current density, thus approaching a potential where CO can no longer be oxidized [55]. This adsorption, desorption, readsorption of CO repeats, resulting in the voltage oscillating [60]. Perhaps, such voltage oscillations contributed to the erratic voltage behavior observed in Figure 44. However, it should be kept in mind that cell measurements only provide the summation of the overpotential at the anode and cathode, and therefore an exact interpretation seems to be speculative. Also there may be a potential gradient in the electrode as it approaches the membrane electrolyte (i.e. as a result of less IR drop for the protons), but this could not be measured in this work.

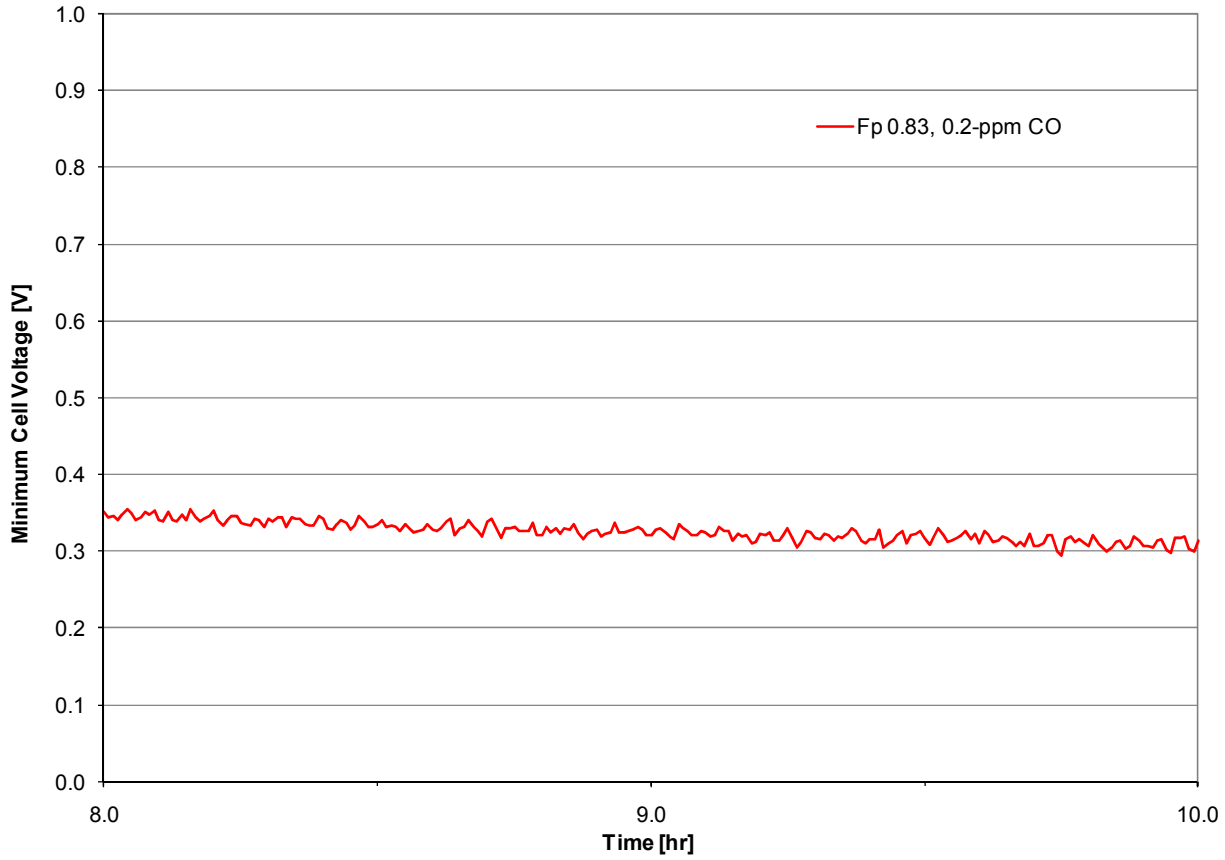

Figure 44: Minimum cell voltage for the last 2 hours of testing for a current density of 920 mA/cm^2, 0.2 ppm CO/H_2 and Fp = 0.83.

The effect of purge on the cell voltage at a current density of 140 mA/cm^2 is discussed separately because the performance losses were far less dramatic than at the higher current densities. Figure 45 demonstrates the effect of Fp on the cell voltage over 10 hours when 0.2 ppm CO/H_2 was supplied at a current density of 140 mA/cm^2. The cell voltage decreases for Fp = 0.5, 0.33, 0.16 and 0.08 was 16, 19, 13 and 17 mV, respectively. Note that the cell voltage is approximately the same for all Fp, so it appears that there is only one horizontal line in Figure 45. Voltage losses as low as these were expected since CO adsorption is weaker at higher potentials (i.e. lower current densities), there is simply less CO injected into the stream (so there is less CO to absorb on the

catalyst), and the fraction of catalyst in use is less, so there remains enough catalyst for hydrogen electrooxidation at this low current density. Also, it was expected that mass transfer polarization was negligible at this low current density. Regarding the fuel savings at these purge levels, a decrease in purge from Fp = 0.5 to Fp = 0.08 results in a 59% reduction in hydrogen fuel requirement. So from the point of view of the minimal effect of 0.2 ppm CO/H_2 on the stack voltage, there is incentive to decrease the purge at low current densities further to effectively increase fuel efficiency.

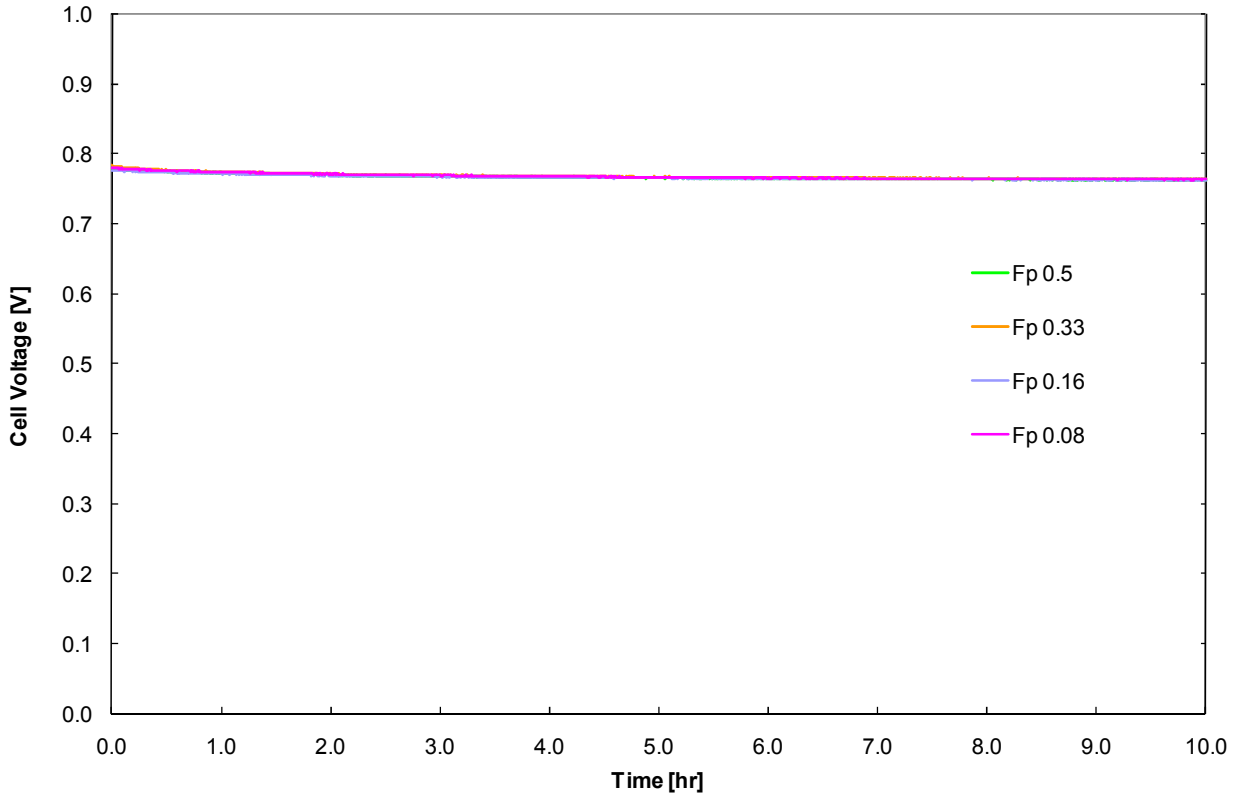

Figure 45: The effect of purge fraction on the cell voltage when 0.2 ppm CO/H_2 is supplied to the anode at a current density of 140 mA/cm^2. At Fp=0.5, 0.33, 0.16 and 0.08, a voltage loss of 16, 19, 13 and 17 mV was observed, respectively. Note that the cell voltage is approximately the same for all Fp, so it appears that there is only one horizontal line.

3.3 Carbon Monoxide Poisoning Mitigation and Recovery Techniques

3.3.1 Effect of Temperature

It was well supported in this study and in the literature that at low temperatures (< 80^{o}C), trace levels of CO can cause significant voltage degradation in a PEMFC. Jiang et al. explained that higher temperatures could effectively reduce CO coverage on the catalyst by promoting CO oxidation with an OH adsorbed group [70]. Figure 46 shows the effect of an increase in temperature from 65^{o}C to 75^{o}C on the cell voltage degradation for two scenarios:

(i) neat hydrogen and,

(ii) 0.2 ppm CO/H_2.

The result for 0.2 ppm CO/H_2 is also presented normalized with the degradation due to N_2 crossover subtracted. The normalized data for 0.2 ppm CO/H_2 degradation was calculated by subtracting the cell voltage degradation value when neat hydrogen was supplied from the cell voltage degradation value when 0.2 ppm was supplied. Given that performance typically increases with temperature (for reasons discussed in Section 1.4.3), the normalized data was calculated to show the effect of temperature on CO poisoning only. As shown in Figure 46, when the anode was fed hydrogen containing 0.2 ppm CO and Fp = 0.71, the voltage degradation decreased by 28 mV when the temperature was increased from 65^{o}C to 75^{o}C. This is comparable to the 27 mV voltage increase that was achieved by increasing the purge at 570 mA/cm^2 from Fp = 0.63 to Fp = 0.71 (Figure 42). However, the increase in purge resulted in an 8% increase in fresh hydrogen feed requirement. Accordingly, there is definitely an incentive to operate at higher temperatures given that with a temperature increase of 10 ^{0}C, the same voltage was achieved at a lower purge resulting in a higher fuel efficiency.

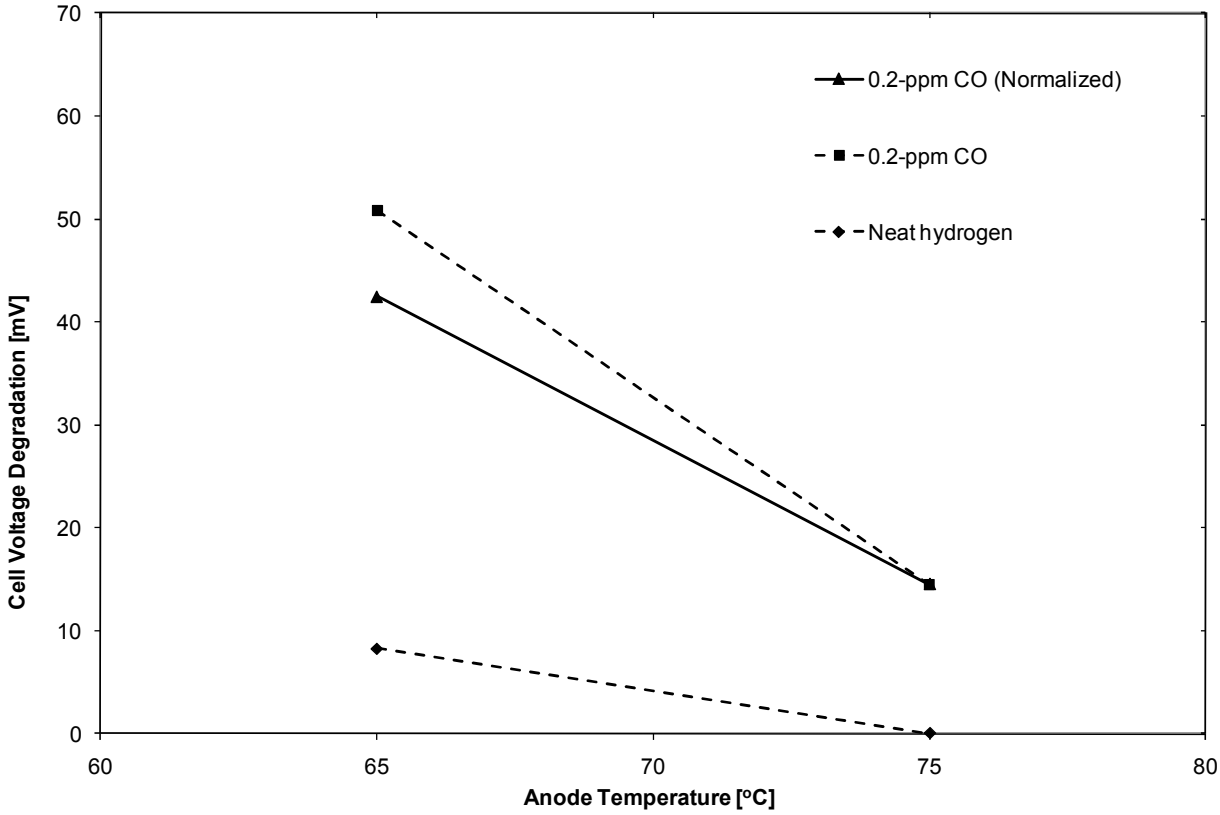

Figure 46: The effect of anode temperature on cell voltage for a current density of 570 mA/cm^2. When the anode was fed hydrogen containing 0.2 ppm CO and Fp =0.71, the voltage degradation decreased by 28 mV when the temperature was increased from 65^{o}C to 75^{o}C

3.3.2 Effect of Switching to Neat Hydrogen

Figure 47 shows the effect of switching from 0.2 ppm CO/H_2 to neat hydrogen on the cell voltage for a current density of 920 mA/cm^2 and Fp = 0.83. In the first 10 hours when 0.2 ppm CO was being supplied the voltage decreased by 164 mV. At t =10 hours, neat hydrogen was supplied and the voltage recovered by 104 mV. An interesting observation was that when the fuel gas was switched, the recovery process proceeded faster than the poisoning process. The reason the recovery was not even faster was probably because CO was still present in the anode

gas stream due to recirculation. Had the test run longer, it was expected that the voltage would have eventually fully recovered.

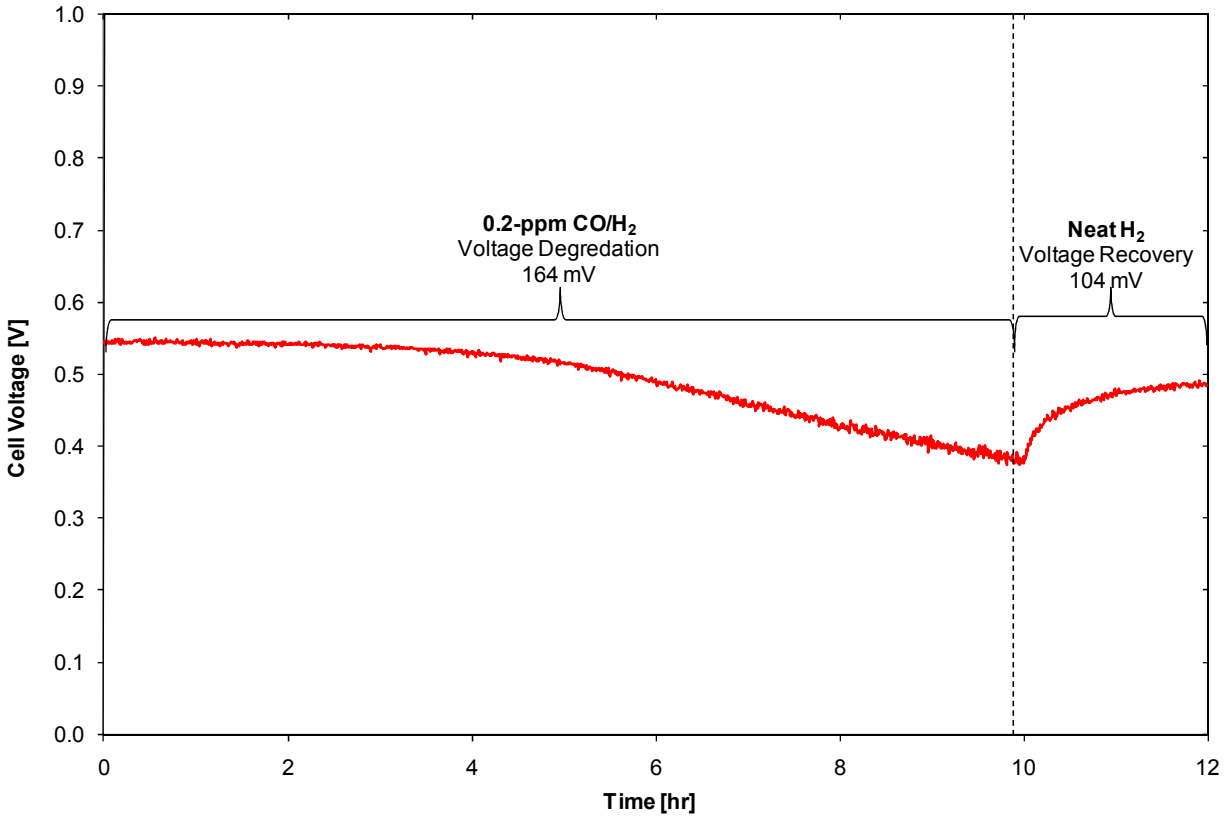

Figure 47: The effect of switching from 0.2 ppm CO/H_2 to neat hydrogen on cell voltage for a current density of 920 mA/cm^2 and Fp =0.83. In the first 10 hours when 0.2 ppm CO was being supplied the voltage decreased by 164 mV. At t =10 hours, neat hydrogen was supplied and the voltage recovered by 104 mV.

3.3.3 Effect of Switching to a Higher Purge Fraction

Figure 48 shows the effect of increasing the purge on the cell voltage for a current density of 920 mA/cm^2 and 0.2 ppm CO/H_2. The left vertical axis represents the cell voltage over the 13 hour test and the right vertical axis represents the purge fraction. At t =10 hours, the purge was

switched from Fp =0.83 to Fp =1.0 but the feed remained at 0.2 ppm CO/H_2. Close examination of Figure 48 shows that after the purge fraction is increased, the voltage continues to decrease but the voltage degradation rate decreases. Two hours prior to switching Fp the voltage degradation rate was 18.4 mV/hr. After the switch, the cell voltage continued to drop but the degradation rate was much lower (6.8 mV/hr).

In comparing these last two techniques, switching to neat hydrogen definitely resulted in a faster recovery from CO poisoning. However this technique is not practical for portable PEMFC applications, whereas increasing the purge rate is practical and easy to execute, but this only decrease the degradation, this method does not lead to voltage recovery.

When operating with a recycle stream there is a clear point where degradation can be observed, and this point is a couple of hours before degradation accelerates to a higher rate. This indicates that online diagnostic testing may be feasible in that voltage degradation can be observed, and mitigation action taken (e.g. increasing purge fraction to lower the rate of degradation, or a short air bleed for recovery) prior to the most significant impact taking place on overall performance.

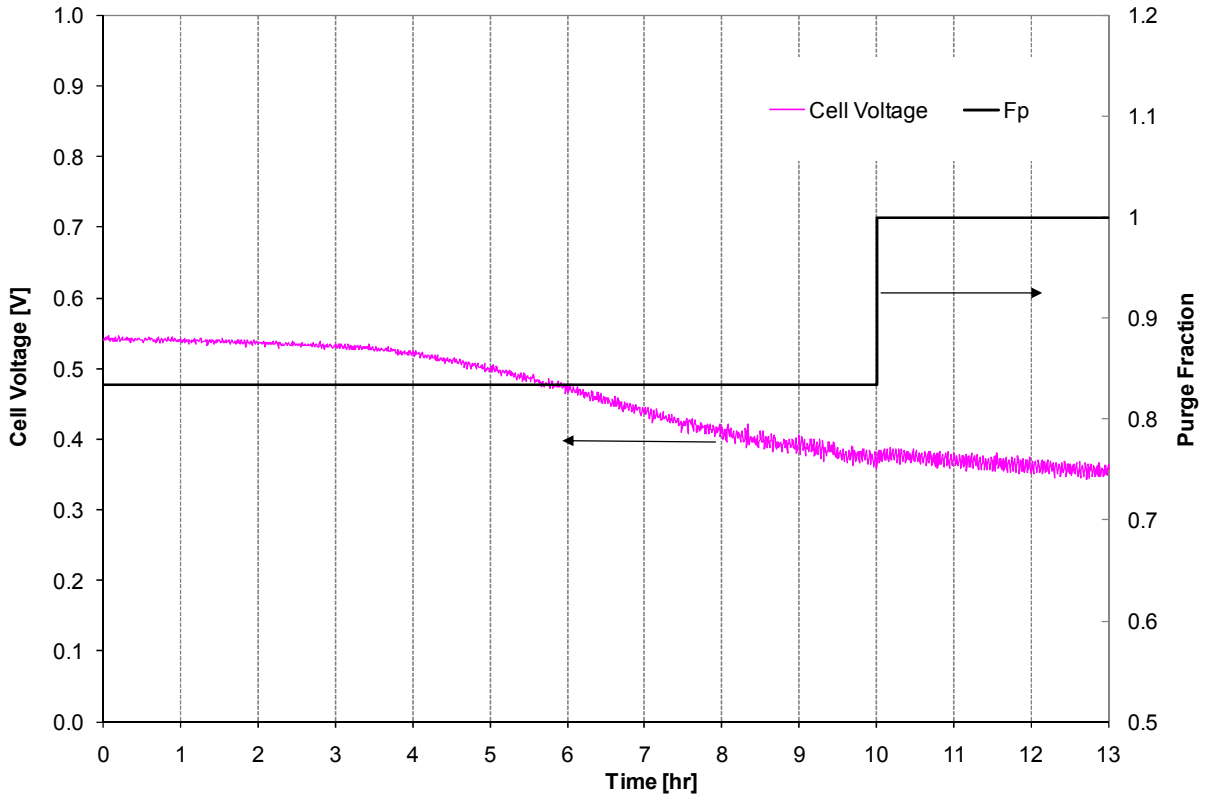

Figure 48: The effect of switching the purge from Fp =0.83 to Fp =1.0 on cell voltage for a current density of 920 mA/cm^2 and 0.2 ppm CO/H$_2$. At t =10 hours, the purge valve was opened and remained open for the duration of the test (i.e. Fp =1.0) causing a decrease in the voltage degradation rate.

Chapter 4 - Conclusions and Recommendations

4.1 Conclusions

For fuel cells to flourish commercially they must provide a clean, energy-efficient technology that performs comparably, if not better than, the current technologies and at a comparable cost. However, the technical issues that constrain fuel cells from prevailing must first be overcome. This work addressed the critical issue of the effect of the anode stream purge on the performance of a PEMFC operating with a recirculating anode. This issue is critical for fuel cell operation for the foreseeable future where the majority of hydrogen will originate from fossil fuel reformation, and thus likely to contain trace levels of CO. Specifically, studies that examined the effect of the purge fraction on the cell voltage were performed.

This study was undertaken on a shortened stack based on the Hydrogenics 8kW Hydrogen Fuel Cell Power Module (HyPM® HD8) stack, and the purge rate simulated the actual power module system operation. Like most fuel cell systems, the HyPM HD8 utilizes an anode recirculation system which recycles the anode outlet stream to the anode inlet. Such an arrangement not only increases the fuel efficiency but also permits dry fuel supply since water vapor, evaporating from the membrane, in the anode gas is recycled thus humidifying the inlet gas. This has considerable benefits for a fuel cell system because the humidification system on the anode can be eliminated, saving both space and cost in the design of the balance of plant of a fuel cell system. Recirculation, however, can adversely affect PEMFC performance if impurities in the anode stream are allowed to enrich. The accumulation of impurities is controlled by continuously purging a portion of the anode outlet gas to the exhaust. Purging must be kept to a minimum because any unconsumed hydrogen will be lost irrecoverably, thus lowering the overall fuel efficiency.

Of the many impurities that adversely affect the anode performance, nitrogen and carbon monoxide were studied in this work. Nitrogen in the anode gas reduces the concentration of hydrogen. In this study, nitrogen present in the anode gas was the result of nitrogen crossing over the membrane from the cathode to the anode. In contrast, carbon monoxide was delivered to the anode in the fresh hydrogen fuel supply. Carbon monoxide poisons the anode by adsorbing onto the platinum catalyst sites and inhibiting hydrogen adsorption and electrooxidation. Carbon monoxide (CO) concentrations as low as 0.2 ppm have been shown to degrade the cell voltage. This poses a problem for the HyPM HD8 because hydrogen-rich fuel produced from reformation is the realistic future for systems used for transportation applications. Reformate may contain 0.2 ppm CO and furthermore, the concentration of CO in the anode gas can enrich beyond this level from the recirculation operation. Given that in practical situations the HyPM HD8 will be operating with anode impurities, it is critical to operate with an anode purge rate that minimizes the associated performance losses.

The experimental setup used in this work consisted of a fuel cell stack, anode recirculation balance of plant, and a Hydrogenics Fuel Cell Automated Test Station (FCATS). Together, these components mimicked the operation of the HyPM HD8 and permitted the manipulation of the purge and the measurement of all the desired parameters. The stack used in this work contained 10 cells, each with a surface area of 196.5 cm^2. The G-Series FCATS^{TM} encompassed custom options to operate the anode in dead end mode with the ability to manipulate the purge. The purge fraction (Fp) controls the time the purge valve is open and therefore the amount of gas exiting the anode outlet to the exhaust. Fp is defined as the ratio of the time the purge valve is open (t_{duty}) to the total cycle time. To mimic the operation of the HyPM HD8, t_{duty} was set constant at 500 ms for all current densities. A positive displacement pump connected between the anode outlet and anode inlet formed the anode recirculation loop. The recirculation flow rate was 6.5 lpm for all current densities and all Fp. A dew point sensor was connected at the anode outlet in order to calculate the relative humidity in the anode stream.

The objective of Phase 1 testing was to determine the effect of Fp on the average cell voltage when pure hydrogen fuel was fed to the anode. In this case the only impurity in the anode stream was nitrogen from crossover. Three current densities representing a low load condition (140 mA/cm^2), medium load condition (570 mA/cm^2), and high load condition (920 mA/cm^2) were tested and each experiment tested a different Fp. For each current density, the cell voltage, fresh hydrogen savings and anode relative humidity were plotted against Fp. Also, two key purge fractions, Fp_{min1} and Fp_{min2}, were determined (Table 7 displays the results of Fp_{min1} and Fp_{min2}). Fp_{min1} represented the minimum purge fraction that could sustain a voltage without the stack shutting down. Fp_{min2} represented the minimum purge fraction which avoided the excessive loss of hydrogen in the purge gas, while also avoiding the excessive buildup of nitrogen that results in a relatively higher voltage loss.

Table 7: Summary of the results of Fp_{min1} and Fp_{min2} from Phase 1 tests.

Current Density	Fp_{min1}	Fp_{min2}
140 mA/cm^2	0.001	0.05
570 mA/cm^2	0.05	0.5
920 mA/cm^2	0.71	0.71

Fp_{min2} was selected based on the average cell voltage degradation and fresh hydrogen savings at a given purge fraction. It was rationalized that a purge fraction resulting in a voltage loss too large did not merit testing in Phase 2 as the voltage loss would be far greater with CO present in the anode gas. However, a purge fraction too large resulted in a greater fresh hydrogen feed requirement. Based on these the optimum purge fraction (i.e. Fp_{min2}) was chosen. For the Fp_{min2} values selected at each current density, the voltage degradation was 5 mV or less and the fresh hydrogen savings was greater than 20%. In the presence of carbon monoxide in the fuel, the

voltage degradation was expected to be greater so Phase 2 tests would be conducted using $Fp \geq Fp_{min2}$.

Some general trends were observed with a decrease in purge at each current density in Phase 1 of the test program:

- The cell voltage decreased because of nitrogen accumulation in the anode stream. Nitrogen buildup leads to reduced mass transfer rates causing polarization and decreases the partial pressure of hydrogen which lowers the equilibrium cell potential.
- The anode outlet relative humidity increased due to water vapor accumulation owing to the increased recycle stream.

Trends observed as the current density increased included:

- Fp_{min1} and Fp_{min2} decreased because nitrogen accumulation amplified the effect of concentration polarization, which dominates at higher current densities.
- The anode relative humidity increased due to a greater net flux of water to the anode via back diffusion from the cathode, as happens when more product water is produced at higher currents. In fact, the relatively high value of Fp_{min1} =0.71 at 920 mA/cm^2, was expected to be the cause of water flooding.

In conclusion for Phase 1, the results showed that nitrogen buildup, in the absence of carbon monoxide, did not significantly penalize the cell performance for purge fractions greater than or equal to Fp_{min2}. Above this optimum purge fraction significant voltage degradation was associated with nitrogen build-up at 140 and 570 mA/cm^2, while flooding was the cause at 920 mA/cm^2.

The objective of Phase 2 testing was to determine the effect of purge fraction on the average cell voltage when 0.2 ppm CO was present in the fresh hydrogen fuel supply. With the exception of an additional fuel supply stream called Fuel B, the same experimental setup was used as in Phase

1. Fuel B was a gas mixture containing ppm levels of CO in hydrogen. This stream mixed with the pure hydrogen stream before entering the anode. The protocol followed for Phase 2 tests differed from that of Phase 1 in that a stack recovery procedure was performed before stack conditioning and the test ran for 10 hours rather than 20 minutes. The stack recovery procedure performed before each test was shown to be effective in removing some of the adsorbed CO from the previous test. The introduction of oxygen, from air, allowed for the oxidation of CO to CO_2, resulting in available catalyst sites for hydrogen adsorption and electrooxidation.

The first set of experiments performed in Phase 2 assessed the impact of the concentration of CO in the hydrogen fuel gas. The trend of increasing voltage degradation with increasing CO concentration was attributed to there being fewer active anode catalyst sites available for the adsorption and electrooxidation of hydrogen. The voltage decrease was assumed to reflect an increase of anode overpotential.

The second set of experiments assessed the impact of the purge fraction when the fuel stream contained CO. A decrease in cell voltage with a decrease in purge was observed at all three current densities. The trend of decreasing performance with a decrease in purge was assumed to be the result of an increasing CO concentration in the anode gas due to a smaller purge fraction.

At 570 mA/cm^2 the voltage loss was 162 mV at the lowest purge (Fp =0.63) and 96 mV at Fp=1.0. By increasing the temperature from 65^oC to 75^oC at Fp =0.71, the voltage degradation decreased by 28 mV. This is comparable to the 27 mV voltage increase that was achieved by increasing the purge from Fp =0.63 to Fp = 0.71 at 570 mA/cm^2. However, the increase in purge resulted in an 8% increase in fresh hydrogen feed requirement. Accordingly, there is definitely incentive to operate at higher temperatures given that with a temperature increase of just 10^0C a lower purge fraction can be used.

At 920 mA/cm^2 a voltage loss of 178 mV occurred at the lowest purge (Fp =0.83). This voltage loss was reduced to 155 mV when Fp =1.0, but at the cost of a 13% increase in the fuel requirement. After the 10 hour test, two techniques were used to reduce the CO poisoning. First, by switching from 0.2 ppm CO/H_2 to neat hydrogen after 10 hours of testing, the voltage recovered by 104 mV in only 2 hours. Second, by switching the purge from Fp =0.83 to Fp =1.0 after ten hours, the voltage continued to decrease but the degradation rate was much slower at the higher purge. In comparing these two techniques, switching to neat hydrogen definitely resulted in a faster recovery from CO poisoning, while higher purge only slowed the degradation.

Also observed at 570 mA/cm^2 and 920 mA/cm^2 was that voltage degradation accelerated with time. As one example at 570 mA/cm^2 and Fp= 0.63, the voltage degradation rate was 3.8 mV/hr over the first 4 hours and 30.8 mV/hr in the last 4 hours. The smaller degradation rate in the first hours was thought to be the result of slight CO coverage and that coverage being limited to the catalyst sites closest to the gas diffusion layer. As time progressed, the CO coverage increased and the distribution had an amplifying effect of the voltage loss. The distribution now included sites near the membrane, and these sites play a more crucial role in determining the electrode performance.

When operating with a recycle stream there is a clear point where degradation can be observed, and this point is a couple of hours before degradation accelerates to a higher rate. This indicates that online diagnostic testing may be feasible in that voltage degradation can be observed, and mitigation action taken (e.g. increasing the purge fraction to lower the rate of degradation, or a short air bleed for recovery) prior to the most significant impact taking place on overall performance.

The effect of purge on the cell voltage was less dramatic at a current density 140 mA/cm^2. The average voltage decrease for the range of Fp tested ($0.5 \geq Fp \geq 0.08$) was only 16 mV. Given the minimal effect that 0.2 ppm CO/H_2 had on the stack voltage at low current densities, there is

incentive to operate the HyPM HD8 at a lower purge to increase fuel efficiency if operation is at a low current density.

4.2 Recommendations/Future Work

- Water balance studies could be performed to determine the amount of water entering and exiting the anode and cathode, as well as that retained inside the membrane and GDL at various current densities. This will allow for a better examination of the role flooding may have played in the voltage degradation of the cell.

- Nernst law analyses could be developed with additional experimental runs in order to estimate the steady state concentrations of nitrogen in the anode stream. Also more runs could be conducted in order to more clearly characterize stack performance transient conditions.

- Electrochemical techniques such as cyclic voltammetry and impedance spectroscopy can be used to better characterize and isolate the catalyst aging.

- Scanning Electron Microscopy (SEM) is a valuable tool in characterizing the surface of fuel cell membranes and is capable of achieving both high resolution and magnification. This tool could be used to characterize failure modes such a pinhole formation, membrane and electrode thinning, and electrode delamination.

- Energy Dispersive X-ray (EDX) is a useful tool in determining the atomic composition of the surface of a sample and could be used to observe changes in the level of contaminants found.

- In this work (and on the actual fuel cell power module) the anode recirculation flow rate cannot be reasonably controlled by the constant speed of the recirculation pump. The development and/or selection of a variable speed pump, and then the development of a control algorithm for the pump may help to improve the overall system efficiency.

- Hydrogen sulfide (H_2S) is a contaminant found in reformate and ppm levels of H_2S are known to severely, and irreversibly, poison the catalyst. Studying the effect of H_2S in a study similar to this one would provide useful information for practical operating situations.

References

[1] Thomas, S., Zalbowitz, M., & Gill, D. (2006). Fuel Cells - Green Power.

[2] Mathias, M. F., Makharia, R., Gasteiger, H. A., Conley, J. J., Fuller, T. J., Gittleman, C. J., Kocha, S. S., Miller, D. P., Mittelsteadt, C. K., Tao Xie, Yan, S. G., & Yu, P. T. (2005). **Two fuel cell cars in every garage**? *Electrochem. Soc. Interface (USA), 14*(3), 24-35.

[3] Heywood, J. B. (2006). Fueling our transportation future *Scientific American, USA, 25*, 60-63.

[4] Van Mierlo, J., & Maggetto, G. (2007). Fuel Cell or Battery: Electric Cars are the Future. *Fuel Cells, 7*(2), 165-173.

[5] National Hydrogen Association, N. (2009). The Energy Evolution: An Analysis of Alternative Vehicles and Fuels to 2100. *Washington: National Hydrogen Association,*

[6] Canadian Hydrogen Fuel Cell Association. (2008). *About Fuel Cells.*, 2008, from http://www.chfca.ca/itoolkit.asp?pg=ABOUT_FUEL_CELLS

[7] Larminie, J., & Dicks, A. (2001). *Fuel Cell Systems Explained*. Chichester; Weinhein; New York; Brisbane; Singapore; Toronto: John Wiley & Sons.

[8] U.S. Dept. of Energy. (2009). *Electrochemical reaction within a PEM Fuel Cell.*, June 22, 2009, from http://alternativefuels.about.com/od/researchdevelopment/ig/Fuel-Cell-Diagrams/PEM-Fuel-Cell.htm

[9] Hoogers, G. (2002). *Fuel Cell Technology Handbook* CRC Press.

[10] Japan Hydrogen & Fuel Cell Demonstration Project. (2009). *Fuel Cell Battery Configuration.*, 2009, from http://www.jhfc.jp/e/beginner/about_fc/img/img_03.gif

[11] Kundu, S. (2004). Structure-Property-Performance Relationships in Fuel Cell Materials. (Masters, University of Waterloo).

[12] Appleby, A. J., & Foulkes, F. R. (2002). *Fuel Cell Handbook (Sixth Edition)* (6th ed.) Krieger Pub Co.

[13] Kocha, S. S., Yang, J. D., & Yi, J. S. (2006). Characterization of gas crossover and its implications in PEM fuel cells. *AIChE Journal, 52*(5), 1916-1925.

[14] Quan, P., Zhou, B., Sobiesiak, A., & Liu, Z. (2005). Water behavior in serpentine micro-channel for proton exchange membrane fuel cell cathode. *Journal of Power Sources, 152*, 131-145.

[15] Lee, Y., Jang, Y. H., Jung, T., Chung, J. T., & Kim, Y. (2006). Performance Characteristics of a Polymer Electrolyte Fuel Cell with the Anodic Supply Mode. *ECS Transactions, 3*(1), 871-878.

[16] U.S. Department of Energy. (2001). *Hydrogen Fuel Cell Engines and Related Technologies Course Manual*. Palm Desert, California: College of the Desert.

[17] St-Pierre, J., Wilkinson, D. P., Knights, S., & Bos, M. L. (2000). Relationships between water management, contamination and lifetime degradation in PEFC. *Journal of New Materials for Electrochemical Systems, 3*(2), 99-106.

[18] Cheng, X., Shi, Z., Glass, N., Zhang, L., Zhang, J., Song, D., Liu, Z., Wang, H., & Shen, J. (2007). A review of PEM hydrogen fuel cell contamination: Impacts, mechanisms, and mitigation. *Journal of Power Sources, 165*(2), 739-756.

[19] Kandlikar, S. G. (2008). Microscale and Macroscale Aspects of Water Management Challenges in PEM Fuel Cells. *Heat Transfer Engineering, 29*(7), 575.

[20] Fuller, T. F., & Newman, J. (1992). Experimental Determination of the Transport Number of Water in Nafion 117 Membrane. *Journal of the Electrochemical Society, 139*(5), 1332-1337.

[21] Choi, K., Peck, D., Kim, C. S., Shin, D., & Lee, T. (2000). Water transport in polymer membranes for PEMFC. *Journal of Power Sources, 86*(1-2), 197-201. doi:DOI: 10.1016/S0378-7753(99)00420-6

[22] Kreuer, K., Paddison, S. J., Spohr, E., & Schuster, M. (2004). Transport in Proton Conductors for Fuel-Cell Applications: Simulations, Elementary Reactions, and Phenomenology. *Chemical Reviews, 104*(10), 4637-4678.

[23] Falcão, D. S., Rangel, C. M., Pinho, C., & Pinto, A. M. F. R. (2009). Water Transport through a Proton-Exchange Membrane (PEM) Fuel Cell Operating near Ambient Conditions: Experimental and Modeling Studies. *Energy & Fuels, 23*(1), 397-402.

[24] Canut, J. L., Abouatallah, R. M., & Harrington, D. A. (2006). Detection of Membrane Drying, Fuel Cell Flooding, and Anode Catalyst Poisoning on PEMFC Stacks by Electrochemical Impedance Spectroscopy. *Journal of the Electrochemical Society, 153*(5), A857-A864.

[25] Grot, W. G. (1994). *Polymerization of fluorinated copolymers*. Patent GB1286859

[26] Kreuer, K. D. (2001). On the development of proton conducting polymer membranes for hydrogen and methanol fuel cells. *Journal of Membrane Science, 185*(1), 29-39.

[27] Zawodzinski Jr., T. A., Springer, T. E., Uribe, F., & Gottesfeld, S. (1993). Characterization of polymer electrolytes for fuel cell applications. *Solid State Ionics, 60*(1-3), 199-211. doi:DOI: 10.1016/0167-2738(93)90295-E

[28] Nguyen, T. V., & White, R. E. (1993). A Water and Heat Management Model for Proton-Exchange-Membrane Fuel Cells. *Journal of the Electrochemical Society, 140*(8), 2178-2186.

[29] Zawodzinski Jr., T. A., Derouin, C., Radzinski, S., Sherman, R. J., Smith, V. T., Springer, T. E., & Gottesfeld, S. (1993). Water Uptake by and Transport Through Nafion[sup [registered sign]] 117 Membranes. *Journal of the Electrochemical Society, 140*(4), 1041-1047.

[30] Watanabe, M., Satoh, Y., & Shimura, C. (1993). Management of the Water Content in Polymer Electrolyte Membranes with Porous Fiber Wicks. *Journal of the Electrochemical Society, 140*(11), 3190-3193.

[31] Buchi, F. N., & Srinivasan, S. (1997). Operating Proton Exchange Membrane Fuel Cells Without External Humidification of the Reactant Gases. *Journal of the Electrochemical Society, 144*(8), 2767-2772.

[32] Hakenjos, A., Muenter, H., Wittstadt, U., & Hebling, C. (2004). A PEM fuel cell for combined measurement of current and temperature distribution, and flow field flooding. *Journal of Power Sources, 131*(1-2), 213-216. doi:DOI: 10.1016/j.jpowsour.2003.11.081

[33] Lee, W., Shimpalee, S., & Zee, J. W. V. (2003). Verifying Predictions of Water and Current Distributions in a Serpentine Flow Field Polymer Electrolyte Membrane Fuel Cell. *Journal of the Electrochemical Society, 150*(3), A341-A348.

[34] Yoon, Y., Lee, W., Yang, T., Park, G., & Kim, C. (2003). Current distribution in a single cell of PEMFC. *Journal of Power Sources, 118*(1-2), 193-199. doi:DOI: 10.1016/S0378-7753(03)00093-4

[35] SAE International. (2005). *Information Report on the Development of Hydrogen Quality Guideline for Fuel Cell Vehicles* No. 11). 2005: SAE International.

[36] Cheng, X., Zhang, J., Tang, Y., Song, C., Shen, J., Song, D., & Zhang, J. (2007). Hydrogen crossover in high-temperature PEM fuel cells. *Journal of Power Sources, 167*(1), 25-31.

[37] Dhanushkodi, S. R., Mahinpey, N., Srinivasan, A., & Wilson, M. (2008). Life cycle analysis of fuel cell technology. *Journal of Environmental Informatics, 11*(1), 36-44.

[38] S. R. Dhanushkodi, N. Mahinpey, A. Srinivasan and M. Wilson. (2008). **Life Cycle** Analysis of Fuel Cell Technology. *Journal of Environmental Informatics, 11*(1), 36-44.

[39] Neburchilov, V., Martin, J., Wang, H., & Zhang, J. (2007). A review of polymer electrolyte membranes for direct methanol fuel cells. *Journal of Power Sources, 169*(2), 221-238.

[40] Moore, J. M., Adcock, P. L., Lakeman, J. B., & Mepsted, G. O. (2000). The effects of battlefield contaminants on PEMFC performance. *Journal of Power Sources, 85*(2), 254-260.

[41] Kundu, S., Fowler, M. W., Simon, L. C., Abouatallah, R., & Beydokhti, N. (2008). Degradation analysis and modeling of reinforced catalyst coated membranes operated under OCV conditions. *Journal of Power Sources, 183*(2), 619-628. doi:DOI: 10.1016/j.jpowsour.2008.05.074

[42] Ahluwalia, R. K., & Wang, X. (2007). Buildup of nitrogen in direct hydrogen polymer-electrolyte fuel cell stacks. *Journal of Power Sources, 171*(1), 63-71.

[43] Scholta, J., Rohland, B., & Wendt, H. (2000). Hydrogen fired PAFCs: an experimental investigation into the optimal utilization of impure, recycled hydrogen. *Journal of Applied Electrochemistry, 30*(3), 323-331.

[44] Bhatia, K. K., & Wang, C. (2004). Transient carbon monoxide poisoning of a polymer electrolyte fuel cell operating on diluted hydrogen feed. *Electrochimica Acta, 49*(14), 2333-2341.

[45] Gu, T., Lee, W. K., Zee, J. W. V., & Murthy, M. (2004). Effect of Reformate Components on PEMFC Performance: Dilution and Reverse Water Gas Shift Reaction.*151*(12), 2100-2105.

[46] Halseid, R., & Tunold, R. (2006). Hydrogen Oxidation on PtRu PEM Anodes. *Journal of the Electrochemical Society, 153*(12), A2319-A2325.

[47] Springer, T. E., Rockward, T., Zawodzinski, T. A., & Gottesfeld, S. (2001). Model for polymer electrolyte fuel cell operation on reformate feed - Effects of CO, H-2 dilution, and high fuel utilization. *Journal of the Electrochemical Society, 148*(1), A11-A23.

[48] Springer, T. E., Zawodzinski, T. A., & Gottesfeld, S. (1991). Polymer Electrolyte Fuel-Cell Model. *Journal of the Electrochemical Society, 138*(8), 2334-2342.

[49] Ahluwalia, R. K., & Wang, X. (2008). Effect of CO and CO2 impurities on performance of direct hydrogen polymer-electrolyte fuel cells. *Journal of Power Sources, 180*(1), 122-131.

[50] Wang, X., Hsing, I., Leng, Y., & Yue, P. (2001). Model interpretation of electrochemical impedance spectroscopy and polarization behavior of H2/CO mixture oxidation in polymer electrolyte fuel cells. *Electrochimica Acta, 46*(28), 4397-4405.

[51] Baschuk, J. J., & Li, X. (2003). Modelling CO poisoning and O_2 bleeding in a PEM fuel cell anode. *International Journal of Energy Research, 27*(12), 1095-1116. doi:10.1002/er.934

[52] Chan, S. H., Goh, S. K., & Jiang, S. P. (2003). A mathematical model of polymer electrolyte fuel cell with anode CO kinetics. *Electrochimica Acta, 48*(13), 1905-1919.

[53] Ralph T. R., & Hogarth M. P. (2002). Catalysis for Low Temperature Fuel Cells. *Platinum Metals Review, Volume 46, Number 3, 1 July 2002 , Pp. 117-135(19), 46*(3), 117-135(19).

[54] Oetjen, H. -., Schmidt, V. M., Stimming, U., & Trila, F. (1996). Performance Data of a Proton Exchange Membrane Fuel Cell Using H[sub 2]/CO as Fuel Gas. *Journal of the Electrochemical Society, 143*(12), 3838-3842. doi:10.1149/1.1837305

[55] Ciureanu, M., & Wang, H. J. Electrochem. Soc.(1999). *Electrochemical Impedance Study of Electrode-Membrane Assemblies in PEM Fuel Cells: I. Electro-oxidation of H2 and H2/CO Mixtures on Pt-Based Gas-Diffusion Electrodes*146114031-4040

[56] Gu, T., Lee, W. -., & Zee, J. W. V. (2005). Quantifying the 'reverse water gas shift' reaction inside a PEM fuel cell. *Applied Catalysis B: Environmental, 56*(1-2), 43-50.

[57] Ianniello, R., Schmidt, V. M., Stimming, U., Stumper, J., & Wallau, A. (1994). CO adsorption and oxidation on Pt and PtRu alloys: dependence on substrate composition. *Electrochimica Acta, 39*(11-12), 1863-1869. doi:DOI: 10.1016/0013-4686(94)85176-X

[58] Benesch, R., & Jacksier, T. (2006). Hydrogen and material quality issues for PEM fuel cells. *2005 IEEE Vehicle Power and Propulsion Conference* Chicago, IL, USA. 646-51.

[59] Jambunathan, K., Shah, B. C., Hudson, J. L., & Hillier, A. C. (2001). Scanning electrochemical microscopy of hydrogen electro-oxidation. Rate constant measurements and carbon monoxide poisoning on platinum. *Journal of Electroanalytical Chemistry, 500*(1-2), 279-289. doi:DOI: 10.1016/S0022-0728(00)00344-2

[60] Qi, Z., He, C., & Kaufman, A. (2002). Effect of CO in the anode fuel on the performance of PEM fuel cell cathode. *Journal of Power Sources, 111*(2), 239-247.

[61] Choudhary, T. V., Sivadinarayana, C., & Goodman, D. W. (2003). Production of COx-free hydrogen for fuel cells via step-wise hydrocarbon reforming and catalytic dehydrogenation of ammonia. *Chemical Engineering Journal, 93*(1), 69-80.

[62] Garcia, A. C., Paganin, V. A., & Ticianelli, E. A. (2008). CO tolerance of PdPt/C and PdPtRu/C anodes for PEMFC. *Electrochimica Acta, 53*(12), 4309-4315.

[63] Pitois, A., Davies, J. C., Pilenga, A., Pfrang, A., & Tsotridis, G. (2009). Kinetic study of CO desorption from PtRu/C PEM fuel cell anodes: Temperature dependence and associated microstructural transformations. *Journal of Catalysis, 265*(2), 199-208.

[64] Schmidt, T. J., Gasteiger, H. A., & Behm, R. J. (1999). Rotating Disk Electrode Measurements on the CO Tolerance of a High-Surface Area Pt/Vulcan Carbon Fuel Cell Catalyst. *Journal of the Electrochemical Society, 146*(4), 1296-1304. doi:10.1149/1.1391761

[65] Isono, T., Suzuki, S., Kaneko, M., Akiyama, Y., Miyake, Y., & Yonezu, I. (2000). Development of a high-performance PEFC module operated by reformed gas. *Journal of Power Sources, 86*(1-2), 269-273.

[66] Iwasita, T., Hoster, H., John-Anacker, A., Lin, W. F., & Vielstich, W. (2000). Methanol Oxidation on PtRu Electrodes. Influence of Surface Structure and Pt−Ru Atom Distribution. *Langmuir, 16*(2), 522-529.

[67] Lee, S. J., Mukerjee, S., Ticianelli, E. A., & McBreen, J. (1999). Electrocatalysis of CO tolerance in hydrogen oxidation reaction in PEM fuel cells. *Electrochimica Acta, 44*(19), 3283-3293.

[68] Zamel, N., & Li, X. (2008). Transient analysis of carbon monoxide poisoning and oxygen bleeding in a PEM fuel cell anode catalyst layer. *International Journal of Hydrogen Energy, 33*(4), 1335-1344.

[69] Das, S. K., Reis, A., & Berry, K. J. (2009). Experimental evaluation of CO poisoning on the performance of a high temperature proton exchange membrane fuel cell. *Journal of Power Sources, 193*(2), 691-698.

[70] Jiang, R., Kunz, H. R., & Fenton, J. M. (2005). Electrochemical Oxidation of H[sub 2] and H[sub 2]/CO Mixtures in Higher Temperature (T[sub cell] > 100[degree]C) Proton Exchange Membrane Fuel Cells: Electrochemical Impedance Spectroscopy. *Journal of the Electrochemical Society, 152*(7), A1329-A1340.

[71] Ehsasi, M., Matloch, M., Frank, O., Block, J. H., Christmann, K., Rys, F. S., & Hirschwald, W. (1989). Steady and nonsteady rates of reaction in a heterogeneously catalyzed reaction: Oxidation of CO on platinum, experiments and simulations.*19*(8), 4949-4960.

[72] Gottesfeld, S., & Pafford, J. (1988). A New Approach to the Problem of Carbon Monoxide Poisoning in Fuel Cells Operating at Low Temperatures. *Journal of the Electrochemical Society, 135*(10), 2651-2652. doi:10.1149/1.2095401

[73] Chung, C., Chen, C., Lin, H., & Yan, Y. (2005). Improvement of CO tolerance of proton exchange membrane fuel cell (PEMFC) by an air-bleeding technique. *Proceedings of the 3rd International Conference on* ***Fuel Cell*** *Science, Engineering, and Technology, 2005,* Ypsilanti, MI, United states. 215 -221.

[74] Inaba, M., Sugishita, M., Wada, J., Matsuzawa, K., Yamada, H., & Tasaka, A. (2008). Impacts of air bleeding on membrane degradation in polymer electrolyte fuel cells. *Journal of Power Sources, 178*(2), 699-705.

[75] Shah, A. A., Ralph, T. R., & Walsh, F. C. (2009). Modeling and Simulation of the Degradation of Perfluorinated Ion-Exchange Membranes in PEM Fuel Cells. *Journal of the Electrochemical Society, 156*(4), B465-B484.

[76] Collier, A., Wang, H., Zi Yuan, X., Zhang, J., & Wilkinson, D. P. (2006). Degradation of polymer electrolyte membranes. *International Journal of Hydrogen Energy, 31*(13), 1838-1854.

[77] Janssen, G. J. M., & Overvelde, M. L. J. (2001). Water transport in the proton-exchange-membrane fuel cell: measurements of the effective drag coefficient. *Journal of Power Sources, 101*(1), 117-125.

[78] Rama, P., Chen, R., & Thring, R. (2005). A polymer electrolyte membrane fuel cell model with multi-species input.*219*(4), 255-271.

[79] Hirano, S., Kim, J., & Srinivasan, S. (1997). High performance proton exchange membrane fuel cells with sputter-deposited Pt layer electrodes. *Electrochimica Acta, 42*(10), 1587-1593.

[80] Chan, K. W. (2005). Performance, Diagnostics, and Forensic Analyses of PEMFC in Dry Cathode Operation. (Master of Applied Science, University of Waterloo).

Appendix A

HyAL Automation Scripts

PHASE 1 - CONDITION

```
BEGIN
set_parameter logging_duration 30 Sec.
set_parameter averaging_duration 300 Sec.
autologging_on
log_data_now startup
override_safety
clear_alarms
set_valve valve_anode_dry_bypass ON
load_following_on
load_ctrl_mode
log_data_now start_up
set EP_ramp_dp 5 Kpa 0 999 0
set EP_ramp_rate 10 Kpa/step 0 999 0
set min_flow 0 mAmp/cm^2 0 10000 3
set_load load_value_set 0 Amps 0 1000 0
set_variable var_coolant_flow active_area $$$ 0 10000 0
mult var_coolant_flow no_of_cells $$$ 0 100000 0
divide var_coolant_flow 1000 $$$ 0 100000 0
set_flow flow_coolant_set var_coolant_flow lpm 0 5 20
BEGINGROUP
set_valve valve_anode_n2_purge OFF
ENDGROUP
DELAY 10
BEGINGROUP
set_valve valve_anode_n2_purge ON
ENDGROUP
DELAY 2
set_pressure pressure_anode_inlet_set 5 kPag 0 300 20
set_pressure pressure_cathode_inlet_set 5.4 kPag 0 300 20
DELAY 30
set anode_stoich_set 1.5 $$$
set cathode_stoich_set 2.46 $$$
set min_flow 200 mAmp/cm^2 0 10000 30
DELAY 30
set_temperature temp_stack_control_set 60 C 0 95 0
dewpt_readback_tracking_mode
DELAY 5
```

```
inlet_readback_tracking_mode
DELAY 5
;
set_valve valve_anode_deadend_bypass ON
set dead_end_flag ON
set total_cycle_time_set 0.5 0 140 0
DELAY 5
load_connect_on
DELAY 5
set current_density_set 100 mAmp/cm^2 0 10000 60
DELAY 80
enable_safety
set current_density_set 200 mAmp/cm^2 0 10000 60
DELAY 80
set_pressure pressure_anode_h2_forward_set 7 Kpa 0 420 10
DELAY 5
set current_density_set 400 mAmp/cm^2 0 10000 60
DELAY 80
dewpt_tracking_mode_off
DELAY 5
inlet_tracking_mode_off
DELAY 5
set_temperature temp_anode_reheat_loop_temp_set 65 C 0 120 0
set_temperature temp_anode_dewpoint_set 0 C 0 95 0
set_temperature temp_anode_gas_inlet_set 65 C 0 110 0
set_temperature temp_cathode_reheat_loop_temp_set 60 C 0 120 0
set_temperature temp_cathode_dewpoint_set 59 C 0 90 0
set_temperature temp_cathode_gas_inlet_set 60 C 0 110 0
;
DELAY 5
IF all_alarm_flags <= 0
enable_safety
ENDIF
set_pressure pressure_anode_h2_forward_set 9.7 Kpa 0 420 10
DELAY 5
set current_density_set 570 mAmp/cm^2 0 10000 100
DELAY 2000
log_data_now end_conditioning
END
```

PHASE 1 - 140 mA/cm^2

total_cycle_time_set = 0.5

```
BEGIN
```

```
GOTO skip_comments
; Accelerated Durability (Gore) Start Up Script
; Start up to 600 mA/cm^2, 80/80/80 degC, 100/100 kPa, 1.5/2.5 stoich conditions;
; Written by: Frank van den Bosch
; Revision 1: Jan 12, 2007 Original script for G-series stands
LABEL skip_comments
log_data_now i=140mA/cm2
set_temperature temp_stack_control_set 60 C 0 95 0
DELAY 2
set current_density_set 400 mAmp/cm^2 0 10000 60
DELAY 80
set_pressure pressure_anode_h2_forward_set 5 Kpa 0 420 10
set_pressure pressure_cathode_inlet_set 2.4 kPag 0 300 10
DELAY 10
;
set current_density_set 140 mAmp/cm^2 0 10000 160
DELAY 180
set cathode_stoich_set 4.69 $$$
DELAY 2
set_temperature temp_anode_reheat_loop_temp_set 67 C 0 120 0
set_temperature temp_anode_dewpoint_set 0 C 0 95 0
set_temperature temp_anode_gas_inlet_set 67 C 0 110 0
set_temperature temp_cathode_reheat_loop_temp_set 60 C 0 120 0
set_temperature temp_cathode_dewpoint_set 59 C 0 90 0
set_temperature temp_cathode_gas_inlet_set 60 C 0 110 0
;
DELAY 200
set total_cycle_time_set 0.5 $$$ 0 420 0 ; THIS IS THE ONLY CHANGING VARIABLE
start_new_datafile
log_data_now TCT=0.5_[CO]=0
DELAY 7200
start_new_datafile
END
```

PHASE 1 - 570 mA/cm^2

total_cycle_time_set = 0.5

```
BEGIN
GOTO skip_comments
; Accelerated Durability (Gore) Start Up Script
; Start up to 600 mA/cm^2, 80/80/80 degC, 100/100 kPa, 1.5/2.5 stoich conditions;
; Written by: Frank van den Bosch
; Revision 1: Jan 12, 2007 Original script for G-series stands
LABEL skip_comments
log_data_now i=570mA/cm2
```

```
set_temperature temp_stack_control_set 60 C 0 95 0
DELAY 2
set current_density_set 570 mAmp/cm^2 0 10000 60
DELAY 80
set_pressure pressure_anode_h2_forward_set 9.7 Kpa 0 420 10
set_pressure pressure_cathode_inlet_set 5.4 kPag 0 300 10
DELAY 10
;
set cathode_stoich_set 2.46 $$$
DELAY 2
set_temperature temp_anode_reheat_loop_temp_set 65 C 0 120 0
set_temperature temp_anode_dewpoint_set 0 C 0 95 0
set_temperature temp_anode_gas_inlet_set 65 C 0 110 0
set_temperature temp_cathode_reheat_loop_temp_set 60 C 0 120 0
set_temperature temp_cathode_dewpoint_set 59 C 0 90 0
set_temperature temp_cathode_gas_inlet_set 60 C 0 110 0
;
DELAY 200
set total_cycle_time_set 0.5 $$$ 0 8000 0
start_new_datafile
log_data_now TCT=0.5_Fp=1.0
DELAY 1200
autologging_off
END
```

PHASE 1 - 920 mA/cm^2

total_cycle_time_set = 0.5

```
BEGIN
GOTO skip_comments
; Accelerated Durability (Gore) Start Up Script
; Start up to 600 mA/cm^2, 80/80/80 degC, 100/100 kPa, 1.5/2.5 stoich conditions;
; Written by: Frank van den Bosch
; Revision 1: Jan 12, 2007 Original script for G-series stands
LABEL skip_comments
log_data_now i=800mA/cm2
set_temperature temp_stack_control_set 63 C 0 95 0
DELAY 2
set cathode_stoich_set 2.36 $$$
DELAY 2
set_pressure pressure_anode_h2_forward_set 16.6 Kpa 0 420 10
set_pressure pressure_cathode_inlet_set 9.6 kPag 0 300 10
DELAY 10
set current_density_set 920 mAmp/cm^2 0 10000 200
DELAY 220
```

```
;
set_temperature temp_anode_reheat_loop_temp_set 65 C 0 120 0
set_temperature temp_anode_dewpoint_set 0 C 0 95 0
set_temperature temp_anode_gas_inlet_set 65 C 0 110 0
set_temperature temp_cathode_reheat_loop_temp_set 60 C 0 120 0
set_temperature temp_cathode_dewpoint_set 59 C 0 90 0
set_temperature temp_cathode_gas_inlet_set 60 C 0 110 0
;
DELAY 200
set total_cycle_time_set 0.5 $$$ 0 8000 0
start_new_datafile
log_data_now TCT=0.5_Fp=1
DELAY 1200
autologging_off
END
```

PHASE 1 – SHUTDOWN

```
BEGIN
set_parameter logging_duration 10 Sec.
set_signal signal_out_load_relay OFF
override_safety
equivalent_flow_mode
set_load load_value_set 0 Amps 0 1000 0
set equivalent_flow 50 mAmp/cm^3
set_flow flow_anode_special_gas_mfc_set 0 ccm 0 1000 0
set_valve valve_anode_special_gas_mfc OFF
;
IF pressure_anode_in_set > 20
ANDIF pressure_cathode_in_set > 20
set_pressure pressure_anode_in_set 20 kPa 0 350 30
set_pressure pressure_cathode_in_set 20 kPa 0 350 30
DELAY 200
ENDIF
;
set_pressure pressure_anode_in_set 0 kPa 0 350 5
set_pressure pressure_cathode_in_set 0 kPa 0 350 5
DELAY 10
set_valve valve_anode_vent OFF
set_valve valve_cathode_vent OFF
;
set_valve valve_anode_steam OFF
set_valve valve_cathode_steam OFF
set_valve valve_steam_main OFF
;
```

```
set min_flow 0 mAmp/cm^2
set equivalent_flow 0 mAmp/cm^3
set_flow total_anode_stack_flow_set 0 slpm
set_flow total_cathode_stack_flow_set 0 slpm
;
inlet_readback_tracking_mode
dewpt_readback_tracking_mode
set_temperature temp_anode_sat_set 20 C 0 100 0
set_temperature temp_cathode_sat_set 20 C 0 100 0
set_temperature temp_coolant_tank_out_set 20 C 0 100 0
set_temperature temp_stack_control_set 20 C 0 100 0
;
set_valve valve_anode_inert OFF
DELAY 60
set_valve valve_anode_inert ON
;
set_signal signal_out_anode_dewpt_loop OFF
set_signal signal_out_anode_reheat_loop OFF
set_signal signal_out_cathode_dewpt_loop OFF
set_signal signal_out_cathode_reheat_loop OFF
;
; give the stack half an hour to cool to 40 degC
; otherwise e-stop
DO
IF LOOP_TIME >= 1800
print "Stack failed to reach 40 degC in 30 minutes"
GOTO endscript
ENDIF
WHILE temp_stack_control >= 40
;
LABEL endscript
autologging_off
;
set_signal signal_out_coolant_pump OFF
;
e_stop
;
; Shutdown
; comments included at end to allow rapid script execution
;
; Written by: Frank van den Bosch
; Revision 1: May 19, 2003
; Based on 15DOWNq by Branimir Petosic and SOP104
;
e_stop
END
```

PHASE 2 - CONDITION

BEGIN
set_parameter logging_duration 30 Sec.
set_parameter averaging_duration 300 Sec.
autologging_on
log_data_now startup
override_safety
clear_alarms
set_valve valve_anode_dry_bypass ON
set_valve valve_anode_special_gas_mfc OFF
set_flow flow_anode_special_gas_mfc_set 0 ccm 0 1000 0
load_following_on
load_ctrl_mode
log_data_now start_up
set EP_ramp_dp 5 Kpa 0 999 0
set EP_ramp_rate 10 Kpa/step 0 999 0
set min_flow 0 mAmp/cm^2 0 10000 3
set_load load_value_set 0 Amps 0 1000 0
set_variable var_coolant_flow active_area $$$ 0 10000 0
mult var_coolant_flow no_of_cells $$$ 0 100000 0
divide var_coolant_flow 1000 $$$ 0 100000 0
set_flow flow_coolant_set var_coolant_flow lpm 0 5 20
BEGINGROUP
set_valve valve_anode_n2_purge OFF
ENDGROUP
DELAY 10
BEGINGROUP
set_valve valve_anode_n2_purge ON
ENDGROUP
DELAY 2
set_pressure pressure_anode_inlet_set 5 kPag 0 300 0
set_pressure pressure_cathode_inlet_set 5.4 kPag 0 300 0
DELAY 5
set anode_stoich_set 1.5 $$$
set cathode_stoich_set 2.46 $$$
set min_flow 200 mAmp/cm^2 0 10000 30
DELAY 30

PHASE 2 - 140 mA/cm^2

total_cycle_time_set = 0.5

BEGIN

```
GOTO skip_comments
; Accelerated Durability (Gore) Start Up Script
; Start up to 600 mA/cm^2, 80/80/80 degC, 100/100 kPa, 1.5/2.5 stoich conditions;
; Written by: Frank van den Bosch
; Revision 1: Jan 12, 2007 Original script for G-series stands
LABEL skip_comments
log_data_now i=140mA/cm2
set_temperature temp_stack_control_set 60 C 0 95 0
DELAY 2
set current_density_set 400 mAmp/cm^2 0 10000 60
DELAY 80
set_pressure pressure_anode_h2_forward_set 5 Kpa 0 420 10
set_pressure pressure_cathode_inlet_set 2.4 kPag 0 300 10
DELAY 10
;
set current_density_set 140 mAmp/cm^2 0 10000 160
DELAY 180
set cathode_stoich_set 4.69 $$$
DELAY 2
set_temperature temp_anode_reheat_loop_temp_set 67 C 0 120 0
set_temperature temp_anode_dewpoint_set 0 C 0 95 0
set_temperature temp_anode_gas_inlet_set 67 C 0 110 0
set_temperature temp_cathode_reheat_loop_temp_set 60 C 0 120 0
set_temperature temp_cathode_dewpoint_set 59 C 0 90 0
set_temperature temp_cathode_gas_inlet_set 60 C 0 110 0
;
DELAY 200
set_valve valve_anode_special_gas_mfc ON
set_flow flow_anode_special_gas_mfc_set 426 ccm 0 1000 0
set total_cycle_time_set 0.5 $$$ 0 420 0
start_new_datafile
log_data_now TCT=0.5 Fp=1.0
DELAY 7200
autologging_off
END
```

PHASE 2 - 570 mA/cm^2

total_cycle_time_set = 0.5

```
BEGIN
GOTO skip_comments
; Accelerated Durability (Gore) Start Up Script
; Start up to 600 mA/cm^2, 80/80/80 degC, 100/100 kPa, 1.5/2.5 stoich conditions;
; Written by: Frank van den Bosch
; Revision 1: Jan 12, 2007 Original script for G-series stands
```

```
LABEL skip_comments
log_data_now i=570mA/cm2
set_temperature temp_stack_control_set 60 C 0 95 0
DELAY 2
set current_density_set 570 mAmp/cm^2 0 10000 60
DELAY 80
set_pressure pressure_anode_h2_forward_set 9.7 Kpa 0 420 10
set_pressure pressure_cathode_inlet_set 5.4 kPag 0 300 10
DELAY 10
;
set cathode_stoich_set 2.46 $$$
DELAY 2
set_temperature temp_anode_reheat_loop_temp_set 65 C 0 120 0
set_temperature temp_anode_dewpoint_set 0 C 0 95 0
set_temperature temp_anode_gas_inlet_set 65 C 0 110 0
set_temperature temp_cathode_reheat_loop_temp_set 60 C 0 120 0
set_temperature temp_cathode_dewpoint_set 59 C 0 90 0
set_temperature temp_cathode_gas_inlet_set 60 C 0 110 0
;
DELAY 10
set total_cycle_time_set 0.5 $$$ 0 8000 0
set_valve valve_anode_special_gas_mfc ON
set_flow flow_anode_special_gas_mfc_set 27 ccm 0 1000 0
start_new_datafile
log_data_now t0.5_[CO]=0.2
DELAY 36000
start_new_datafile
END
```

PHASE 2 - 920 mA/cm^2

total_cycle_time_set = 0.5

```
BEGIN
GOTO skip_comments
; Accelerated Durability (Gore) Start Up Script
; Start up to 600 mA/cm^2, 80/80/80 degC, 100/100 kPa, 1.5/2.5 stoich conditions;
; Written by: Frank van den Bosch
; Revision 1: Jan 12, 2007 Original script for G-series stands
LABEL skip_comments
log_data_now i=920mA/cm2
set_temperature temp_stack_control_set 63 C 0 95 0
DELAY 2
set cathode_stoich_set 2.36 $$$
DELAY 2
set_pressure pressure_anode_h2_forward_set 16.6 Kpa 0 420 10
```

```
set_pressure pressure_cathode_inlet_set 9.6 kPag 0 300 10
DELAY 10
set current_density_set 920 mAmp/cm^2 0 10000 200
;
set_temperature temp_anode_reheat_loop_temp_set 65 C 0 120 0
set_temperature temp_anode_dewpoint_set 0 C 0 95 0
set_temperature temp_anode_gas_inlet_set 65 C 0 110 0
set_temperature temp_cathode_reheat_loop_temp_set 60 C 0 120 0
set_temperature temp_cathode_dewpoint_set 59 C 0 90 0
set_temperature temp_cathode_gas_inlet_set 60 C 0 110 0
;
DELAY 2400
set total_cycle_time_set 0.5 $$$ 0 8000 0
DELAY 5
start_new_datafile
log_data_now t=0.5_[CO]0.0
set_valve valve_anode_special_gas_mfc OFF
set_flow flow_anode_special_gas_mfc_set 0 ccm 0 1000 0
DELAY 36000
autologging_off
END
```

PHASE 2 – SHUTDOWN

```
BEGIN
; autologging_on
; set_valve valve_anode_special_gas_mfc OFF
; set_flow flow_anode_special_gas_mfc_set 0 ccm 0 1000 0
; set total_cycle_time_set 0.6 sec 0 8000 0
; DELAY 7200
; set current_density_set 0 mAmp/cm^2 0 10000 1
; set_pressure pressure_anode_h2_forward_set 3.6 Kpa 0 420 0
; set_pressure pressure_cathode_inlet_set 1.1 kPag 0 300 0
; set cathode_stoich_set 5.47 $$$
; DELAY 60
; set_pressure pressure_anode_h2_forward_set 9.7 Kpa 0 420 0
; set cathode_stoich_set 2.46 $$$
; set_pressure pressure_cathode_inlet_set 5.4 kPag 0 300 0
; set current_density_set 920 mAmp/cm^2 0 10000 240
; DELAY 2400
; set current_density_set 0 mAmp/cm^2 0 10000 1
; DELAY 180
; set current_density_set 920 mAmp/cm^2 0 10000 240
; DELAY 2400
set_signal signal_out_load_relay OFF
override_safety
```

```
equivalent_flow_mode
set_load load_value_set 0 Amps 0 1000 0
set equivalent_flow 50 mAmp/cm^3
;
IF pressure_anode_in_set > 20
ANDIF pressure_cathode_in_set > 20
set_pressure pressure_anode_in_set 20 kPa 0 350 30
set_pressure pressure_cathode_in_set 20 kPa 0 350 30
ENDIF
;
set_pressure pressure_anode_in_set 0 kPa 0 350 5
set_pressure pressure_cathode_in_set 0 kPa 0 350 5
DELAY 10
set_valve valve_anode_vent OFF
set_valve valve_cathode_vent OFF
;
set_valve valve_anode_steam OFF
set_valve valve_cathode_steam OFF
set_valve valve_steam_main OFF
;
set min_flow 0 mAmp/cm^2
set equivalent_flow 0 mAmp/cm^3
set_flow total_anode_stack_flow_set 0 slpm
set_flow total_cathode_stack_flow_set 0 slpm
;
inlet_readback_tracking_mode
dewpt_readback_tracking_mode
set_temperature temp_anode_sat_set 20 C 0 100 0
set_temperature temp_cathode_sat_set 20 C 0 100 0
set_temperature temp_coolant_tank_out_set 20 C 0 100 0
set_temperature temp_stack_control_set 20 C 0 100 0
;
set_valve valve_anode_inert OFF
DELAY 60
set_valve valve_anode_inert ON
;
set_signal signal_out_anode_dewpt_loop OFF
set_signal signal_out_anode_reheat_loop OFF
set_signal signal_out_cathode_dewpt_loop OFF
set_signal signal_out_cathode_reheat_loop OFF
;
; give the stack half an hour to cool to 40 degC
; otherwise e-stop
DO
IF LOOP_TIME >= 1800
print "Stack failed to reach 40 degC in 30 minutes"
```

```
GOTO endscript
ENDIF
WHILE temp_stack_control >= 40
;
LABEL endscript
autologging_off
;
set_signal signal_out_coolant_pump OFF
;
e_stop
;
; Shutdown
; comments included at end to allow rapid script execution
;
; Written by: Frank van den Bosch
; Revision 1: May 19, 2003
; Based on 15DOWNq by Branimir Petosic and SOP104
;
e_stop
END
```

Appendix B

Leak Check Procedure [80]

Leak checks are performed after each 100 hour cycle of durability in order to determine whether any leaks have formed between the anode, cathode, coolant, and external environment. The test rig is composed of:

various lengths of ¼" nylon/stainless steel pipe
miscellaneous fittings such as tees and unions
4 plugs
1 pressure gauge rated up to 30 psig
4 rotometers of different sizes rated for nitrogen flow:

- 0-50 cm^3min^{-1}
- 0-200 cm^3min^{-1}
- 100-1000 cm^3min^{-1}
- 1000-5000 cm^3min^{-1}

Leak checks are used to detect five different types of leaks that can occur in the fuel cell stack. These are between:

- Anode to cathode
- Cathode to anode
- Anode to coolant
- Cathode to coolant
- External leak

Each one of the five leak checks requires a small modification of the test jig. Thus, leak checking the test rig is also extremely important after each modification has been made. Regardless of the test, the fuel cell stack must be at a temperature of 30°C or less before the test

can be started so that the results are consistent. When the cell membranes are warm, they will expand, changing the pore size of any pinholes that may be present. The test jig illustrating the flow of nitrogen gas for the external leak can be seen in Figure A.1.

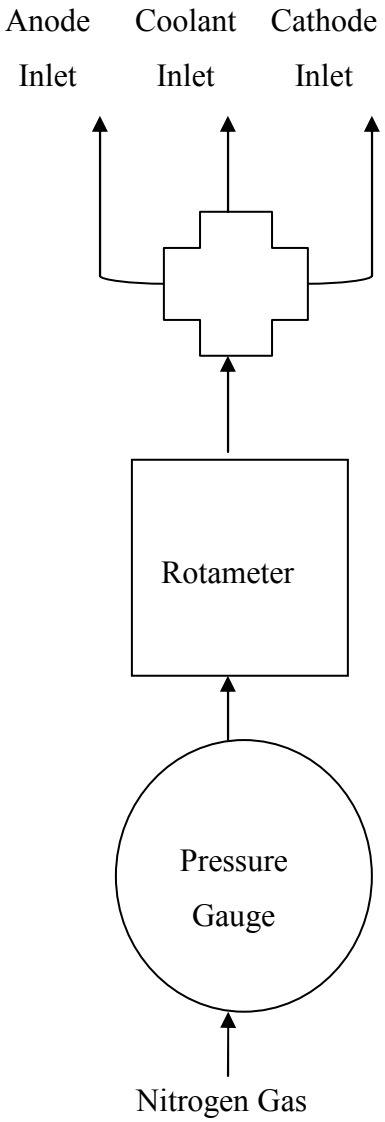

Figure A.1: Flow of nitrogen test gas through the leak check test jig and into fuel cell stack

In all of the leak checks, the three outlet ports are capped off to prevent the nitrogen from flowing out of the stack during the test. For the other four leak checks, a much simpler test rig is used instead. An example of a leak check to test for a leak in the direction of the anode to the cathode can be seen in Figure A.2.

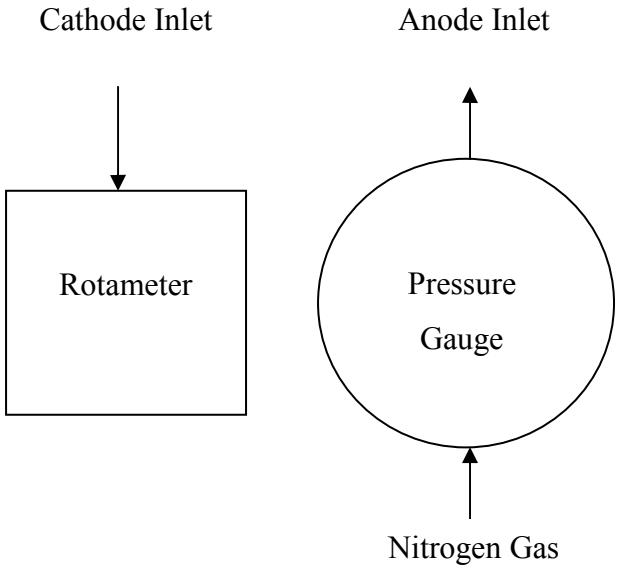

Figure A.2: Leak check test jig for anode to cathode crossover

The side with the pressure gauge always connects to the inlet of the port being tested whereas the side with the rotometer plugs into the outlet. Table A.1 summarizes the connections for all five leak checks.

Table A.1: Fuel cell stack connections for leak checking

Type of leak test	Anode inlet	Coolant inlet	Cathode inlet	N_2 Pressure [psig]

External	See Figure A.1	See Figure A.1	See Figure A.1	30
Anode to cathode	Pressure gauge	Capped	Rotameter	5
Cathode to anode	Rotameter	Capped	Pressure gauge	5
Anode to coolant	Pressure gauge	Rotameter	Capped	20
Cathode to coolant	Capped	Rotameter	Pressure gauge	20

Appendix C

HyWARE Tag Names

Date	flow_cathode_air_mfc_low	pressure_anode_humidifier_inlet	temp_anode_reheat_heattape
Time	flow_cathode_air_mfc_low_set	pressure_cathode_humidifier_inlet	temp_cathode_reheat_heattape
Interval_Time	flow_coolant	pressure_cool_in_out_diff	temp_anode_reheat_loop_temp_set
Cumulative_Time	flow_coolant_set	pressure_coolant_bpc	temp_cathode_dewpoint_gas
Comment	heater_anode_dewpoint_on	pressure_coolant_inlet	temp_cathode_dewpoint_set
MarkPoint	heater_anode_dewpoint_pwm	pressure_coolant_inlet_set	temp_cathode_corrected_dewpoint_set
Alarm	heater_anode_dewpoint_ssr	pressure_coolant_outlet	temp_cathode_corrected_dewpoint_disp
data_cell_001	heater_anode_heattape_pwm	pump_anode_dewpoint_on	temp_cathode_dewpoint_water
data_cell_002	heater_anode_reheat_on	pump_cathode_dewpoint_on	temp_cathode_endplate_set
data_cell_003	heater_anode_reheat_pwm	pump_coolant_old	temp_cathode_exhaust
data_cell_004	heater_anode_reheat_ssr	rad_coolant_pwm	temp_cathode_gas_inlet_set
data_cell_005	heater_cathode_dewpoint_on	rng_cell_voltage	temp_cathode_heattape
data_cell_006	heater_cathode_dewpoint_pwm	signal_in_anode_dewpoint_sensor	temp_cathode_inlet
data_cell_007	heater_cathode_dewpoint_ssr	signal_in_cathode_dewpoint_sensor	temp_cathode_outlet
data_cell_008	heater_cathode_heattape_pwm	signal_in_h2_sensor	temp_cathode_reheat_gas
data_cell_009	heater_cathode_reheat_en	signal_out_coolant_vfd_ref	temp_cathode_reheat_loop_temp
data_cell_010	heater_cathode_reheat_on	signal_out_flow_coolant_ip	temp_cathode_reheat_loop_temp_set
active_area	heater_cathode_reheat_pwm	signal_out_load_en	temp_coolant_hex_outlet
anode_inlet_rel_hum	heater_cathode_reheat_ssr	signal_out_pressure_anode_deadend_ip	temp_coolant_inlet
anode_inlet_rel_hum_set	heater_coolant_pwm	signal_out_pressure_anode_ip	temp_stack_control_set
anode_inlet_rh_temp_set	heater_end_plate_anode_pwm	signal_out_pressure_cathode_ip	temp_coolant_outlet
anode_stoich	heater_end_plate_cathode_pwm	signal_out_shutdown	temp_stack_coolant_delta_t
anode_stoich_set	load_value	dead_end_purge_valve_open_duration_set	temp_stack_coolant_delta_t_set

transitional_anode_stoich_set	load_value_diff	dead_end_pressure_pid_disable	total_anode_stack_flow_avg
averaging_size	load_value_set	dead_end_low_cell_voltage_threshold_set	total_anode_stack_flow
averaging_duration	max_cell_voltage	stack_power	total_anode_stack_flow_set
cathode_inlet_rel_hum	mean_cell_voltage	stack_voltage	total_cathode_stack_flow
cathode_inlet_rel_hum_set	min_cell_voltage	standard_dev	total_cathode_stack_flow_set
cathode_stoich	no_of_cells	temp_an_ca_diff	total_cycle_time
cathode_stoich_set	pressure_anode_bpc	temp_an_cool_diff	total_cycle_time_set
coolant_module_on	pressure_anode_cathode_diff	temp_anode_dewpoint_gas	valve_anode_deadend_bypass
current_density	pressure_anode_coolant_diff	temp_anode_dewpoint_set	valve_anode_dewpoint_hex_outlet
dead_end_flag	pressure_anode_fpc	temp_anode_corrected_dewpoint_set	valve_anode_dewpoint_hex_outlet_pwm
duty_cycle	pressure_anode_inlet	temp_anode_corrected_dewpoint_disp	valve_anode_dry_bypass
duty_cycle_set	pressure_anode_inlet_set	temp_anode_dewpoint_water	valve_anode_h2_mfc_low
flow_anode_h2_mfc_high	pressure_anode_outlet	temp_anode_endplate_set	valve_anode_humid_drain_pwm
flow_anode_h2_mfc_high_set	pressure_cathode_bpc	temp_anode_gas_inlet_set	valve_anode_humid_fill
flow_anode_h2_mfc_low	pressure_cathode_cool_diff	temp_anode_heattape	valve_anode_humid_inlet
flow_anode_h2_mfc_low_set	pressure_cathode_inlet	temp_anode_inlet	valve_cathode_dry_bypass
flow_cathode_air_mfc_high	pressure_cathode_inlet_set	temp_anode_outlet	valve_pilot_air_supply
flow_cathode_air_mfc_high_set	pressure_cathode_outlet	temp_anode_reheat_gas	temp_pc_cabinet
flow_anode_special_gas_mfc	flow_anode_special_gas_mfc_set	pump_power_supply_set	

Appendix D

HyPM HD8 Process Conditions

Total current [A]	Current Density [A/cm^2]	Air flow [slpm]	Cath Stoich	H2 Flow Stoich of 1 [slpm]	Anode Stoich As Seen By The Stack	Coolant Flowrate [slpm]	Anode Stack Inlet Press [kpa]	Cath Stack Inlet Press [kpa]	Cath Stack Inlet Temp [C]	Anode Stack Inlet Temp [C]	Coolant Stack Outlet Temp [C]	Cath Stack Inlet Dew point [C]	Anode Stack Inlet Dew point [C]
181	0.92	567	2.36	101	1.53	39	16.6	9.6	60	65	63	59	33
158	0.8	503	2.4	88	1.61	39	14.3	8.2	60	65	62	59	33
135	0.69	435	2.43	75	1.72	39	11.9	6.8	60	66	62	59	42
112	0.57	367	2.46	63	1.83	39	9.7	5.4	60	65	60	59	41
91	0.46	302	2.51	51	2.00	39	7.9	4.3	60	66	61	59	49
70	0.35	263	2.85	39	2.29	39	6.8	3.6	60	66	60	59	55
49	0.25	190	2.93	27	2.84	39	5.3	2.6	60	67	59	59	57
28	0.14	173	4.69	16	4.23	39	5	2.4	60	67	60	59	59
7	0.04	50	5.47	4	14.06	39	3.6	1.1	60	68	59	59	60

**Based on GEN 1.4-HYPM XR OPERATING CONDITIONS-Mar-21-06-REV-00*